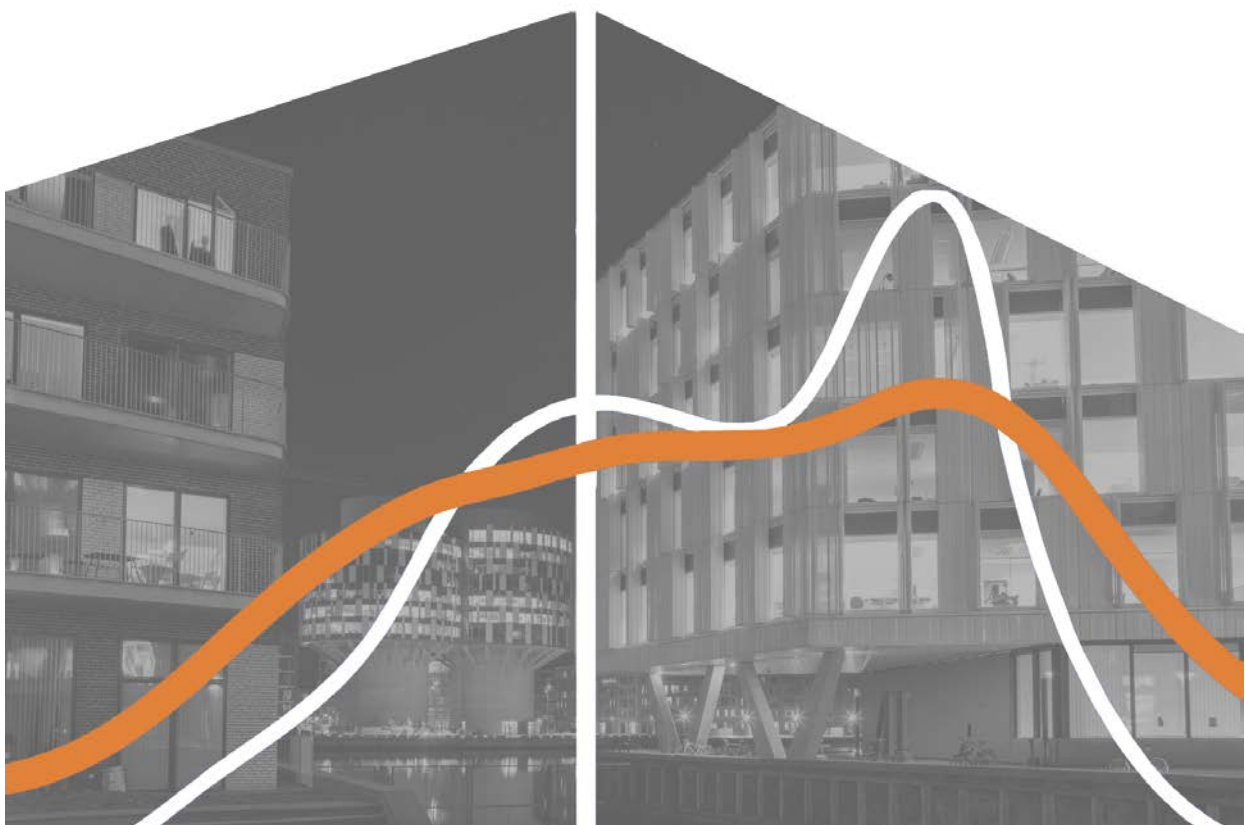


Modelling of possible Energy Flexibility in Single Buildings and Building Clusters



A technical report from IEA EBC Annex 67 Energy Flexible Buildings

Modelling of possible Energy Flexibility in Single Buildings and Building Clusters

Editor

Rongling Li, Technical University of Denmark (DTU), Denmark

Contributors

Rongling Li, Technical University of Denmark (DTU), Denmark

Sarah O'Connell, United Technologies Research Centre, Ireland

Kun Zhang, Polytechnique Montreal, Canada

Krzysztof Arendt, University of Southern Denmark, Denmark

Yuekuan Zhou and Sunliang Cao, Hong Kong Polytechnic University, China

Hussain Kazmi, Katholieke Universiteit Leuven (KU Leuven), Belgium

Zahra Mohammadi, Eindhoven University of Technology, the Netherlands

Reviewers

Søren Østergaard Jensen, Danish Technological Institute (DTI), Denmark

Bart Bleys, Belgian Building Research Institute (BBRI), Belgium

October, 2019



Preface

The increasing global energy demand, the foreseen reduction of available fossil fuels and the increasing evidence of global warming during the last decades have generated a high interest in renewable energy sources. However, renewable energy sources, such as wind and solar power, have an intrinsic variability that can seriously affect the stability of the energy system if they account for a high percentage of the total energy generation.

The Energy Flexibility of buildings is commonly suggested as part of the solution to alleviate some of the upcoming challenges in the future demand-respond energy systems (electrical, district heating and gas grids). Buildings can supply flexibility services in different ways, e.g. utilization of thermal mass, adjustability of HVAC system use (e.g. heating/cooling/ventilation), charging of electric vehicles, and shifting of plug-loads. However, there is currently no overview or insight into how much Energy Flexibility different building may be able to offer to the future energy systems in the sense of avoiding excess energy production, increase the stability of the energy networks, minimize congestion problems, enhance the efficiency and cost effectiveness of the future energy networks. Therefore, there is a need for increasing knowledge on and demonstration of the Energy Flexibility buildings can provide to energy networks. At the same time, there is a need for identifying critical aspects and possible solutions to manage this Energy Flexibility, while maintaining the comfort of the occupants and minimizing the use of non-renewable energy.

In this context IEA EBC Annex 67 Energy Flexible Buildings was started in 2015 with the aim of gaining increased knowledge on the benefits and services the utilization of the Energy Flexibility in buildings may provide to the future energy networks. The present report is one among several outputs from IEA EBC Annex 67. For further information, please visit <http://www.iea-ebc.org/projects/ongoing-projects/ebc-annex-67/>.

Published by Rongling Li, Technical University of Denmark, Denmark
Cover photo credit: Birgitte Torntoft

Disclaimer Notice: This report is not an official IEA EBC report. Although this publication is part of the work conducted within IEA EBC Annex 67 Energy Flexible Buildings, the publication only reflects the viewpoints of the authors. Neither the authors nor the EBC Contracting Parties (of the International Energy Agency Technology Collaboration Programme of Research and Development on Energy in Buildings and Communities) make any representation as to the adequacy or accuracy of the information contained herein, or as to its suitability for any particular application, and accept no responsibility or liability arising out of the use of this publication. The information contained herein does not supersede the requirements given in any national codes, regulations or standards, and should not be regarded as a substitute for the need to obtain specific professional advice for any particular application.

Contents

1. Introduction.....	9
2. Development of a data driven approach to investigate the energy flexibility potential of building clusters.....	11
2.1 Modelling objective.....	12
2.2 Building and system description	12
2.3 Method and modelling tools.....	13
2.3.1 Occupancy modelling.....	14
2.3.2 Building modelling	15
2.3.3 Estimating number of households and generating occupancy model for the building.....	17
2.3.4 Simulation of energy flexibility	17
2.4 Results.....	17
2.4.1 Energy flexibility potential of building clusters with different construction year	17
2.4.2 Energy flexibility potential of building clusters with different construction year	17
2.4.3 Uncertainty of energy flexibility potential of building clusters	19
2.5. Conclusion.....	20
2.6. References.....	21
2.7 Relevant publications.....	21
3. Flexibility Analysis for smart grid demand response.....	22
3.1 Modelling objective.....	23
3.2 Building and system description	23
3.3 Method and modelling tools.....	23
3.4 Results.....	27
3.5 Conclusions	30
3.6 Acknowledgements.....	31
3.7 References.....	31
3.8 Abbreviations	31
3.9 Relevant publications.....	32
4. Investigating the energy flexibility of typical Canadian homes: the potential of building thermal mass and photovoltaic system with battery.....	33
4.1 Objective	34
4.2 Building and system description	34
4.3 Method and modelling tools.....	34
4.3.1 Models	34
4.3.2 KPIs	36
4.4 Results.....	37

4.5 Discussions	42
4.6 Reference	43
4.7 Relevant publications	43
5. Multi-objective genetic algorithm for model predictive control in buildings.....	45
5.1 Modelling objective.....	46
5.2 Building and system description	46
5.3 Method and modelling tools.....	46
5.4 Results	49
5.5 Reference	53
5.6 Relevant publications.....	54
6. The investigation of the energy flexibility of a residential building via the hybrid energy storages in Hong Kong.....	55
6.1 Modelling objective.....	56
6.2 Building and system description	56
6.3 Method and modelling tools.....	56
6.4 Results	59
6.5 References.....	59
6.6 Relevant publications	60
7. Few-shot learning: data-driven modelling of hot water systems with extremely limited data	61
7.1 Modelling objective.....	62
7.2 Building and system description	63
7.3 Method and modelling tools.....	64
7.3.1 Benchmark black-box method	64
7.3.2 A taxonomy of transfer learning.....	64
7.3.3 Towards few-shot learning	65
7.4 Results	66
7.4.1 Storage model.....	66
7.4.2 Heating model	69
7.4.3 Extension to active control	72
7.5 Conclusion	73
7.6 Reference	73
7.7 Relevant publications	74
8. Development of a simulation based design optimization approach for grid independent houses with integrated energy flexibility metrics	75
8.1 Modelling objective.....	76
8.2 Building and system description	76
8.3 Method and modelling tools.....	76

8.3.2 Identify decision makers and performance indicators	78
8.3.3 Defining design space	78
8.3.4 Define future scenarios.....	79
8.4 Results	81
8.4.1 Performance prediction and analysis of the design solutions.....	81
8.4.2 Building performance considering all policy scenarios.....	83
8.4.3 Future-proof building designs with low grid dependency considering all policy scenarios .	86
8.5 Conclusion.....	88
8.6 References.....	89
8.7 Relevant publications.....	89

List of Figures

Figure 1 Flow diagram of quantification of building cluster energy flexibility using a data-driven approach	13
Figure 2 Vacancy profile of groups with different number of households. (a) 64 households, about 100 people; (b) 321 households, about 500 people; (c) 643 households, about 1000 people.....	14
Figure 3 Survival analysis of vacancy for all 144 time points and three household sizes.....	15
Figure 4 4R3C grey-box model structure.	16
Figure 5 Indoor air temperature under different control modes.....	18
Figure 6 Heat pump power curve of building cluster with different construction year.....	18
Figure 7 Energy flexibility potential of building cluster with different construction years	19
Figure 8 Energy flexibility and its uncertainty with scaling-up of apartment blocks.....	20
Figure 9 Flexibility Characterisation Process.....	24
Figure 10 Populating a 2D representation of the Flexibility Matrix.	26
Figure 11 Scenario Generation for 1 Hour event showing Battery system only on left and PV (hatched) with HVAC reduction on right: VRF (purple) and AHU fans (grey).	27
Figure 12 Scenario Generation for 4 Hour event showing Battery system only on left and PV (hatched with HVAC reduction on right: VRF (purple) and AHU fans (grey).	27
Figure 13 Validation of one-hour scenario for PV and HVAC. Modelled flexibility is shown on the left and validation results are shown on the right.	28
Figure 14 Validation of one-hour scenario with Battery system only. Modelled flexibility is shown on the left and validated results are shown on the right.	29
Figure 15 Flexible energy demand of buildings (downward flexibility) with E_f : flexible energy; E_{rb} : rebound energy; P_{fmax} : maximum flexible power; tdr : duration of demand response event.....	36
Figure 16 Downward flexible energy of the heating season.....	38
Figure 17 Upward flexible energy of the heating season.....	39
Figure 18 Downward flexible efficiency of the heating season.....	39
Figure 19 Upward flexible efficiency of the heating season.	39
Figure 20 Self-generation vs battery capacity.....	40
Figure 21 Self-consumption vs battery capacity.	41
Figure 22 Upward flexible energy-grid support mode.	42
Figure 23 Upward flexible energy-UPS mode.	42
Figure 24 Downward flexible energy-UPS mode.....	42
Figure 25 (a) simplified test model limited to 7 zones, (b) actual OU44 building.....	46
Figure 26 Optimization framework setup based on a virtual building.	47
Figure 27 Pareto frontier in the multi-objective genetic algorithm optimization.....	48
Figure 28 Gray-box model of a zone based on the R2C2 thermal network (Modelica).....	49
Figure 29 Indoor temperature profiles within the first five days of simulation. The areas shaded in gray mark occupancy periods.....	50
Figure 30 One-month indoor temperature profiles for the three considered scenarios (RBC, CTRL-EE, CTRL-DK1). Each column represents a single zone (profile name - zone number).	51
Figure 31 Indoor comfort violations for the three considered scenarios	52
Figure 32 Total heating profiles for the three scenarios (top) vs. energy price (bottom).....	52
Figure 33 Total energy cost per scenario.	53
Figure 34 The demonstration of the flexible energy and the flexibility factors for the thermal storage system.....	58
Figure 35 A schematic representation of the sensing employed in the projects and the nonlinear temperature distribution inside the storage, which complicates the state of charge estimation.	63
Figure 36 A graphic representation of the potential benefits of transfer learning.....	64
Figure 37 Storage vessel model accuracy with raw time series learning for increasing amounts of data (1 week, 4 weeks, and 32 weeks).....	66
Figure 38 Storage model accuracy with raw time series learning incorporating transfer learning – data-weeks here represents amount of data in weeks used to train the neural network, the source of the data can be from different households achieving transfer.	67

Figure 39 Estimated state of charge as a function of user hot water consumption and thermodynamic losses; the models having been learned with: (a) one week of data for one household; (b) 32 weeks of data for one household; (c) one week of data for 32 households; (d) 32 weeks of data for 32 households.	67
Figure 40 Estimated state of charge as a function of user hot water consumption and thermodynamic losses after constraints have been imposed; the models having been learned with: (a) one week of data for one household; (b) 32 weeks of data for one household; (c) one week of data for 32 households; (d) 32 weeks of data for 32 households.....	68
Figure 41 Mean Absolute Error [°C] as a function of increasing data collection (weeks) and agency (households).	68
Figure 42 Mean Absolute Error [kWh] as a function of increasing data collection (weeks) and agency (households).	69
Figure 43 Mean Absolute Error [°C] as a function of increasing data collection (weeks) and different learning frameworks.....	71
Figure 44 Results of learning with and without induction learning for the heating model; results shown here are to visualize the trends of the learned model for (a) with induction for 2 agents after 4 weeks, and (b) without induction with 2 agents after 32 weeks; the heating temperature (T_{end} is limited to 55°C, above which a booster heater is used to reheat the hot water.....	72
Figure 45 Results of using the developed models to active control of hot water systems.....	72
Figure 46 Layout of a typical Dutch terraced house, showing different floors, front and back view of the building. All dimensions are in mm.....	77
Figure 47 The investment cost and operational cost for total energy consumption of all designs solutions under net-metering scenario.	81
Figure 49 Two sets of Pareto solutions are presented per graph: dark blue dots represent the Pareto solutions based on operational cost, investment cost and overheating hours. Cyan colored dots represent the Pareto solutions based on the energy matching and grid.	83
Figure 50 Two sets of Pareto solutions for the production-based incentive policies (scenarios 1 and 2). Dots without edge represent solutions based on additional investment cost, operational cost and overheating hours. Dots with black edged-lines represent solutions based on energy matching and grid interaction.	84
Figure 51 Two sets of Pareto solutions for the self-consumption-based incentive policies (scenarios 3 and 4). Dots without edge represent solutions based on additional investment cost, operational cost and overheating hours. Dots with black edged-lines represent solutions based on energy matching and grid interaction.	85
Figure 52 The boxplots show the performance spread for a design parameter value caused by variations in all the other design parameters and by the scenarios. The presented solutions are from the homeowner Pareto set. ...	86
Figure 53 The boxplots show the performance spread for a design parameter value caused by variations in all the other design parameters and by the scenarios. The presented solutions are from the EF Pareto set.	87

List of Tables

Table 1 Numbers of households of different household size and different apartment size in Danish apartment buildings.	14
Table 2 U values of building envelopes, data source: TABULA 2015	16
Table 3 Summary showing Modelled and Validated Flexibility Results for 1 Hour Scenario Model	29
Table 4 Summary showing Modelled and Validated Flexibility Results for 4 Hour Scenario Model	29
Table 5 Benchmark Comparison for Example Building	30
Table 6 Total heating energy consumption per scenario	49
Table 7 Overview of thermal comfort and costs performance indicators.	78
Table 8 Overview of energy matching and grid interaction performance indicators.	78
Table 9 Design parameter options considered in this study	79
Table 10 Overview of the policy scenarios and rate of incentives used in this study	80

1. Introduction

This report is a collection of simulation and modelling based studies within the activity B.1 of Annex 67: Simulation of energy flexibility in single buildings and clusters of buildings. Specifically, this report provides case studies of task B.1.3: Practical potential of different energy storage and on-site generation solutions in new and existing buildings, and task B.1.4: Modelling of possible energy flexibility in single buildings and cluster of buildings.

In the Annex 67 working group, different methods have been applied to simulate energy flexibility potential of building components, single buildings and building clusters. We investigated the performance of different storage and generation solutions concerning e.g. power, energy, ramp up and down time, peak shaving, time shifting, uncertainty, etc. and their deployment in both new and existing buildings. The objective of this report is to show cases of these different approaches. In each chapter, one case study is described focusing on methodology used and the table below is the summary of each study. Each chapter is written based on relevant publications listed in the end of the chapter.

The aim of the following case studies is further to inspire peoples who wish to perform simulations for determination of the possible energy flexibility of actual buildings.

Author, institute	Simulated system	Method and software	Scale	Conclusion
Rongling Li, DTU	Heat pump based floor heating	Data-driven grey box and statistical models, MATLAB	Building cluster	This model can be a tool for simulating the building energy flexibility potential for district/city energy planning. When the size of a building cluster was scaled up, the uncertainty became negligible.
Sarah O'Connell, NUIG	VRF heat pump, AHU fans, PV, 2nd life EV batteries	Mathematical model with human-in-the-loop, Python and Excel	Single building	The scenario modelling validation at the case study building demonstrated accurate predictions for mature technologies such as HVAC VRF heat pumps and AHU fans.
Kun Zhang, PolyMTL	Electric resistance heating, PV with battery system	Detailed physical models, TRNSYS and MATLAB	Single building	The flexibility potential of thermal mass and battery system in residential buildings is significant, but subject to weather, building occupancy and baseline control strategy.

Krzysztof Arendt, SDU	Hydronic radiator heating in a 7-zone building	Grey-box (Modelica), white-box (EnergyPlus)	Single building	The dynamic energy pricing based on the Nord Pool market provided insufficient incentives for load shifting in the multi-objective optimization aimed at minimization of discomfort and total energy cost.
Yuekuan Zhou & Sunliang Cao, HKPolyU	Residential building with hybrid energy storages and electric vehicles	White box, TRNSYS	Single-family house	22.1% of the cooling load can be reduced by BIPVs in Hong Kong. Building energy flexibility can be enhanced with the implementation of the excess REe-recharging strategies and the integration of an electric vehicle.
Hussain Kazmi, KU Leuven	Heat pump hot water systems	Data-driven black box, Keras in Python	Building cluster	The data-driven models can be utilized to both estimate device flexibility, and leverage it to improve operational performance of a hot water system. Modeling performance improves as the number of hot water systems used to gather data increases.
Zahra Mohammadi, TU/e	A residential house with heat pump, PV and battery	White box, TRNSYS	Single building	Energy flexible designs can provide higher self-consumption and lower dependency to the grid, but are more expensive for homeowners. They are, however, more future proof in accordance to the probable future policy scenarios.

Insert a list of abbreviations here

VRF heat pump: Variable Refrigerant Flow (VRF) heat pump

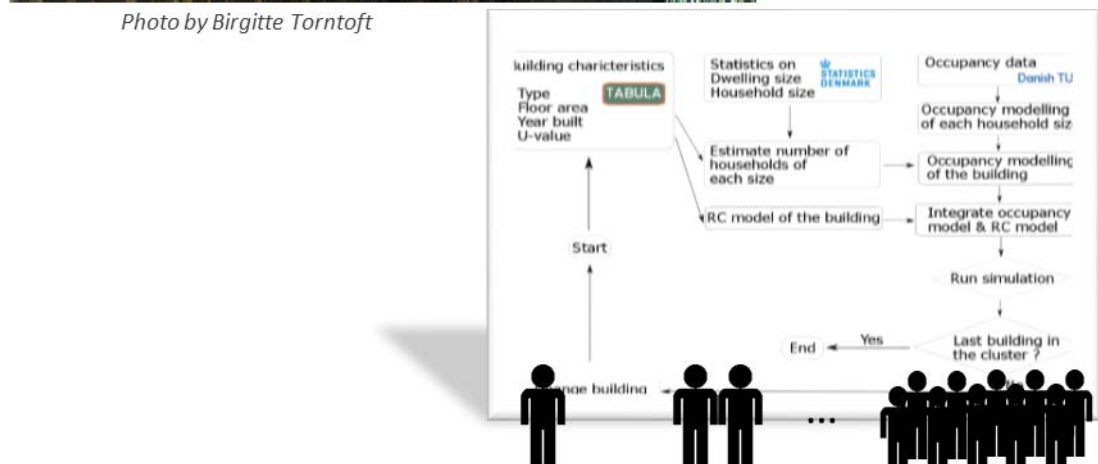
AHU: Air handling unit

PV: Photovoltaic panels

2. Development of a data driven approach to investigate the energy flexibility potential of building clusters



Photo by Birgitte Torntoft



Institution

Section of Energy and Services,
Department of Civil Engineering,
Technical University of Denmark

Technical
University of
Denmark



Contact persons

Dr., Assistant prof. Rongling Li
liron@byg.dtu.dk
+45 45251806

2.1 Modelling objective

In this study, we developed a data driven approach to simulate a generic building cluster that could resemble any mix of building archetypes and occupancy. The energy flexibility potential of apartment building clusters was estimated by using data from surveys and available statistics in Denmark for the worst case scenario, i.e. when the end users do not allow any disturbance when they are at home, so that energy flexibility is only available when residents are not at home. In this scenario, no energy flexibility is assumed when buildings are occupied, which yields a conservative estimation. The uncertainty of the energy flexibility potential due to uncertain occupancy and various archetypes was quantified for different scales of building cluster. The resulting hybrid-model is a combination of a building model and an occupancy model and includes the different factors that influence the potential energy flexibility of buildings.

The first contribution of the present study is its data driven approach to estimating the energy flexibility potential of building clusters containing various archetypes during the time that they are unoccupied. The second contribution is the quantification of the uncertainty of the available energy flexibility for different scales of building cluster with different numbers of households. This approach is generic and scalable can be used to aggregate any number of dwellings. The value of the uncertainty quantification is in the planning of the energy supply. A typical case is when a grid operator must have information on the reliability of deploying a certain number of households and buildings to achieve demand flexibility and balance the grid. Based upon existing state of the art research on energy flexibility in buildings, the present study goes further:

1. The presented model is generic and scalable, implying it can be used to simulate the flexibility of building clusters with three key features: varying the size of a building cluster, flexible combinations of occupancy pattern and building archetypes in each building cluster, and the control solutions applied to enable the provision of building flexibility. Previous studies in this field have tended to focus on only one or two of these three aspects.
2. Each feature of the model is comprehensively modelled and studied based on three different data sources, i.e. TABULA, Danish Statistics and Danish Time Use Survey. Models based on these three data sources are then closely integrated. This combination of data sources is new. On the one hand the study uses Danish information as an example for developing, validating and proving the value of this model; on the other hand, it allows for replicable research if data collected from other sites/countries are available.

2.2 Building and system description

In this study, heat pumps are assumed to be used for space heating to provide energy flexibility. The following principles were applied:

- Heat pumps can be controlled for flexible electricity usage only during the time period when occupants are away, i.e. when the home is unoccupied. This is the worst case scenario, i.e. the minimum amount of flexibility offered by a dwelling assuming that end users do not allow any disturbance of their energy supply when they are at home, so external control can only be applied when they are not at home.
- The occupancy pattern is considered at the household level.

The energy flexibility is thus defined as the adjustable range of heat pump power during the period the apartments are unoccupied. Due to the stochastic nature of occupancy in households, the energy flexibility in this study is a probabilistic distribution with uncertainties instead of a

determined number. The uncertainty of energy flexibility can be defined as the degree of dispersion of the distribution. Our hypothesis is “The stochasticity of occupancy declines with the scaling-up of a building cluster, as does the uncertainty of energy flexibility”.

2.3 Method and modelling tools

A data-driven approach was developed to model the energy flexibility of a building cluster, using MATLAB. The energy flexibility of a given building cluster is greatly influenced by the physical characteristics of the building and the occupancy pattern of individual households. A hybrid-model approach was used that consists of two parts: Thermal resistance and capacity (RC) models for the buildings with each building represented as one zone RC model, and occupancy models for buildings considering occupancy at the household level. The construction of the model is flexible, in that a building cluster can in principle be modeled with any mix of parameters such as the number of buildings, building types and construction year. Fig. 1 shows the model structure and simulation diagram. Four steps were used in modelling a single building:

- RC model of the building was developed based on the TABULA.
- Statistical data on dwelling size and Danish household size from the Statistics Denmark (2017) was then used to estimate the number of households of each size, i.e. one-person, two-person and three-person in the modelled building.
- Data from the Danish Time Use Survey (DTUS) 2008/09 was used to generate occupancy models of each size of household, which were then used to generate the occupancy model of the building according to the number of households of each size the building contains.
- The RC model and the occupancy model of the building were integrated, then simulation was started for this building.

For simulating a cluster of buildings, the four steps above were applied to all the buildings. After the simulation of each building, the decision to end or continue the simulation was, therefore, based on whether the building simulated was the last building in the cluster. If it was, then the simulation ends; if not, it continues with the next building. This is a generic approach that can be used to simulate any dwelling types and to aggregate of any number of dwellings. Each step is explained in more detail in the following section.

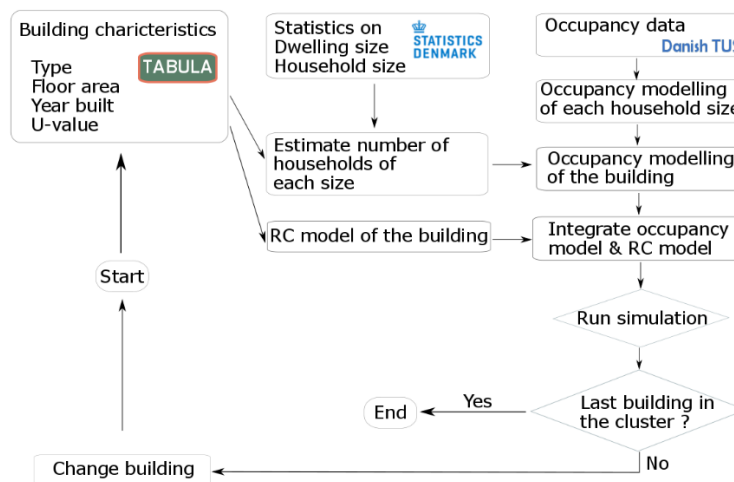


Figure 1 Flow diagram of quantification of building cluster energy flexibility using a data-driven approach

2.3.1 Occupancy modelling

Occupancy models were developed using occupancy data from DTUS 2008/09, which consists of 9640 individuals and 4679 households. Individuals' daily activities were logged in two diaries, one for a weekday and another for a weekend day with 10 min intervals starting at 4:00 and ending at 3:50 the next day.

Vacancy modelling for Danish households

To assign the above probability distribution of vacancy to Danish households, we used the data from Statistics Denmark (2017). Table 1 shows the numbers of households of different household size and different floor area in apartment buildings in Demark in 2017.

Table 1 Numbers of households of different household size and different apartment size in Danish apartment buildings.

Area(m2)	1 person	2 persons	3 persons
<50	124660	23316	3249
50-74	369649	125687	27181
75-99	266876	206708	73749
100-124	115590	173653	69038
125-149	64284	152127	54997
150-174	34275	103633	40123
>175	33985	110574	46796

Fig. 2 shows distributions of vacancy from three different sample sizes in the matrix *Probability distribution of vacancy_{aggregated}*.

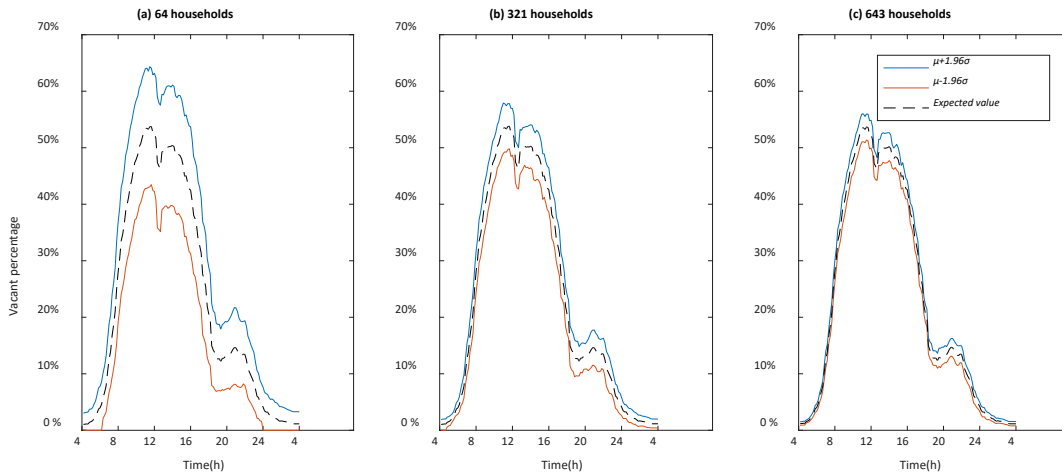


Figure 2 Vacancy profile of groups with different number of households. (a) 64 households, about 100 people; (b) 321 households, about 500 people; (c) 643 households, about 1000 people.

As shown in Fig. 2, the expected value of the vacant percentage does not change with the number of households. However, σ becomes smaller and smaller with more households aggregated. In

other words, the uncertainty of the vacant percentage decreases when the number of households becomes larger.

Vacancy duration estimation using a Kaplan-Meier estimator

The probabilities of vacancy duration for all three household sizes are shown in Fig. 3. It is the aggregation of results from all 144 points (10 minute values). The figure shows the probability that a dwelling is vacant at any observation states and onwards. For example, for one-person households, if a dwelling is unoccupied at 8:00 (see x-axis), the probability that it is still unoccupied after two hours (see y-axis) is around 80% (colour bar) and after six hours it is around 60%.

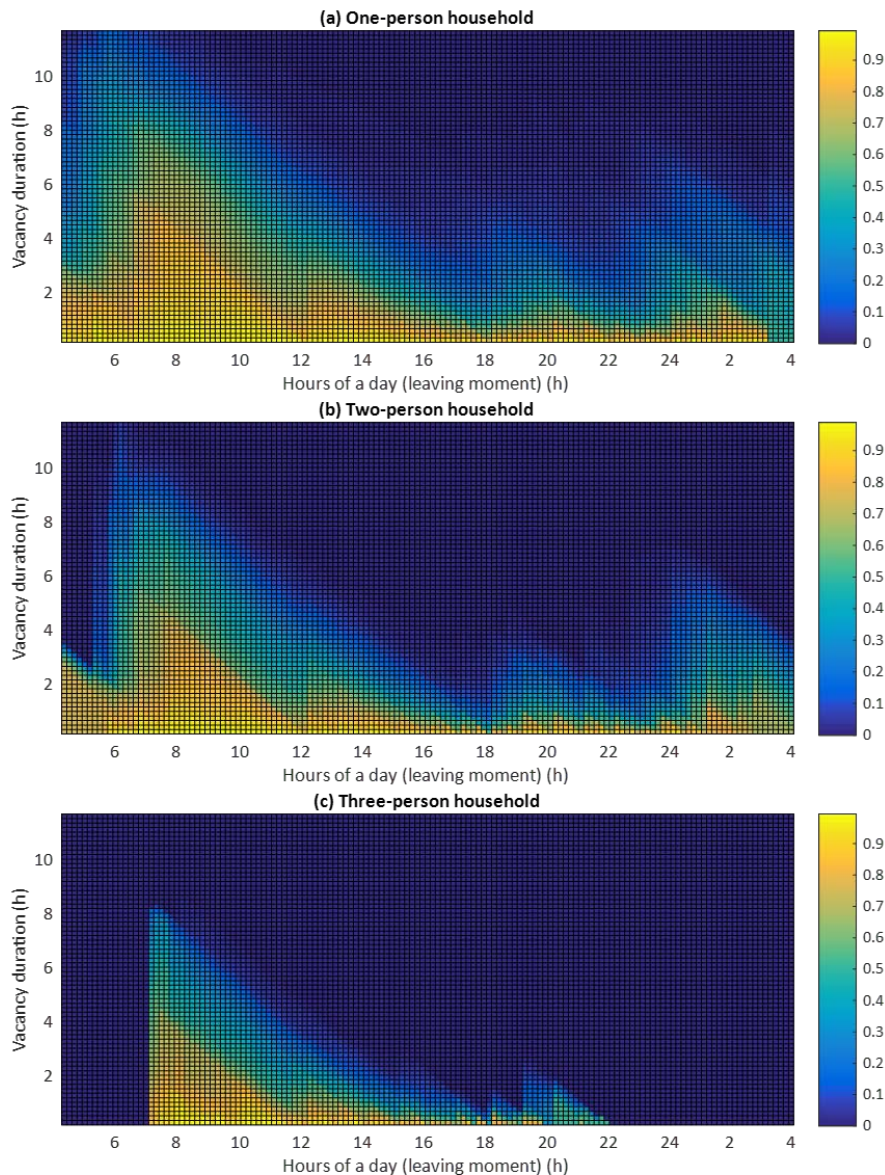


Figure 3 Survival analysis of vacancy for all 144 time points and three household sizes.

2.3.2 Building modelling

In this study, grey-box models were developed for building simulation. The grey-box model consists of a space heating system, a building RC model (a lumped parameter model) and building thermal parameters.

RC model

An RC model is a lumped parameter model, regarding a building as a whole for the purpose of simulation. There are three states used to describe the development of the indoor temperature. The first state T_i (°C) is indoor air temperature. The second state T_{om} (°C) is building envelope temperature as influenced by the building heat transfer with outside air. The last state T_{im} (°C) is the inner walls temperature that reflects the influence of the buildings' thermal inertia on the indoor temperature. Fig. 4 shows the structure of the model used in this study.

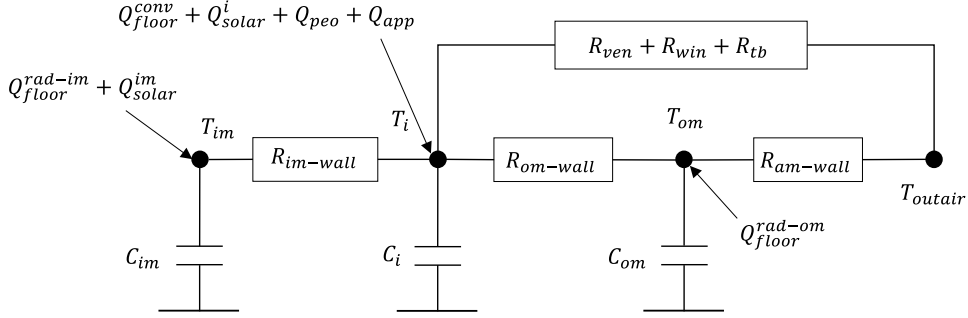


Figure 4 4R3C grey-box model structure.

T_i (°C) is the indoor air temperature, T_{om} (°C) is the building envelope temperature, T_{im} (°C) is the inner walls temperature, C_i (J/K) is the thermal capacity of the indoor air, C_{om} (J/K) is the thermal capacity of the building envelope, C_{im} (J/K) is the thermal capacity of the inner walls, Q_{floor}^{rad-im} (W) is the heat transfer through radiation between the floor and the inner walls, Q_{floor}^{rad-om} (W) is the heat transfer through radiation between the floor and the envelope, and Q_{floor}^{conv} (W) is the heat transfer through convection.

Building thermal parameters

Using the developed RC model and the space heating model, the building model was established. Based on the TABULA database, representative building types can be extracted for case study-based analysis. We chose only apartment blocks for the case study, as they have a large energy demand. Table 2 shows the U values of the building envelope of apartment blocks used in the case study.

Table 2 U values of building envelopes, data source: TABULA 2015.

Year of construction	Energy standard	U values (W/(m ² K))			
		Roof	Wall	Floor	Window
1961–1972	Existing state	0.33	0.51	0.99	2.7
	Usual Refurbishment	0.12	0.34	0.24	1.4
	Advanced Refurbishment	0.09	0.33	0.14	0.9
1979–1998	Existing state	0.19	0.34	0.19	2.7
	Usual Refurbishment	0.12	0.34	0.19	1.4
	Advanced Refurbishment	0.09	0.34	0.19	0.9
2011~	National minimum requirement	0.1	0.18	0.14	1.05
	Improved standard	0.1	0.16	0.1	0.8
	Ambitious standard/NZEB	0.08	0.16	0.08	0.8

2.3.3 Estimating number of households and generating occupancy model for the building

For each apartment block, the number of households of each size, i.e. one-person, two-person and three-person, were estimated according to Statistics Denmark 2017. The dwelling size of an apartment block in Denmark approximately follows the normal distribution shown in Equation (1).

$$DwellingSize_{apartment} \sim N(\mu, \sigma^2), \mu = 79, \sigma = 25 \quad (1)$$

For a one apartment building, a random dwelling size can be generated from the above normal distribution. Then, the number of households can be calculated by the following division formula.

$$N_{household} = \text{round}\left(\frac{\text{Floor Area}}{\text{Dwelling Size}}\right) \quad (2)$$

Next, the household size can be estimated according to the distributions of household sizes in different dwelling areas, as shown in Table 1.

Finally, an occupancy model of the building can be generated according to the estimation result of number of households of different sizes using the method in 2.3.1. In the timeline of one day, there are 144 time points with a 10-minute interval. For each point, the mathematical expectation, $\mu + 1.96\sigma$ and $\mu - 1.96\sigma$ of vacancy percentage was determined. In the simulation of this building, the occupancy model was then integrated with the building model.

2.3.4 Simulation of energy flexibility

The estimation of the energy flexibility potential of a building cluster was performed in three steps: (i) upward modulation in which heat pumps are turned on at max. power when buildings are unoccupied, (ii) downward modulation in which heat pumps are turned off when buildings are unoccupied, and (iii) subtract power of heat pumps under downward modulation from the power of heat pumps under upward modulation to obtain energy flexibility potential.

The uncertainty of the energy flexibility potential was quantified for building clusters with different scales, to be specific, different numbers of buildings and different numbers of households. This is because the uncertainty of occupancy varies when the number of households changes. The simulation was run for one day with typical winter weather conditions in Copenhagen.

2.4 Results

2.4.1 Energy flexibility potential of building clusters with different construction year

Fig. 5 is an example showing how the indoor air temperature varies under the extreme conditions that all households are vacant for six hours from 9:00 to 15:00. Heat pumps are switched on or off from 9:00 to 14:30 for energy flexibility, but back to normal operation 30 minutes before residents return, to ensure that the room temperature is within the comfort range when residents return.

2.4.2 Energy flexibility potential of building clusters with different construction year

The heat pump power curve of apartment blocks with three different construction years is shown in Fig. 6, where the gap between the red line and the blue line is the building energy flexibility potential. In Fig. 6, curves of the three building types indicate that, with a similar number of residents and number of households, the energy consumption by heat pumps in new buildings with better insulation is much less than it is in old buildings due to a much lower heat demand. However, old buildings with worse insulation have larger energy flexibility potential (Fig. 7). Fig. 7 shows the subtraction of the red curve and the blue curve in Fig. 6.

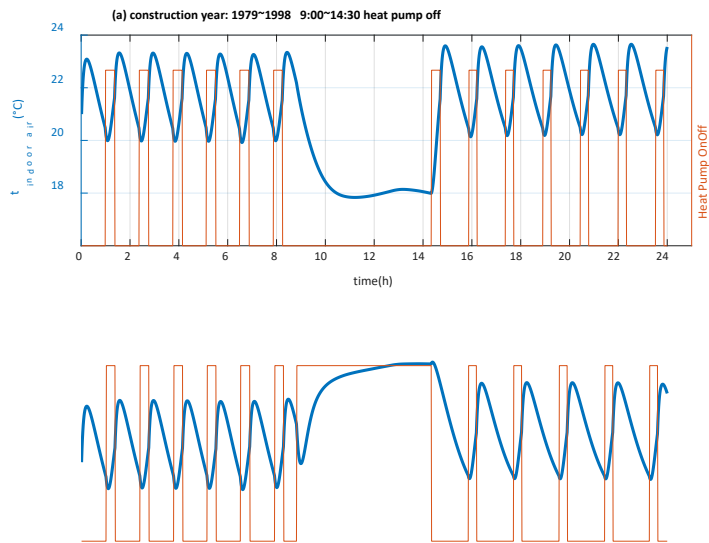


Figure 5 Indoor air temperature under different control modes.

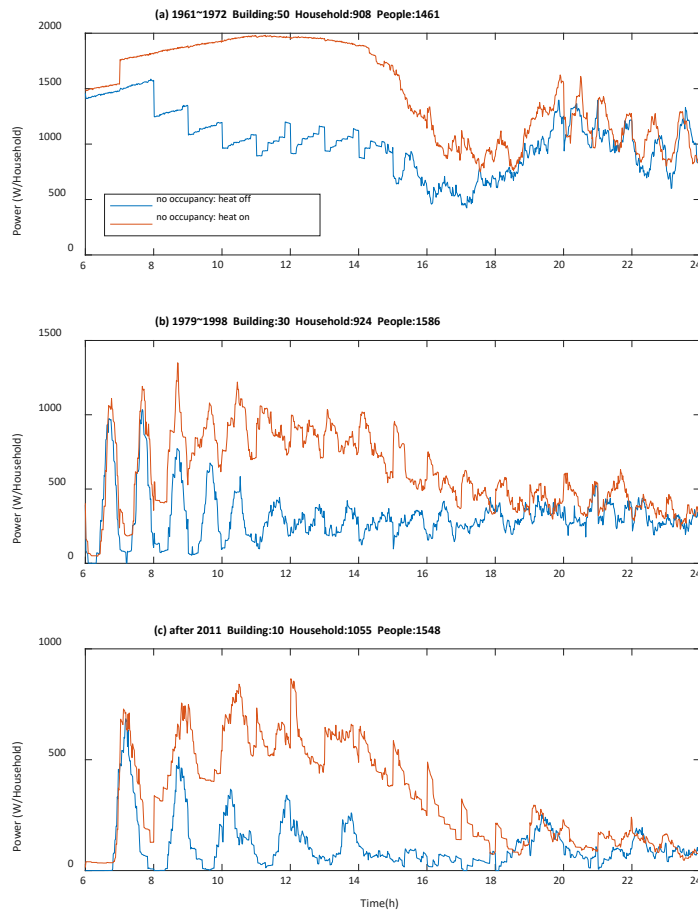


Figure 6 Heat pump power curve of building cluster with different construction year.

The red curve indicates the operation of heat pumps switched on during a vacancy period, while the blue curve indicates heat pumps switched off when the household is vacant.

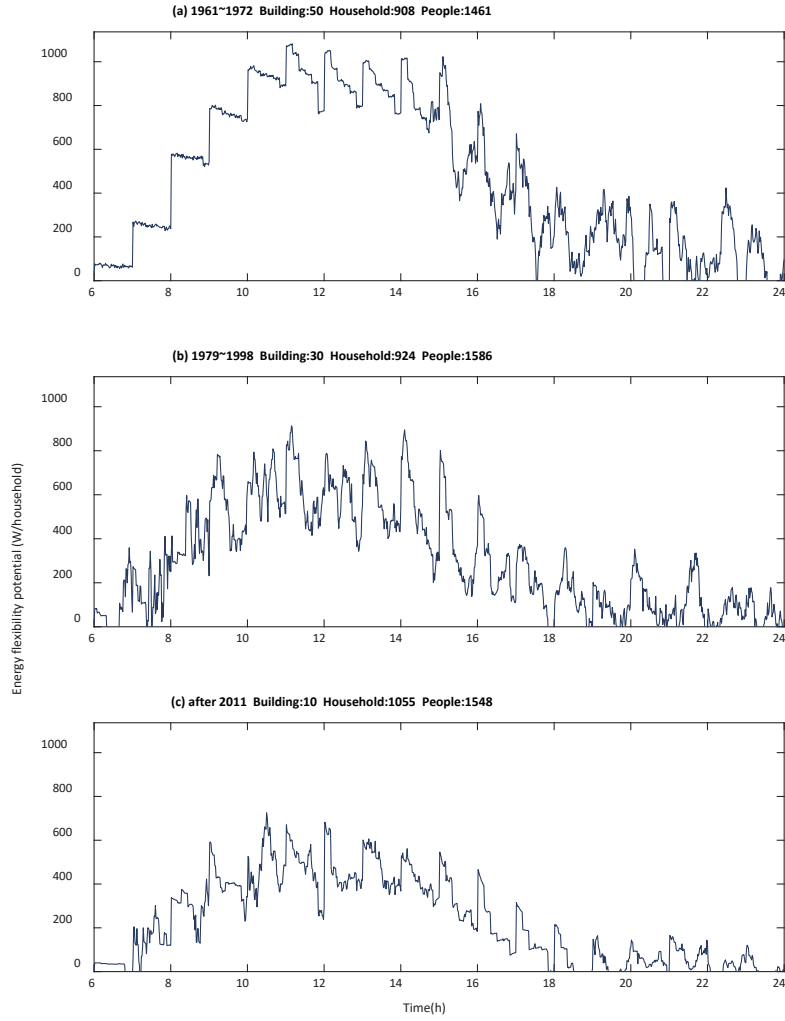


Figure 7 Energy flexibility potential of building cluster with different construction years

2.4.3 Uncertainty of energy flexibility potential of building clusters

For the occupancy model, with the scaling-up of number of residents and number of households, the mathematical expectation is almost invariable while $\mu + 1.96\sigma$ value and $\mu - 1.96\sigma$ value gradually converge to the mathematical expectation. On condition that heat pumps are switched on or off for energy flexibility according to occupancy patterns, the mean value of the energy flexibility potential is determined by the mathematical expectation while the uncertainty of the energy flexibility potential is determined by $\mu + 1.96\sigma$ value and $\mu - 1.96\sigma$ value. The uncertainty of the building energy flexibility potential is defined as follows:

$$Uncertainty = \frac{EF_{max} - EF_{min}}{EF_{mean}} \% \quad (3)$$

Where EF_{mean} is the mean value of the energy flexibility potential at any time, which is also the mean value of the adjustable range in Fig. 8. EF_{max} and EF_{min} are the maximum value and minimum value of the energy flexibility potential in Fig. 8.

In Fig. 8, it can be seen that the uncertainty declines with the scaling-up of a building cluster. When the number of households is more than 600 and the number of residents is larger than 1000, the uncertainty almost disappears, and the energy flexibility potential can be accurately estimated. The uncertainty is less than 10% when the number of households is around 700. In addition, a building cluster with 1102 households and 1767 residents has energy flexibility with less than 6% uncertainty.

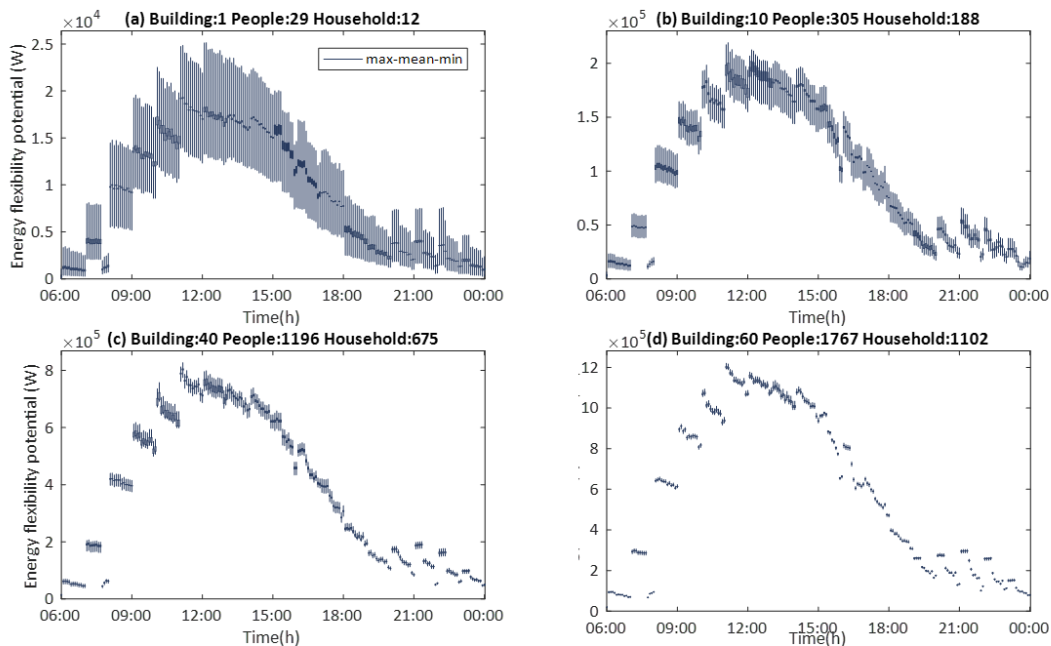


Figure 8 Energy flexibility and its uncertainty with scaling-up of apartment blocks.
Existing state, construction year: 1961~1972.

2.5. Conclusion

In this study, a generic energy flexibility model was developed in MATLAB for the simulation of any dwelling types and for the aggregation of any number of dwellings with high computing speed, usually only a few minutes. Heat pumps were controlled for flexible energy usage when occupants were absent. The heat pump power adjustable range was defined as the energy flexibility during each period. At times when the home was occupied, the indoor temperature was maintained within a comfortable range.

The uncertainty of the building energy flexibility potential caused by the stochasticity of occupancy patterns was evaluated. It was found that when the size of a building cluster was scaled up, the uncertainty became negligible. In other words, the uncertainty of the occupancy decreases when the aggregated number of residents increases. The uncertainty of energy flexibility was less than 10%, when about 700 households were aggregated. In comparison with new buildings with good thermal insulation, older buildings have higher energy flexibility potential. In addition, it was found that the older the building is, the higher the energy flexibility it has due to a higher energy demand.

This model can be a tool for simulating the building energy flexibility potential for district or even regional level energy planning when using the available flexibility to address various chal-

lenges caused by fluctuations in the power available from renewable energy sources. The methods developed are being considered for a number of practical applications, e.g. 1) to support the design of flexibility service products in electricity and heat markets; 2) to help building demand aggregators to create a building-based portfolio that has a statistically steady and predictable performance relation to flexibility control, operation, management and trading; and 3) to facilitate city planning and network planning by providing improved prediction of building clusters' energy profiles, since the original energy profiles are dramatically influenced by using the flexibility of buildings for different purposes.

2.6. References

EU, 2009. Directive 2009/28/EC of the European Parliament and of the Council of 23 April 2009 on the Promotion of the Use of Energy from Renewable Sources and Amending and Subsequently Repealing Directives 2001/77/EC and 2003/30/EC. <http://eur-europa.eu/eli/dir/2009/28/oj>.

Wittchen and Kragh 2012. SBi 2012:01 Danish building typologies-Participation in the TABULA project. Danish Building Research Institute, Aalborg University.

TABULA WebTool 2015. <http://webtool.building-typology.eu/#bm>.

EN/DS 15251. Indoor environmental input parameters for design and assessment of energy performance of buildings addressing indoor air quality, thermal environment, lighting and acoustics. Dansk Stand., p. 54, 2007.

2.7 Relevant publications

Further information of this study can be found: Andong Wang, Rongling Li and Shi You. Development of a data driven approach to explore the energy flexibility potential of building clusters. *Applied Energy*, 232: 89-100, 2018. <https://doi.org/10.1016/j.apenergy.2018.09.187>

More information of Danish Time Use Survey: V. Barthelmes, R. Li, R. K. Andersen, W. Bahnfleth, S. P. Corgnati, and C. Rode. Profiling Occupant Behaviour in Danish Dwellings using Time Use Survey. *Energy and Buildings*, 177: 329-340, 2018. <https://doi.org/10.1016/j.enbuild.2018.07.044>

3. Flexibility Analysis for smart grid demand response



Institution

United Technologies Research Centre Ireland Ltd.,
Ireland



&

National University of Ireland, Galway



Contact persons

Sarah O'Connell
s.oconnell19@nuigalway.ie

Dr. Marcus Keane
NUI Galway
marcus.keane@nuigalway.ie

3.1 Modelling objective

The aim of this study is to generate scenario models to define the flexibility ranges for contracts between buildings, aggregators and grid operators. Flexibility ranges are then visualised through scenario generation.

Contracts with aggregators, Transmission System Operators (TSOs) and Distribution System Operators (DSOs) are based on committing to a defined range of flexibility. For single source applications, for example, running a backup generator, flexibility is easily assessed, but for buildings or sites where multiple sources of flexibility are available, determining what can be offered becomes more complex. The building or site manager/operator needs to know the flexibility range, firstly to decide if participation is appropriate and if it is, to support them in selecting the most appropriate demand side management or flexibility program to participate in. Aggregators wish to minimize up front time and effort when assessing sites for aggregated portfolios. Having a fast, easily implementable and standardized modelling approach is an enabler for building and site managers, aggregators and grid operators.

3.2 Building and system description

The building that is modelled in this study is the Gateshead College Skills Academy for Sustainable Manufacturing and Innovation (SASMI). It is a 5,700 m² building consisting of classrooms, offices and workshops and located adjacent to the Nissan manufacturing site in Sunderland, UK. The peak power load of the building is approximately 140 kW and its base load at evenings and weekends is between 20 kW and 40 kW.

The systems that are modelled for flexibility in the SASMI building are Nissan Leaf second life Electric Vehicle (EV) batteries (Nissan are a partner in the ELSA project), a 50 kWp Photovoltaic (PV) array and Heating, Ventilation and Air Conditioning (HVAC) loads in the building. The 3 x 16 kWh second life EV batteries have a combined system capacity of 48 kWh. The first life capacity of the EV batteries, when they were newly installed in the Electric Vehicle, was 72 kWh. The HVAC loads in the building which have the capability to provide flexibility include variable speed fans in Air Handling Units (AHUs) and a Toshiba Carrier Variable Refrigerant Flow (VRF) heat pump system.

3.3 Method and modelling tools

Scenario modelling using flexibility characterization is the proposed method. The method developed transforms data into actionable information using flexibility characterization and a simple mathematical model. The flexibility characterization process is represented as a flowchart through which to navigate the avalanche of data available for buildings to select flexible systems early on, identify the key parameters of each system and avoid unproductive analysis of systems which are not relevant. The mathematical model uses the key parameters to calculate flexibility as a percentage of total load. The method is designed to be implemented by technical individuals who are not experts in energy or flexibility analysis, thereby overcoming the barrier to participation in demand response whereby flexibility is either underestimated by a cursory examination or a comprehensive evaluation by a domain expert is expensive and time consuming. The output of the modelling process is scenario generation, a means of visualizing the available flexibility against a standard daily load profile, detailed in section 1.4 Results.

To implement the flexibility characterisation, a flexibility audit, structured using elements of the energy audit standard ISO 50002:2014 is recommended. Activities such as data collection, site visit, analysis and reporting, based on a Type 2 audit, greatly assist in gathering the necessary

information to implement the model. A Type 2 energy audit is a detailed audit which is more rigorous than a walk-through assessment and includes a detailed analysis of energy systems in the building and operating conditions at the site. Opportunities for improvement are identified and there is a comparison with benchmarks. Using an audit structure reduces the specialized expertise needed to implement the characterisation while addressing the key objectives of the flexibility modelling. In addition, existing flexibility assessment methods including (Ma et al. 2013) (Alcazar-Ortega et al. 2015) (Siebert et al. 2015) were reviewed, identifying gaps which the method addresses.

The flexibility characterisation process is shown in Figure 9. Even for a small-medium sized commercial building there are 1,000s of specification documents and equipment data sheets, 100s of drawings and 1,000s sensors, equipment parameters and meters continuously generating hundreds of thousands of values every day. The objective of the flexibility characterisation process is the elimination of non-flexible systems and identification of key parameters for flexible storage, on-site generation and loads. These key parameters are then captured in a flexibility matrix. Starting with the load branch of the process, for a load to be flexible, it must be sheddable, controllable and acceptable. Sheddable means can a load be reduced or turned off, controllable means controlled by an automated system such as a Building Management System (BMS) and acceptable means is it acceptable to the building occupants, manager and or owner to reduce or turn off the load e.g. if it impacts the thermal comfort of occupants. If the answer to the question ‘is it sheddable, controllable AND acceptable’ is not ‘yes’ for all three, then the load is not flexible and the assessor moves on to the next load, storage or renewable generation. Renewable generation may not be controllable but it is possible to predict its output to reduce the net power import to the site and so it may be considered flexible.

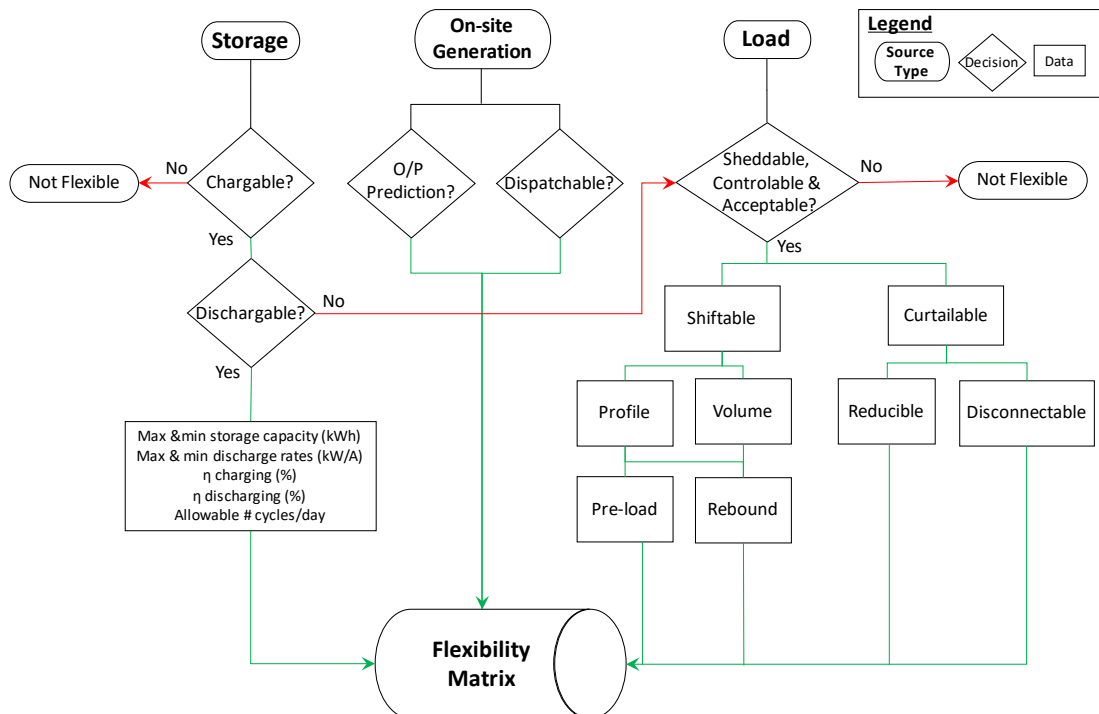


Figure 9 Flexibility Characterisation Process.

An example of the application of the flexibility characterisation process is shown in Figure 9. A Variable Refrigerant Flow (VRF) heat pump system is a type of HVAC load. It is possible to reduce the load over a short period; therefore it is Sheddable. These are typically controlled by a dedicated manufacturer's controller or a Building Management System (BMS) so it is Controllable. It must be determined if it is Acceptable, to the building operator to reduce the VRF power consumption by reducing or increasing temperature set points or by displacing electrical heating by gas fired systems. HVAC loads, including VRF are generally shiftable, but it may be partly curtailable. E.g. if thermal energy is reduced during a flexibility event, there is often a rebound effect afterwards where more energy is needed to restore the building to the temperature set point. However, if the duration of the event is short, it may be possible to curtail the load with minimal impact on indoor air temperature, depending on building thermal mass and air changes per hour, and thereby avoid rebound.

The parameters gathered through this process are then input into the flexibility matrix, and the process is repeated for other loads, storage and on-site generation sources on site. The parameters in the flexibility matrix may include flexible power [kW], duration of event [h], Time In Advance (TIA) notification [h], minimum time between events [h], pre-load (P, t) [kW, h], rebound (P, t) [kW, h], load availability [days, h], financial or other shed time [s/min] and time frame when requests are permitted. A two-dimensional representation of the flexibility matrix is captured using Flexibility System Parameter tables as shown in Figure 10.

The models are calculated as follows: the total flexibility at any given time interval, j , is the sum of all the individual sources i , which have flexibility in that time interval. Flexibility, f , is expressed in power (kW or MW).

$$f_{Total}(t_j) = \sum_{i=1}^n f_i(t_j) \quad (1)$$

To calculate flexibility as a percentage of peak load, F , the following formula is used:

$$F = \left(\frac{f_{Total}(t_j)}{P_{Peak}} \right) \cdot 100 \quad (2)$$

Where P_{peak} is the peak power load for the building in kW or MW and f_{Total} is as defined in equation (1). Human reasoning is required to evaluate the flexibility of each source for a specific timeframe from the flexible system parameters, a step which may be automated in future. The flexibility, F , for storage, generation and loads for specific time frames are then plotted as a percentage of peak power load against typical daily profiles for the building as shown in section 3.4 Results. This is performed both for individual energy systems and a combination of systems.

HVAC System – AHUs			
Type	Description	Value	Unit
Specifications	Ventilation (Supply Heating & Cooling)	AHU01, AHU 02, AHU 03, AHU 05	
	Fan Size	Supply and Extract fans in each AHU01	
			1.5 x 2 = 3 kW
			4.0 x 2 = 8 kW
			3 x 2 = 6 kW
			0.75 x 2 = 1.5 kW
Communications	BMS		
Control	Fan Speed	Set on commissioning but requested change to set point	%
Parameters	CO ₂	On AHU01 at present but requested for all	750 - 1,125 ppm
	Temperature	Return duct sensor set point	20 - 22 °C
	Duct Pressure	Fan speed control on AHU02 only	150 Pa
	Recirculation Damper	AHU01 only	%
	Recuperator Damper	AHU02, 03, 05	%
Flexibility	Max	Estimated 20%	1.4 kW
	Min	Estimated 10%	2.8 kW
	4 Hour Average	10-20%	kW
	Pre-load/Rebound	Not for ventilation, may occur on AHU01 on cooling	n/a
	TIA		10 - 15 min
	Load Availability	As per occupancy schedule	
	Min time between events	Provided max ppm of CO ₂ is met, no restriction on ventilation control, may be restriction due to interactions	TBD h

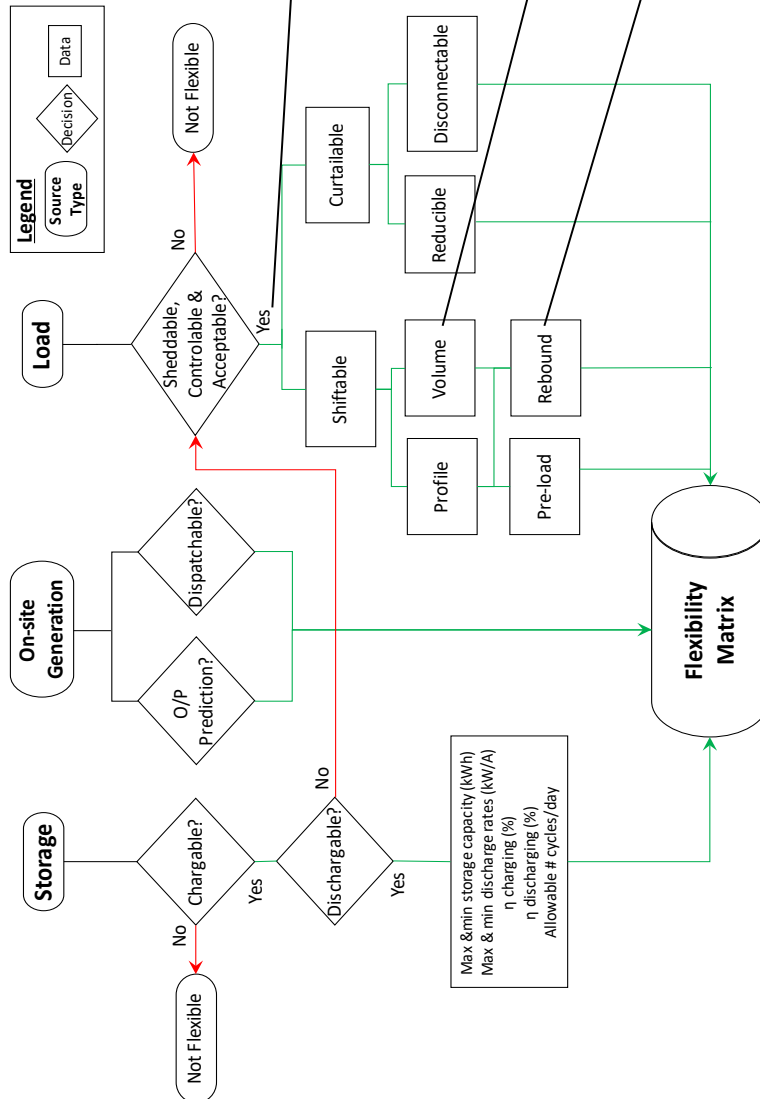


Figure 10 Populating a 2D representation of the Flexibility Matrix.

3.4 Results

The quantity, in power (kW) and duration (time) of flexibility available are visualized through scenario generation. Two sets of sample scenarios for flexibility are generated. The first is for a one-hour flexibility event, the second is a four-hour flexibility event. Flexibility is denoted as a percentage of total peak load. The scenarios are then validated by conducting one-hour and four-hour experiments in the SASMI building. The recorded data was analysed to compare it against the modelled scenarios.

The one-hour flexibility event scenario, shown in Figure 11, illustrates the percentage of total load which the storage, on-site generation and loads have the capability to provide in response to a request for services from an aggregator or grid. If only the battery system was used, it could provide up to 26% flexibility as a percentage of the building peak load. PV combined with a HVAC reduction in summer gives flexibility of 19%. The HVAC reduction consists of decreasing the load on the Variable Refrigerant Flow (VRF) heat pump system and curtailing Air Handling Unit (AHU) fan speed. Combining both of these scenarios gives a total modelled flexibility of 45%.

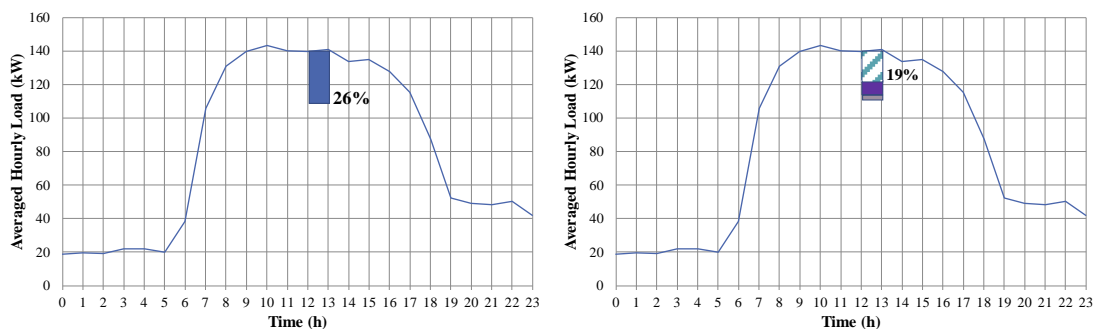


Figure 11 Scenario Generation for 1 Hour event showing Battery system only on left and PV (hatched) with HVAC reduction on right: VRF (purple) and AHU fans (grey).

The four-hour flexibility event scenario, shown in Figure 12 illustrates the flexibility that may be achieved using the same sources over a longer time frame. The battery system can achieve 8% flexibility by itself. On the right hand side of the figure, HVAC load reduction can achieve 8% while adding PV generation results in a total flexibility of up to 20% in summer.

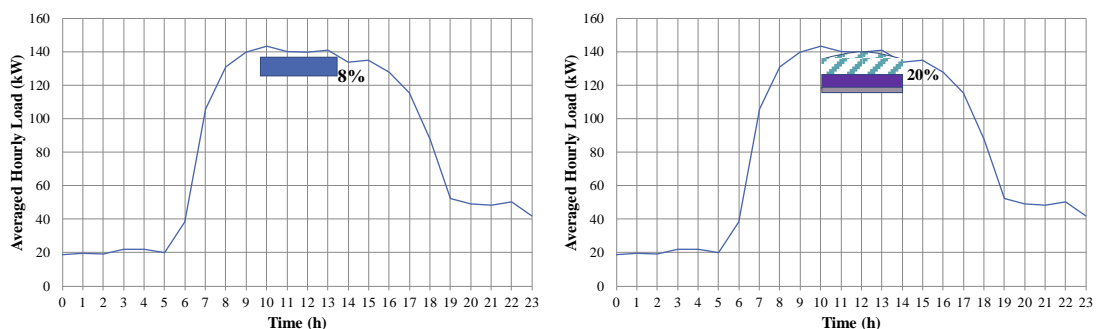


Figure 12 Scenario Generation for 4 Hour event showing Battery system only on left and PV (hatched with HVAC reduction on right: VRF (purple) and AHU fans (grey).

Analysis: In the one-hour scenario, the contribution of the battery is most significant. However, for the four-hour scenario, the contribution of the battery is limited by its capacity (kWh) and as this is spread over a four-hour period, the amount of flexibility it can provide is much reduced. In contrast, for the four hour event, the contribution of HVAC systems is much more significant than in the one hour event as they double the flexibility available from 8% (battery only) to 16% (battery & HVAC).

In summary, the results demonstrated:

- the capacity and maximum discharge rate of the battery system had a significant impact on the available flexibility, particularly for the one hour scenario;
- during longer events, such as the four-hour scenario, load sources such as HVAC become much more significant, with a flexibility range more than double that of the battery system.

Validation of the results was conducted at the SASMI building for both the one hour and four-hour scenarios. The validation profiles are strongly influenced by volatility in the PV output causing significant fluctuation in the overall load profile. This creates noise in the recorded data, requiring analysis to extract the actual flexibility achieved.

Validation of the one-hour scenario is shown in Figure 13. The PV and HVAC systems gave a flexibility of 18 % of peak power load as shown in Figure 13. This was very close to the modelled flexibility of 19 %. A slight drop in PV output was compensated by larger than predicted HVAC load reductions. The AHU fan flexibility gave a steady load reduction whereas the VRF system was more volatile. Overall, intermittency in PV output created significant variations in the overall load profile for power imported from the grid (P_Main_kW).

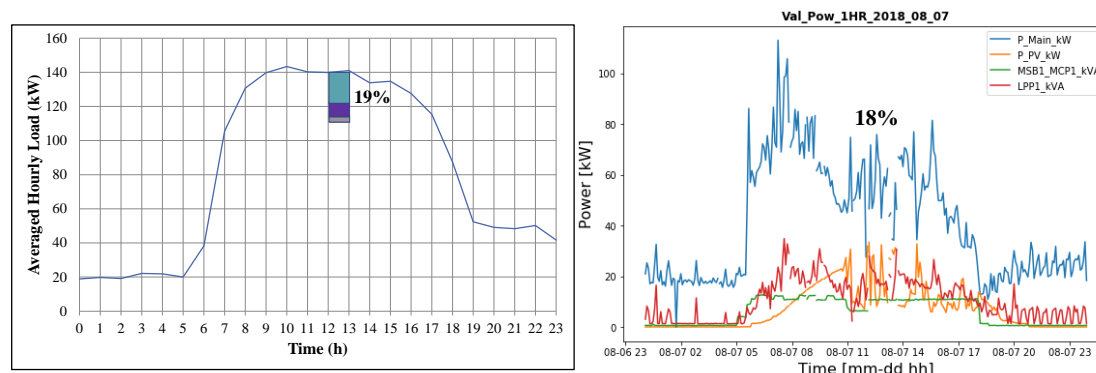


Figure 13 Validation of one-hour scenario for PV and HVAC. Modelled flexibility is shown on the left and validation results are shown on the right.

The battery system provided a flexibility of 17% of peak load as shown in Figure 14. This was lower than the modelled flexibility of 26 %. The reason for this is the 2nd life battery system installed in the SASMI building is an early prototype at technology readiness level (TRL) 5/6, and of the three 2nd life EV battery modules in the system, only two were operational at any given time. The individual maximum discharge rate for each EV battery is 12 kW, giving a total maximum discharge rate of 24 kW which is equivalent to 17 % of the building peak load of 140

kW. If the predicted flexibility was reset to the actual available capacity, the achieved flexibility would be equal to the modelled flexibility.

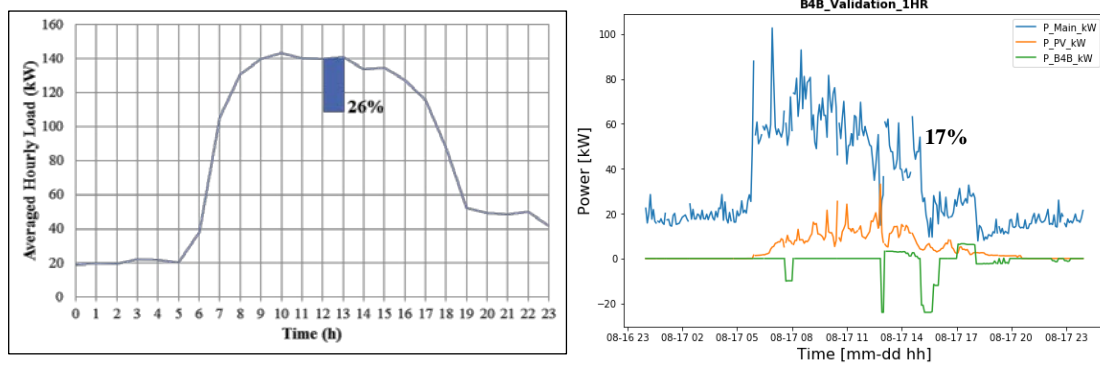


Figure 14 Validation of one-hour scenario with Battery system only. Modelled flexibility is shown on the left and validated results are shown on the right.

A summary of the validated results is shown in the tables below.

Table 3 Summary showing Modelled and Validated Flexibility Results for 1 Hour Scenario Model.

1 Hour Scenario	HVAC & PV	Battery	Total
Modeled Flexibility	19 %	26 %	45 %
Validated Flexibility	18 %	17 %	35 %

Table 4 Summary showing Modelled and Validated Flexibility Results for 4 Hour Scenario Model.

4 Hour Scenario	HVAC & PV	Battery	Total
Modeled Flexibility	20 %	8 %	28 %
Validated Flexibility	12 %	5 %	17 %

Validation of the four-hour scenario for PV and HVAC loads gave a flexibility 12.5 %, shown in Table 4, lower than the modelled value of 20%. The reason for this was a significant drop in PV output during the flexibility event. For the battery system only, validation of the four-hour scenario resulted in almost half the predicted flexibility. The scenario gave an 8% flexibility whereas during the validation, the battery system only achieved 5%. The reason for this is the reduced battery system capacity due to only two of the three EV batteries being in operation at the time of validation.

Modelling of predicted PV output is challenging as it is highly dependent on extremely localised weather conditions e.g. a cloud passing the PV panel. This raises questions around PV volatility & its reliability as a source of flexibility. In addition, it supports the case for electrical storage to implement PV power smoothing to avoid intermittent demand creating issues on the grid side.

However, if the battery storage system is engaged in PV power smoothing, it may not be available for flexibility events such as demand response.

Accurate modelling of battery systems requires reliable system specification which is challenging when dealing with a prototype battery management system at TRL 5/6. A mature technology at TRL 9 will give certainty around the available flexibility of second life battery systems for modelling and system operation.

Benchmarking: To understand how much flexibility is typical for a building of this type with similar systems providing flexibility, benchmarking is required. Standardized benchmarks, similar to CIBSE TM46 for energy consumption in buildings, have not yet been developed for flexibility in buildings. To benchmark the results, a number of other demonstration projects were reviewed (Picault et al. 2015) (Piette et al. 2006) (Grid4EU 2016) (Siebert et al. 2015). Of these, the two most relevant for the building in this example were chosen. Benchmark 1 is a Californian study in the US which measured HVAC load reduction in 28 buildings participating in a utility demand response program (Piette et al. 2006). The study was chosen as the sample size is significant and the HVAC systems were used in this example. Benchmark 2 is a demonstration project involved 8 pilot sites, battery storage and a PV array in France (Siebert et al. 2015). The pilot sites each provided a single load, heating in buildings or pumps in industrial sites. The PV and storage elements were similar to the example site presented here but were managed centrally by an aggregator, instead of the building managing its own renewable generation and storage. As before, flexibility is denoted as a percentage of total peak load.

Table 5 Benchmark Comparison for Example Building

Benchmark 1 [CA, USA; 28 Buildings] (Piette et al. 2006)	Benchmark 2 [FR; Battery, PV & Loads] (Siebert et al. 2015)	Validated Flexibility (%)	Duration (h/min)
Average 7 – 9 %	Min ~7 %	4 % - 12.5 %	4 h
Max 28 - 56 %	Max ~ 18 %	35 %	1 h

The flexibility modelled and validated for the Example building, SASMI, is within the range of Benchmark 1 and above Benchmark 2 as shown in Table 5. This means that the flexibility the Example building can provide is typical or slightly better than a building of this type with similar systems used for flexibility (HVAC, PV & Battery).

3.5 Conclusions

A standardized scenario modelling approach for early stage flexibility assessment in buildings was developed and validated. It is an enabler for building and site managers, aggregators and grid operators to effectively navigate through the 1,000s of specification documents and equipment data sheets, 100s of drawings and 1,000s of data points to generate scenario models which predict the available flexibility in the building. The scenario modelling proved to be accurate for mature technologies such as the HVAC systems but high frequency variations in PV output and some technical issues with the prototype battery system resulted in the total validated flexibility differing from the modelled flexibility.

Future work in the development of standardized benchmarks for a range of building types e.g. apartments, hospitals, offices etc. would be a welcome development.

3.6 Acknowledgements

This work was done as part of the project Energy Local Storage Advanced system (ELSA) which receives funding from the European Union's Horizon 2020 research and innovation programme under grant agreement No. 646125. <https://elsa-h2020.eu/>

3.7 References

Alcázar-Ortega, M., C. Calpe, T. Theisen, J. Rodríguez-García. "Certification prerequisites for activities related to the trading of demand response resources." *Energy* vol. 93, Part 1, pp. 705-715. December 2015a.

Alcázar-Ortega, M. C. Calpe, T. Theisen, J. Rodríguez-García. "Methodology for the identification, evaluation and prioritization of market handicaps which prevent the implementation of Demand Response: Application to European electricity markets." *Energy Policy* 86: 529-543, November 2015b.

Grid4EU. Spotlight on clients' peak shaving flexibilities in the Demo6. Published on <http://www.grid4eu.eu/results/grid4eu-technical-spotlights.aspx>, April 2016.

ISO 50002: 2014 "Energy audits - Requirements with guidance for use." International Organization for Standardization, Switzerland, July 2014.

Ma, O., et al. "Demand Response for Ancillary Services." *IEEE Transactions on Smart Grid* vol. 4, pp. 1988 – 1995, Dec 2013.

Piette, M.A., D. Watson, N. Motegi, S. Kiliccote, and E. Linkugel. "Automated Demand Response Strategies and Commissioning Commercial Building Controls." National Conference on Building Commissioning. April 2006.

Picault, D., O. Cottet, and T Ruez,. "Demand response: A solution to manage loads in the smart grid." 2015 IEEE 15th International Conference on Environment and Electrical Engineering (EEEIC), June 2015.

Siebert, N. et al. "Scheduling demand response and Smart Battery flexibility in a market environment: Results from the Reflexe demonstrator project." PowerTech, 2015 IEEE Eindhoven, July 2015.

3.8 Abbreviations

AHU Air Handling Unit

BMS Building Management System

EV Electric Vehicle

HVAC Heating, Ventilation & Air Conditioning

SASMI Skills Academy for Sustainable Manufacturing and Innovation, Gateshead College, UK.

VRF Variable Refrigerant Flow

Time In Advance (TIA)

3.9 Relevant publications

O'Connell, S. and Riverso, S. 'Flexibility Analysis for Smart Grid Demand Response', arXiv:1704.01308 [cs.SY], April 2017, United Technologies Research Centre Ireland, Cork, ROI. Available at <https://arxiv.org/>

4. Investigating the energy flexibility of typical Canadian homes: the potential of building thermal mass and photovoltaic system with battery



Institution

Department of Mechanical Engineering,
Polytechnique Montreal



**POLYTECHNIQUE
MONTREAL**

LE GÉNIE
EN PREMIÈRE CLASSE

Contact persons

Kun Zhang
kun.zhang@polymtl.ca

Behzad B. Bafrouei
behzad.barzegar-bafrouei@polymtl.ca

Prof. Michaël Kummert
Michael.kummert@polymtl.ca

4.1 Objective

This section aims at investigating the energy flexibility of typical Canadian homes. The energy flexibility potential is studied separately for passive thermal storage i.e., the building thermal mass and photovoltaic solar system with or without battery.

4.2 Building and system description

The selected residential building for the present study are the twin houses at Canadian Centre for Housing Technology (CCHT), which were built in 1998 according to the Canadian R-2000 building standard [1]. They represent the common three-story single-family homes with a basement, the first floor (living zone) and the second floor (sleeping zone). The construction are typically North-American with wood frame structure and brick veneer as exterior finish. The thermal mass is relatively low compared to European heavy-weight houses. The time constant for a response to heating power is in the order of 18 h. A brief summary of the CCHT houses are presented in Table 6 [2].

Table 6 Brief summary of CCHT houses.

Feature	Details
Livable area	210 m ² (2 stories)
Insulation	Attic: R=8.6 m ² K/W; Walls: R=3.5 m ² K/W; Rim joists: R=3.5 m ² K/W
Basement	Poured concrete, full basement Floor: concrete slab, no insulation Walls: R=3.5 m ² K/W in a framed wall
Windows	Low-e coated, argon filled windows Area: 35 m ² total, 16.2 m ² south facing
Airtightness	1.5 h ⁻¹ @ 50 Pa

The heating system investigated in this work is an electric resistance heating system, commonly seen in the Canadian province of Quebec. The PV panels and battery bank is sized according to the available south-facing roof area and on an autonomy of 1½ day. The PV array nominal power is 16.1 kW (three 270 W panels are wired in series at each string) and the storage capacity of the battery bank is 61.2 kWh (48 V-1275 Ah). Twenty-four sealed advanced glass mat (AGM) lead acid battery modules, type Rolls (model S2-1275), 2V 1275Ah, are connected in series.

4.3 Method and modelling tools

4.3.1 Models

A detailed building model is implemented in TRNSYS [3], which is calibrated using measured data. The CWEC weather file for Montreal, Canada is used in the study.

To investigate the general energy flexibility of buildings, it is assumed that the demand response (DR) event can occur at any hour of the year. To assure that each DR event is independent, one

simulation corresponds to only one event. Matlab was used to run the simulation in batches for different DR events in different scenarios. Note that for the building thermal mass case, only the heating season is simulated starting from October 15th to April 29th (altogether 196 days); in other words, the DR event happens at 4704 different hours (196×24 hr.). For the PV system, the DR event happens for all 8760 hours.

Building thermal mass

The electric baseboard heating system was modeled using the idealized heating in TRNBuild; therefore, the setpoint control was also idealized in the simulation. Simple setpoint temperature modulation is investigated. The setpoint control scenario during the DR event is [4]:

- Decreasing the reference setpoint by 2 °C for the downward flexibility;
- Increasing the reference setpoint by 2 °C for the upward flexibility.

The reference setpoint case represents a typical setpoint profile as shown in Table 7.

Table 7 Reference setpoint scenario

Zone	Reference setpoint	DR event
First floor	21 °C	2 °C change
Second floor	21 °C	2 °C change
Basement	17 °C	Not adjusted

PV system with battery

The detailed grid-tied solar system is modeled in TRNSYS, which is composed of PV panels, charge controller, inverter and battery bank. The solar system is coupled with the detailed building model with the all-electric HVAC system and water heater.

Two rule-based control methods are investigated in the study, which represent two extreme operation modes typically available in commercial grid-tied inverters: grid-support mode (PV priority) and Uninterrupted power system (UPS) mode.

In the grid-support mode, the system supplies the required load by prioritizing the electricity generation sources in the following order: 1st. PV panels, 2nd. Battery and 3rd Grid. This reduces the dependency on the grid, but it will not necessarily minimize the electricity bill since discharging the battery during off or mid peak hours is not always economically beneficial.

In the UPS mode the primary task is to keep the battery fully charged in order to back up the grid for supplying the load over interruption or instability. Utilizing this mode of operation let the households have access to the electricity over blackout as well as supporting the sensitive AC loads. In this mode, since the battery bank is always fully charged, the surplus electricity is either dumped or exported to the grid. Therefore, the system is unable to store the extra-generated electricity during the day to meet the load in absence of solar energy. It is interesting to note that, since the battery is not used under normal operation, this references scenario is very close to what a PV system without battery would provide.

4.3.2 KPIs

To quantify the energy flexibility, we introduce the four indices below in the present study. Figure 15 presents a conceptual energy flexibility of buildings with a downward flexibility event happening from 8 am to 10 am.

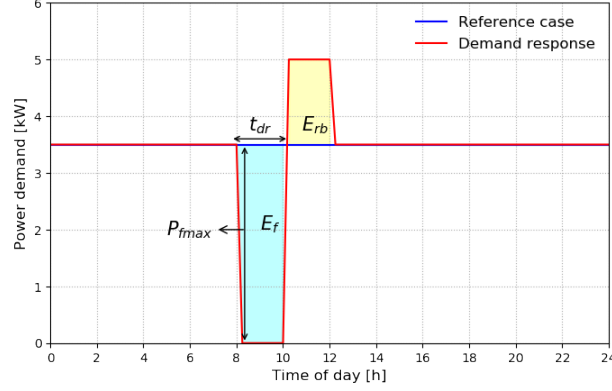


Figure 15 Flexible energy demand of buildings (downward flexibility) with E_f : flexible energy; E_{rb} : rebound energy; P_{fmax} : maximum flexible power; t_{dr} : duration of demand response event.

Flexible energy E_f

The flexible energy quantifies the amount of energy that has been shifted compared with the reference scenario, either downward or upward. It indicates the decreased or increased energy usage during the DR event. The cyan shaded area shown in Figure 15 indicates the downward flexible energy amount during a DR event.

$$\mathbf{E}_f = \int_0^{t_{dr}} (P_{dr} - P_{ref}) dt \quad (1)$$

Note that P_{dr} and P_{ref} in the equation are electric power, unlike the terms shown in Table 6 are thermal. This index also shows the amount of shifted power in average during the DR duration (the average shifted power equals E_f divided by the time of DR duration t_{dr}).

Rebound energy E_{rb}

After the DR event, there is a high possibility in an energy rebound, positively or negatively. If energy have been saved during the peak (the case of downward flexibility), it is immediately seen that the power demand go up after the peak. Similarly, if energy instead have been increase during the demand valley (upward flexibility), the energy need may ramp down after the event because the thermal mass have stored part of the excessive energy. The rebound energy E_{rb} is used to denote this amount of energy rebounded after the DR event (as shown by the yellow shaded area in Figure 15).

$$\mathbf{E}_{rb} = \int_{t_{dr}}^{t_{\infty}} (P_{dr} - P_{ref}) dt \quad (2)$$

Note that the upper bound for the integration in Equation (2) is infinite, but 48 hours are here used in the calculation. In all simulation results, we have confirmed that no rebound effect lasts longer than this horizon; therefore, 48 hours is effectively infinite for the study; it may however be different for other situations.

Flexible energy efficiency η

The DR action does not necessarily save energy consumption for the electricity users. The flexible energy efficiency is introduced to quantify the energy consumption change. Similarly, a cost efficiency could also be introduced to take into account the price change, for instance time-of-use or dynamic electricity price; however, this study intends to be general and not to address the price signals.

$$\eta = \left| \frac{E_f}{E_{rb}} \right| \times 100\% \quad (3)$$

Maximum flexible power P_{fmax}

This indicator is helpful to identify the maximum potential of a power change during a DR event against the reference case. Eq. (4) is separated into the downward and upward cases instead of using absolute values to take into consideration that the rebound phenomenon may occur during the DR event.

$$P_{fmax} = \begin{cases} \max_{t_{dr}} (P_{ref} - P_{dr}) & \text{downward} \\ \max_{t_{dr}} (P_{dr} - P_{ref}) & \text{upward} \end{cases} \quad (4)$$

Two additional yearly KPIs are applied to the PV systems: self-generation and self-consumption. The self-generation (or load cover factor) estimates the share of the demand met by on-site generation through various generator types (e.g. PV panels) [5].

$$\mathbf{Self - generation} = \frac{\int_0^T \min[g(t) - S(t) - \zeta(t), l(t)] dt}{\int_0^T l(t) dt} \quad (5)$$

Whereby the $g(t)$ is the solar panels power at time t and $S(t)$ represent the battery power balance. $\zeta(t)$ is corresponding to the losses and $l(t)$ indicates the load power.

The self-consumption (or supply cover factor) displays the proportion of on-site generation which is utilised by the end-user. In fact, this indicator quantifies the system potential to store and use the surplus generation.

$$\mathbf{Self - consumption} = \frac{\int_0^T \min[g(t) - S(t) - \zeta(t), l(t)] dt}{\int_0^T g(t) dt} \quad (6)$$

4.4 Results

4.4.1 Building thermal mass

Figure 16 presents the downward flexible energy for 2-h DR events happening every hour during the whole heating season (note the negative values in the y axis). Each independent DR event lasts for 2 hours with 2 °C modulation of the set point temperatures for the first and second floor. Each data point in the figure represents one simulation result, and all the data points were sorted out by the hour of day as well as their correspondent months. The transparent boxes are the same as in boxplots with the top edge indicating the 75th percentiles and the bottom edge indicating the 25th percentiles.

The blue curve in the middle shows the median value of the flexible energy. It can be observed that the amount of energy which can be shifted is highly correlated to the hour of day. During the night time, the shifted energy is much more significant than during daytime with maximum value three times of the minimum. This is because the building generally experiences higher

ambient temperatures during the day and can have solar gains as well. This daily cycle of temperature results in lower energy demand in the reference case and therefore reduced DR potential.

The colors of data points indicate the months. Among the 7 months investigated, it is clear to see that the coldest months (January and December) have higher flexibility than the shoulder months (like March, April and October). The small values of flexible energy that are spread out in the top part of the figure are mainly during the three shoulder months. This seasonal trend is the same as explained for the daily phenomenon in that the reference case has lower energy demand, therefore the DR has also lower potential to shift the energy demand.

Figure 17 shows the upward energy flexibility in a same format as shown in Figure 16. A similar daily and seasonal trend for the upward flexibility is found due to the same reasons discussed above. The spread of values shows a strong daily variation, but the median upward flexible energy is approximately constant (and close to the available heating capacity). This shows that the thermal mass capacity of the studied building is large enough to store the heating energy provided during the 2-h DR event.

The maximum power shift shows the same trends as the flexible energy for both cases. Based on the discussion above, it can be concluded that the potential of buildings to shift heating power demand is higher during colder weather. This is beneficial for the utility, which experiences a higher demand during these periods. The ability to use more power by buildings is also higher in colder weather but the weather impact on the median values is not as significant. The building can still have the potential to use more energy when the grid would experience a significant solar power input during the day.

Figure 18 presents the downward flexible efficiency. A nearly constant median efficiency around 1.2 is found. This means that the rebound energy is almost always 20% less than the saved energy (the several zero points represent cases when both the flexible energy and rebound energy are 0). The upward flexible efficiency shows similar results as the downward one as shown in Figure 5. This confirms that the DR strategy in this study is energy efficient – i.e. save energy.

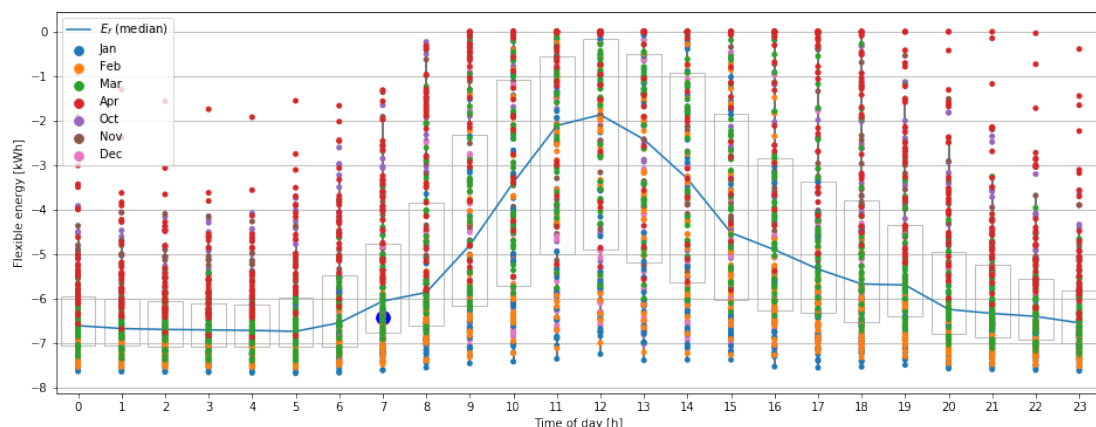


Figure 16 Downward flexible energy of the heating season.

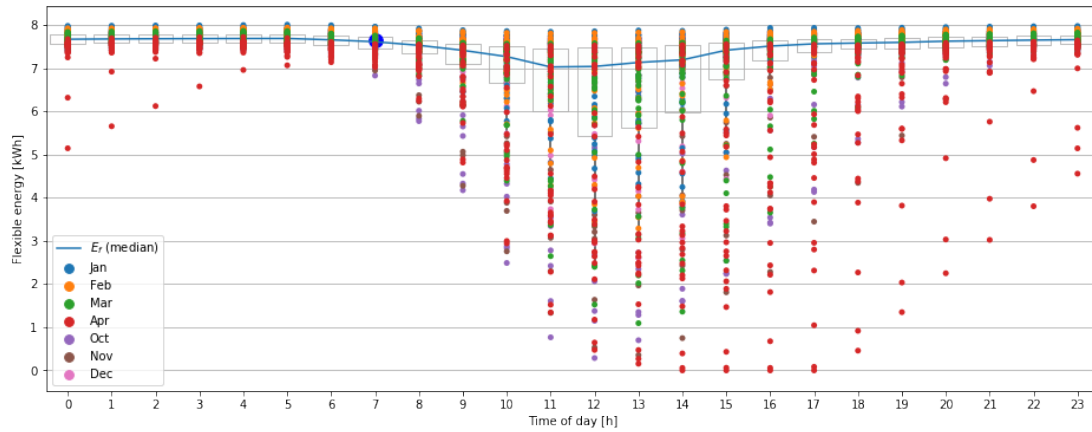


Figure 17 Upward flexible energy of the heating season

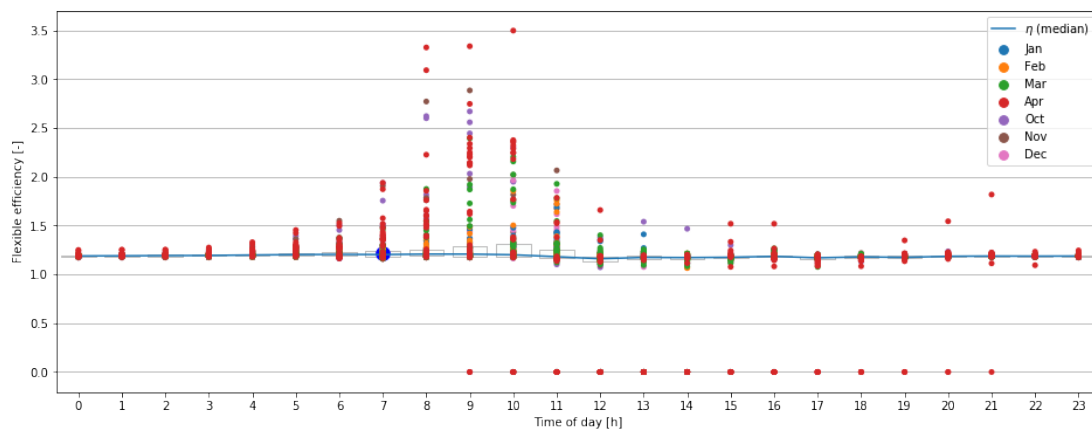


Figure 18 Downward flexible efficiency of the heating season.

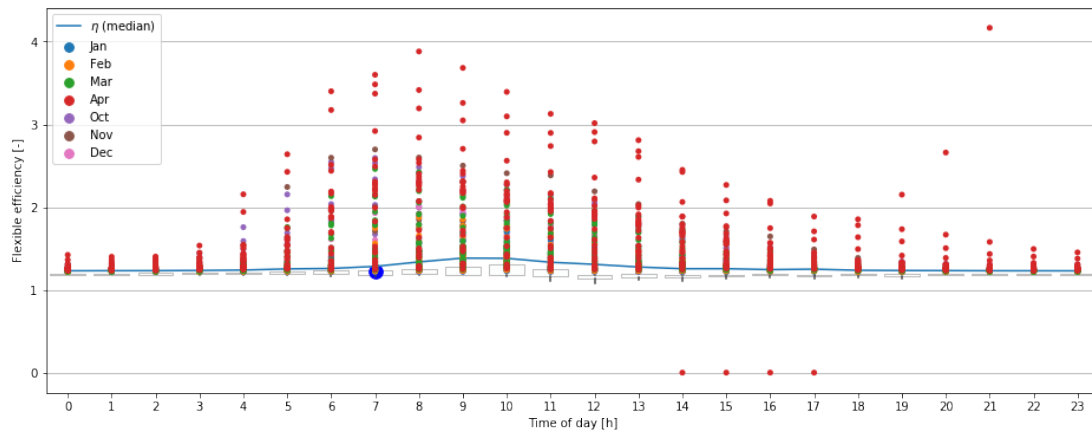


Figure 19 Upward flexible efficiency of the heating season.

4.4.2 PV system with battery

Figure 20 shows the self-generation for a whole year for three different load profiles associated with low, average and high electricity consumption patterns. The results are related to the “grid-support” mode of operation where the battery stores the surplus generation to supply the load over peak hours.

Points with a zero value on the x-axis represent conventional grid-tied photovoltaic systems without batteries. As mentioned above, the performance obtained is the same as a HPVS running in UPS mode, as in that case the battery is maintained fully charged under normal operation and not used to compensate for the solar generation variations.

Adding a battery to a PV system allows to almost double the self-generation and more than double the self-consumption, and there appears to be a saturation of the battery benefits above a value of 4 kWh/kWp for the selected load profiles.

Figure 20 shows that the installed PV capacity has a large impact on self-generation, which was expected. A more surprising result is that self-generation is also strongly affected by the total electrical load, with higher loads corresponding to higher self-generation. For the same HPVS configuration, the solar fraction (the potential share of on-site generation to cover the load) will decrease if the building load increases, but in all cases (with the selected assumptions and configurations) the self-generation will increase. This KPI does not “credit” the system for any exported energy, and increasing the building load will shift some of that exported energy towards directly used energy and, therefore, improving the self-generation.

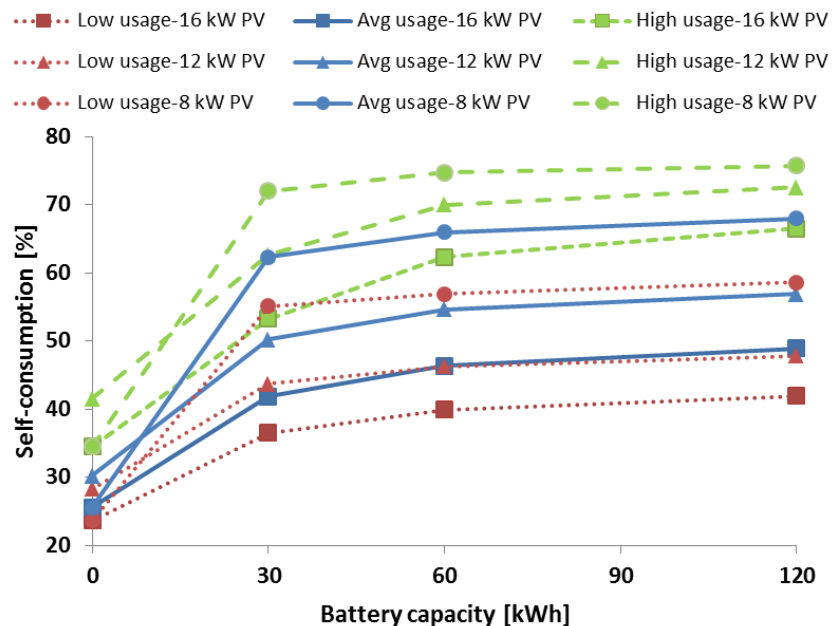


Figure 20 Self-generation vs battery capacity.

Figure 21 shows the results obtained for self-consumption. There is a direct relationship between the amount of exported (or dumped) energy and self-consumption, so adding a battery has a large impact on that KPI. The saturation effect observed for self-generation is even more present, showing that the sizing of HPVS systems will have a large impact on their energy flexibility, without necessarily requiring much larger investment costs than conventional (battery-less) PV systems.

A possible explanation for the relatively quick saturation of the two KPIs with increasing battery sizes is that the system performance is largely influenced by two extreme periods. In winter, an all-electric building load will be very high due to space heating, and solar generation will be low. So, the need for storage is relatively small, only representing a few extremely sunny days. In summer, on the other hand, the building load will typically be much lower, and the solar

generation will be much higher. Adding a relatively small battery capacity allows dealing with the winter period, but not with the summer period. And the results seem to show that the investigated battery sizes (up to 15 kWh/kWp) do not result in significant improvements over much lower battery sizes – improving the self-consumption significantly would require a longer-term energy storage (closer to seasonal storage than to the type of short-term storage investigated in this study).

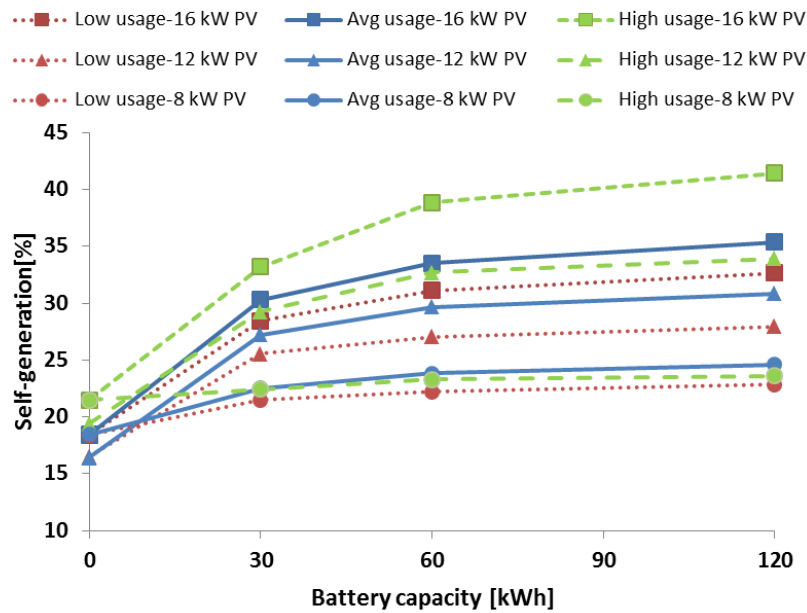


Figure 21 Self-consumption vs battery capacity.

Figure 8 shows that the available energy flexibility E_f ranges from 0 to slightly over 12 kWh, the lower values taking place during the day. The minimum flexibility at night is at 4 kWh except when the battery is full, as discussed above. The median value is relatively constant during the day, with higher values immediately after a sunny day, when the battery is more likely to be charged and the load increases at late afternoon/early evening activities.

During the night time the higher E_f occurred over the months with higher solar radiation (e.g. June and July), when the surplus of generation during the day can be used at night to meet the load. Over the day time, usually on-site generation supplies the load and the system operates in semi-standalone mode. In these conditions, upward flexibility is gained by shutting down the PV panels and supplying the load with the grid, so that the shape of the flexibility matches the shape of the building load, and is higher during the winter months (e.g. December and January).

Figure 23 and Figure 24 display the upward and downward energy flexibility for UPS mode respectively in a same format as shown in Figure 21. As it is expected and explained previously for both upward and downward energy flexibility, the correspondent KPI depends on the share of on-site generation in supplying the load. The upward flexibility is a direct representation of PV generation that can be shut down, and the downward flexibility represents the share of the load that is not covered by PV, up to the maximum battery discharge current (about 8 kW here).

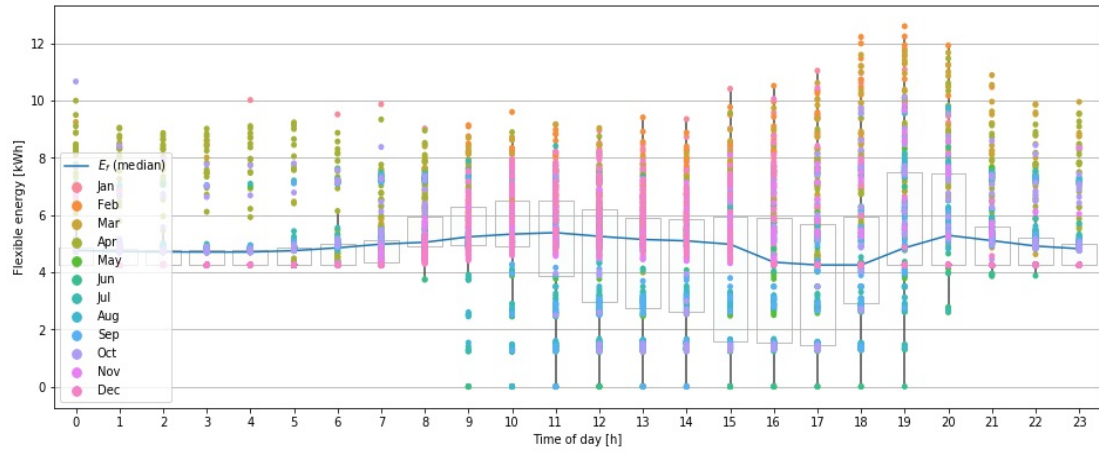


Figure 22 Upward flexible energy-grid support mode.

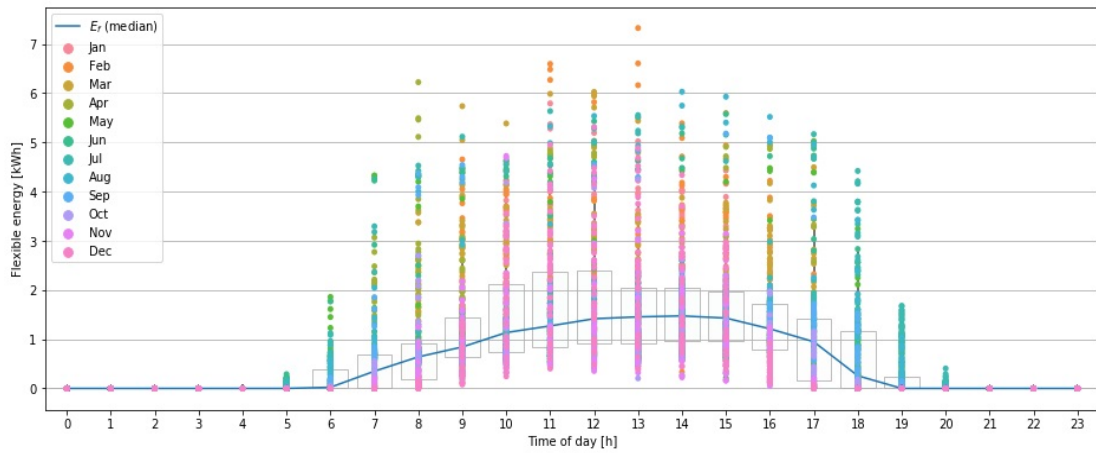


Figure 23 Upward flexible energy-UPS mode.

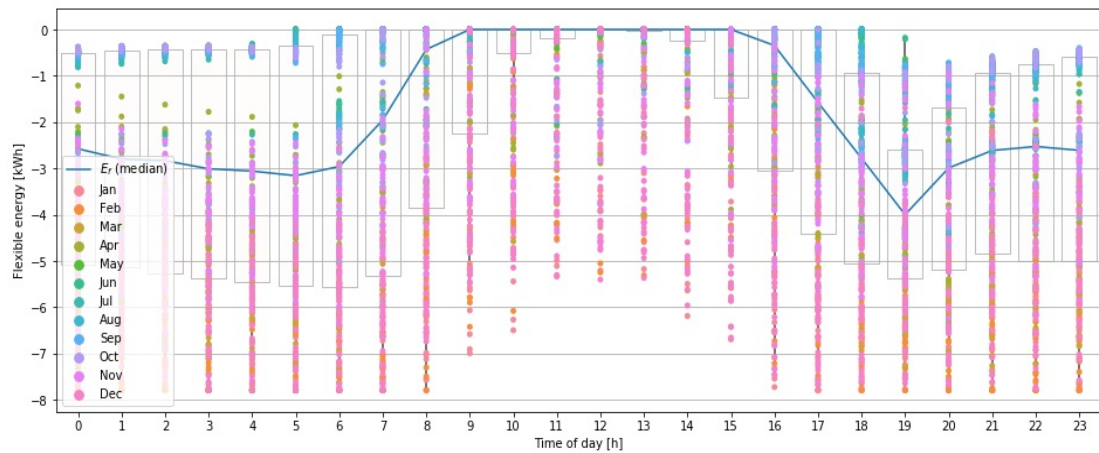


Figure 24 Downward flexible energy-UPS mode.

4.5 Discussions

This section assessed the energy flexibility of an all-electric Canadian house. The energy flexibility was categorized into two scenarios: downward and upward flexibility. The former scenario is similar to load shifting, which shows the ability of buildings to reduce power demand during

peak periods. The upward flexibility denotes the ability to use more energy when the power demand is low on the grid.

Simulation results show that the energy flexibility potential of using thermal mass is significant. The studied house shows a median decrease of the energy use by 6 kWh and a median increase by 7.5 kWh for 2-h DR events. The flexibility depends on the time of the DR event, as it is affected by weather and building operation. The flexible energy amount is higher during colder weather because the normal operation of the house has a higher energy demand during these periods. In addition, the maximum flexible power is also very promising, especially for the upward flexibility.

Yearly KPIs such as self-generation and self-consumption show that adding batteries to a conventional grid-tied PV system can dramatically improve the available flexibility, with a saturation of the effects for battery capacity higher than 4 kWh/kWp under the selected assumptions.

Dynamic KPIs calculated for 1 hour upward and downward flexibility events show that there is a large variability in available flexibility, depending on the day and time of the year and on the inverter control strategy. The UPS mode, which results in the lowest yearly self-generation and self-consumption, presents a significant downward flexibility potential, limited by the maximum battery discharge current. Its upward flexibility results from the ability to shut down PV generation and is entirely dependent on solar radiation. On the other hand, the grid-support (or PV priority) operation mode, which already minimizes grid imports, offers no potential for downward flexibility under the current assumptions. Its upward flexibility is variable between 0 and 12 kWh in this study, with a relatively constant median value around 5 kWh.

4.6 Reference

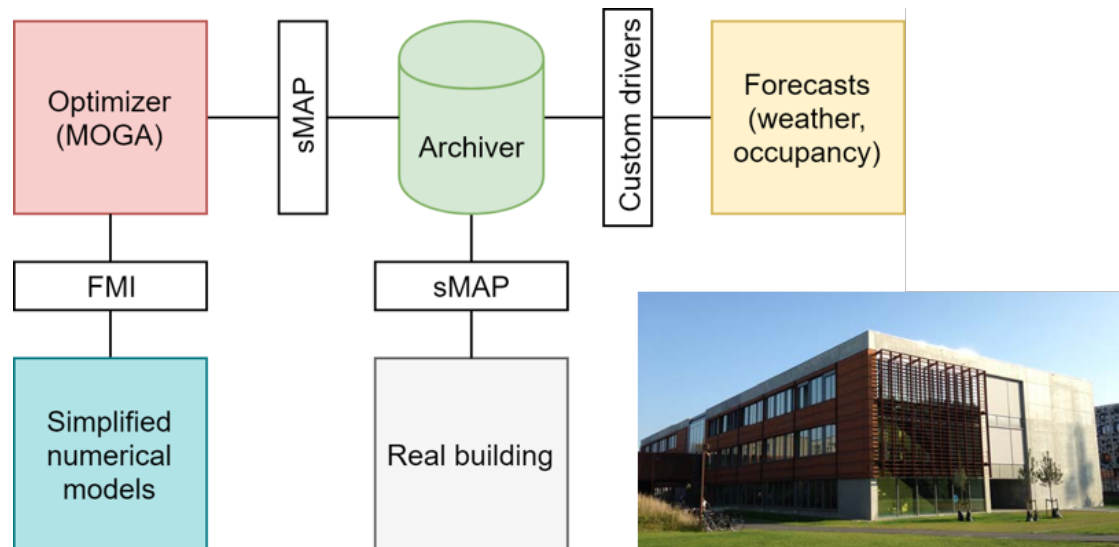
- [1] M. C. Swinton, H. Moussa, and R. G. Marchand, "Commissioning twin houses for assessing the performance of energy conserving technologies," in *Proceedings of Performance of Exterior Envelopes of Whole Buildings VIII: Integration of Building Envelopes, Clearwater Beach, Florida. Dec. 2-7, 2001*, pp. 925–931.
- [2] K. Zhang, H. Quintana, D. Bradley, M. Kummert, and M. Riley, "Air-source integrated heat pumps (AS-IHPs) with smart zoning for residential space and water heating in cold climate," in *Proceedings of Building Simulation 2015: 14th Conference of International Building Performance Simulation Association, Hyderabad, India, Dec. 7-9, 2015*, pp. 1623–1630.
- [3] Thermal Energy System Specialists LLC, "TRNSYS," 2018. [Online]. Available: <http://www.trnsys.com/>. [Accessed: 28-Aug-2018].
- [4] G. Reynders, J. Diriken, and D. Saelens, "Generic characterization method for energy flexibility: Applied to structural thermal storage in residential buildings," *Appl. Energy*, vol. 198, pp. 192–202, 2017.
- [5] J. Salom, A. J. Marszal, J. Widén, J. Candanedo, and K. B. Lindberg, "Analysis of load match and grid interaction indicators in net zero energy buildings with simulated and monitored data," *Appl. Energy*, vol. 136, pp. 119–131, 2014.

4.7 Relevant publications

K. Zhang, M. Kummert. (2018). Potential of building thermal mass for energy flexibility in residential buildings: a sensitivity analysis. Proceedings of eSim 2018 Building Performance Simulation Conference, May 9-10, Montreal, Canada.

B.B. Bafrouei, K. Zhang, M. Kummert (2018). Energy flexibility analysis of photovoltaic system with batteries for residential buildings. Proceedings of eSim 2018 Building Performance Simulation Conference, May 9-10, Montreal, Canada

5. Multi-objective genetic algorithm for model predictive control in buildings



Institution

Center for Energy Informatics,
Mærsk-McKinney Møller Institute,
University of Southern Denmark



Contact persons

Dr. Krzysztof Arendt
krza@mmpi.sdu.dk
+45 6550 2538

Prof. Bo Nørregaard Jørgensen
bnj@mmpi.sdu.dk
+45 6550 3545

5.1 Modelling objective

The aim of this study is to present the implementation and performance of a model predictive control framework based on a multi-objective genetic algorithm. The framework optimizes building control by firstly identifying a Pareto frontier with respect to multiple objectives considered, and then selecting the final strategy based on the user-defined priorities for the respective objectives. Although the approach requires more computing resources than the more traditional constrained convex optimization, it is more flexible in terms of the optimization problem formulation. New objectives can easily be added, and the objective priorities altered during the operation of the system. This flexibility makes the framework attractive for global optimization of multiple systems, including systems based on on/off control. The framework is compatible with the Functional Mock-Up Interface and uses models exported to Functional Mock-Up Units. The framework performance is tested in a virtual experimental testbed using a virtual building modeled in EnergyPlus. It is the first demonstration of applying this framework in a building application.

5.2 Building and system description

The framework was tested on a virtual case study building implemented in EnergyPlus (similarly to e.g. Ascione et al. 2016 or Bianchini et al. 2016). The virtual building is a downscaled version of the OU44 teaching building at the SDU Campus Odense (Fig. 25). It has the same HVAC system type and the building envelope construction as the actual building, but it is limited to just 7 thermal zones. The thermal zones have a similar geometry as the classrooms in OU44. The building is equipped with a hydronic heating loop and a mechanical ventilation system with pre-heating and a heat exchanger unit.

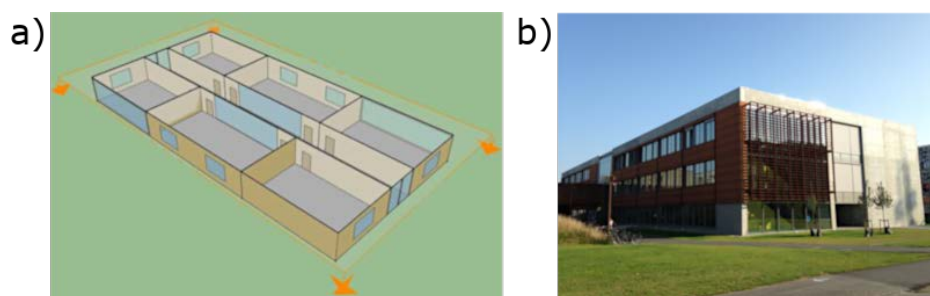


Figure 25 (a) simplified test model limited to 7 zones, (b) actual OU44 building.

5.3 Method and modelling tools

The optimization framework consists of the following parts (Fig. 26):

- multi-objective genetic algorithm (MOGA),
- simplified gray-box models calibrated using ModestPy – Functional Mock-up Unit parameter estimation toolbox (Arendt et al. 2018),
- archiver with the sMAP interface.

Due to the use of Functional Mock-Up Interface (FMI) (Blochwitz et al., 2016) and sMAP interfaces, the framework is model- and system-independent. E.g. the same interface is used to communicate with a virtual building (simulation tests) as with the actual building (real application).

The optimizer is based on a multi-objective genetic algorithm (MOGA) (Sørensen and Jørgensen, 2017) that constructs a Pareto frontier with respect to the considered objectives (Fig. 27). Each individual in the population represents a specific control policy, e.g. specific heating and

ventilation profiles, that is tested in the simulation. The Pareto frontier construction is iterative and based on the genetic algorithm operations: selection, crossover, and mutation. Whenever a new individual appears in the evolution, with a better fitness with respect to at least one of the objectives, it joins the Pareto frontier. When one of the stopping criteria is met, the evolution stops and the algorithm proceeds to the second phase in which the final policy is selected. There two stopping criteria in use: (1) no improvement in the Pareto frontier for a defined number of generations, (2) maximum computational time reached.

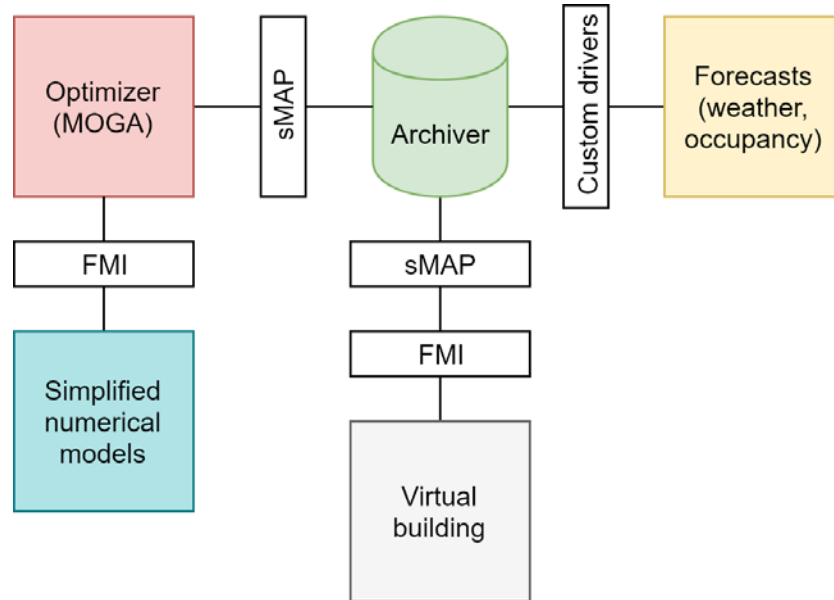


Figure 26 Optimization framework setup based on a virtual building.

The policy selection in the second phase is conducted recursively. In each step i the subset of individuals optimal with respect to the priority level L_i (Fig. 27) is selected. Each priority level can contain either one or more objectives. In the case there are two or more objectives at the same level, the objectives are normalized in order to identify the optimal population subset. However, no normalization is required for priority levels with a single objective. Finally, after traversing through all the levels, one or more equally optimal policies are left, out of which one is selected randomly.

Due to the FMI-compatibility and the use of MOGA the framework is essentially model independent. The models can be implemented in any FMI-compliant tool, and they can be non-linear, non-differentiable or even non-continuous. In addition, since the optimization is not based on a cost function, adding new objectives is straightforward. The objectives do not have to be normalized with respect to one another. Therefore, the framework is potentially more flexible than model predictive control (MPC) systems based on collocation (Magnusson and Åkesson 2015) or shooting methods (Lazutkin et al. 2014). Such features might be especially relevant for building systems, which are often non-linear (e.g. HVAC) and non-continuous (e.g. on/off controllers). On the other hand, MOGA is expected to be more computationally demanding than the gradient-based methods.

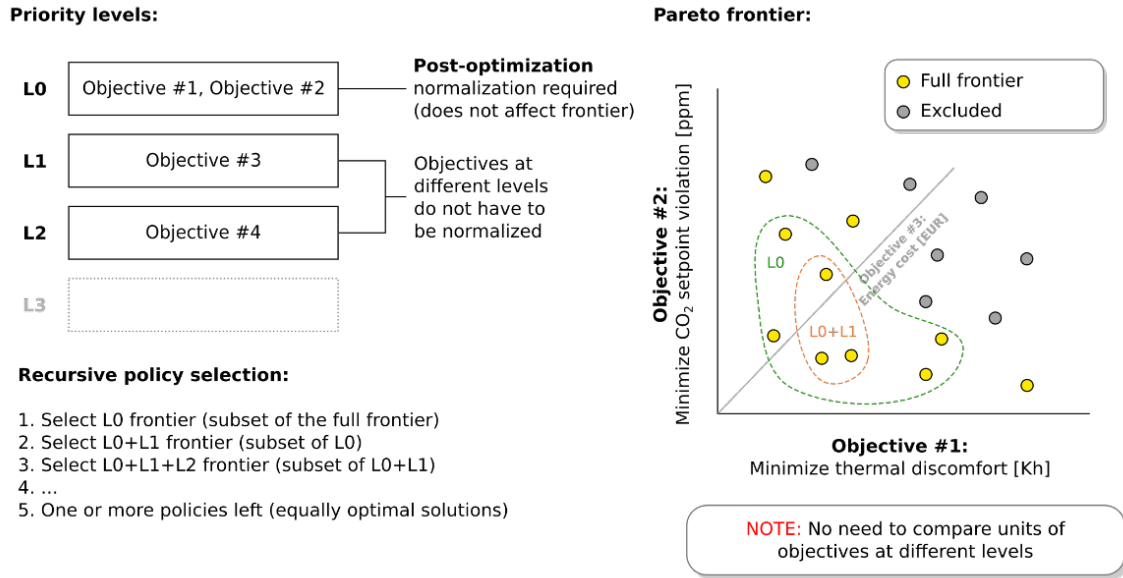


Figure 27 Pareto frontier in the multi-objective genetic algorithm optimization.

MOGA uses 7 gray-box zone models to simulate the effects of control policies on the thermal zones in the analyzed building. The zone models are based on the RC thermal network, and each zone model has the same structure (Fig. 28), but different parameters. The models are implemented in Modelica (Mattsson and Elmqvist, 1997). The zone model parameters were estimated by minimizing the error in indoor temperature and CO₂ compared to the EnergyPlus outputs using the ModestPy toolbox (Arendt et al. 2018).

The performance of the framework is compared with the rule-based control (RBC) in a one-month long simulation, based on the climate data for January from Typical Meteorological Year for Copenhagen. It is assumed that the framework has control over the room temperature setpoints (each room can have a different setpoint) and has access to room occupancy schedules. In the real applications the occupancy schedules would be replaced with occupancy predictions. The influence of the quality of the occupancy predictions on the performance of the framework is not considered in this study. Two MOGA-based scenarios are considered:

1. CTRL-EE – optimization of temperature setpoints to minimize energy consumption and maintain indoor thermal comfort,
2. CTRL-DK1 – optimization of temperature setpoints to minimize energy price (based on the Nord Pool market data) and maintain indoor thermal comfort. Electric heating is assumed in this case.

In both scenarios the maintenance of indoor thermal comfort has the highest priority. In the RBC strategy the temperature setpoints are scheduled to 20 °C during weekdays between 5:00-16:00, and 15 °C otherwise. The RBC strategy is implemented directly in EnergyPlus.

The occupancy schedules for the seven zones were generated based on the reference schedule for office buildings available in OpenStudio, with additional time/value offsets, so that there are no two same schedules in the building.

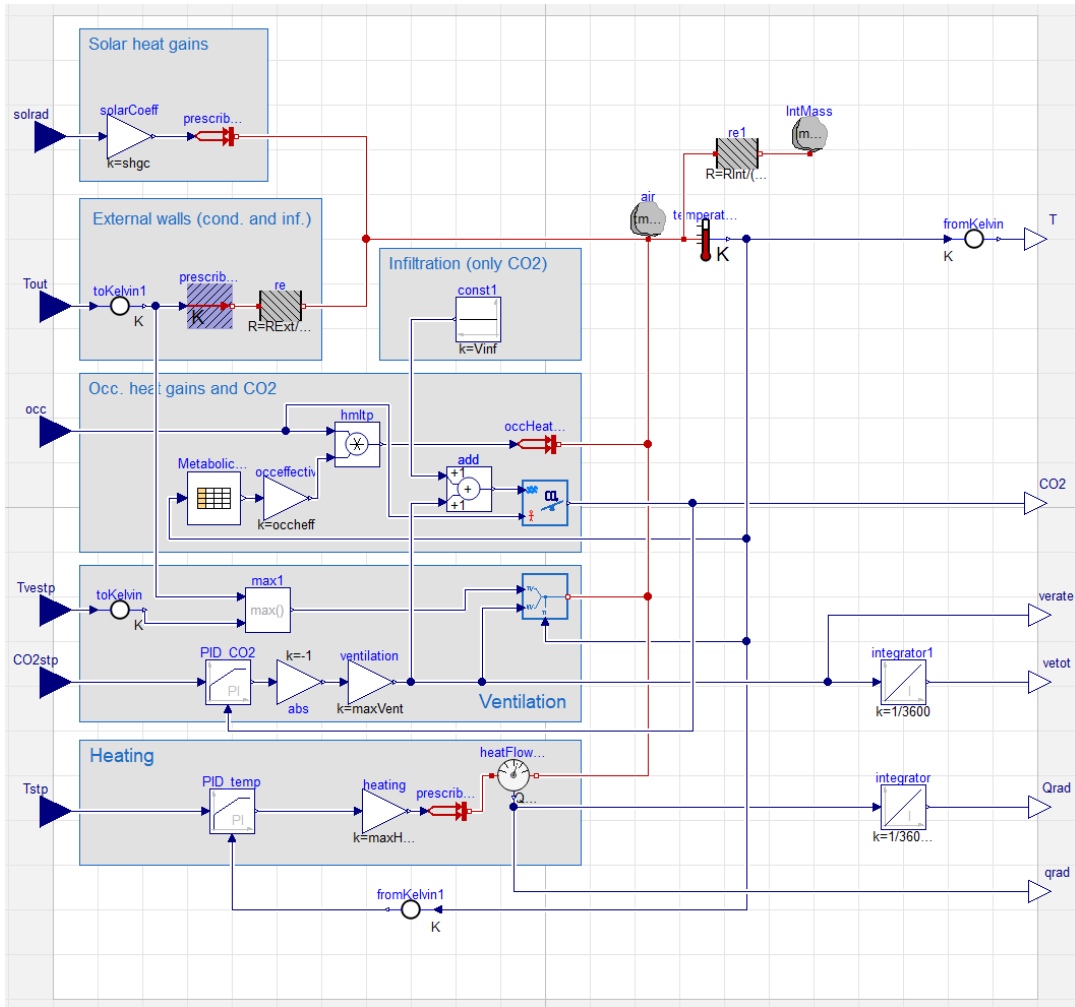


Figure 28 Gray-box model of a zone based on the R2C2 thermal network (Modelica).

5.4 Results

Compared to the implemented RBC, MOGA used around 24-25% less energy for heating (Table 1). Similar savings were achieved in both scenarios, CTRL-DK1 and CTRL-EE.

Table 6 Total heating energy consumption per scenario

Scenario	Total heating energy [kWh]	Relative [% of RBC]
CTRL-EE	4050	75
CTRL-DK1	4092	76
RBC	5369	100

Based on the indoor temperature profiles (Figs. 29-30) it can be concluded that most of the energy savings were due to the demand driven heating, as opposed to the fixed schedule-based behavior in the case of RBC. The indoor temperature profiles in RBC were repetitive and, in many periods, not reflecting the actual occupancy, e.g. see large deviations between RBC and MOGA results on January 4, zones 2-7 in Fig. 29. In addition to the demand-driven behavior, in most cases MOGA was able to preheat the zones before the actual occupancy occurred, with some exceptions when it did not start the preheating early enough, e.g. on January 4, zone 4 in Fig. 29.

The similar monthly profiles of indoor temperature in CTRL-EE and CTRL-DK1 (Fig. 30) suggest that the highest priority objective, i.e. the thermal comfort maintenance, dominated the solution.

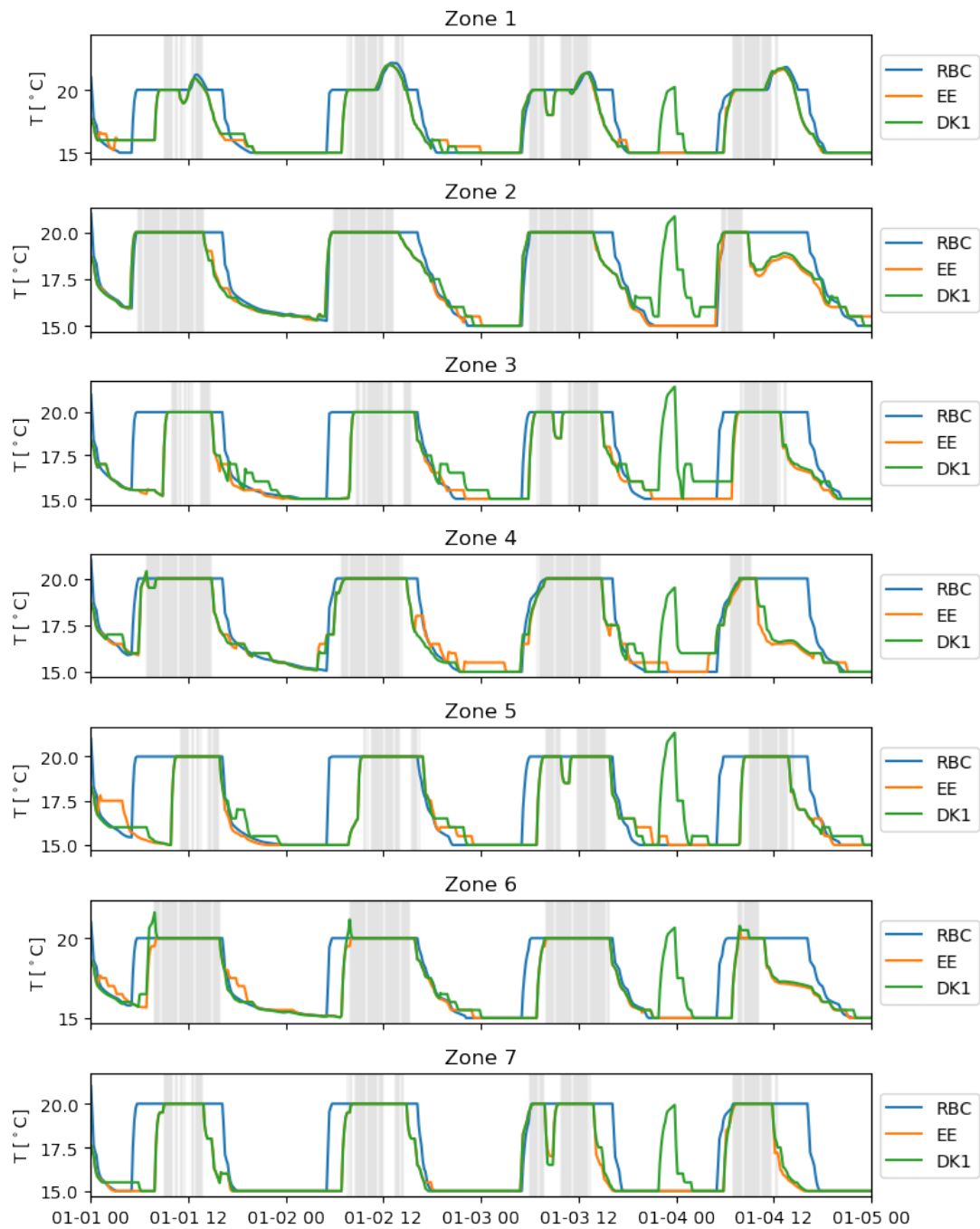


Figure 29 Indoor temperature profiles within the first five days of simulation. The areas shaded in gray mark occupancy periods.

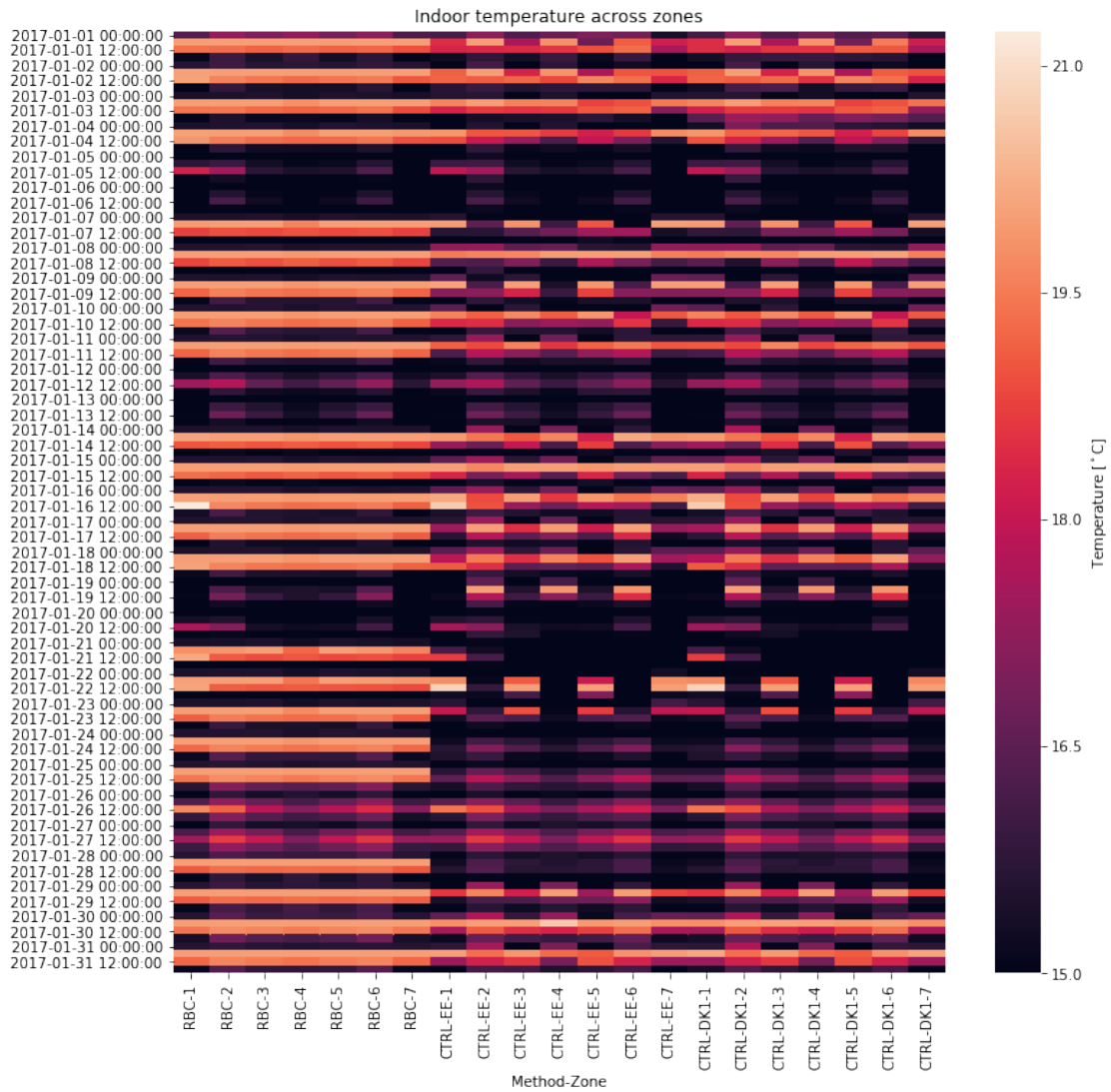


Figure 30 One-month indoor temperature profiles for the three considered scenarios (RBC, CTRL-EE, CTRL-DK1). Each column represents a single zone (profile name - zone number).

The framework reduced the discomfort (measured in Kh) by around 70% (Fig. 31). The discomfort metric used in the study was calculated as the product of the temperature difference between the setpoint of 20°C and the actual temperature and the time in which the difference was observed. Only occupancy periods and only the negative temperature differences were taken into account, i.e. when the indoor temperature was lower than 20°C. E.g. 1 Kh means that the temperature was below the setpoint by 1 degree during 1 h of occupancy. The obtained discomfort metrics were 287.85, 42.18, 41.58 for RBC, CTRL-EE, CTRL-DK1, respectively. The result depends on the chosen reference RBC schedules, however the discomfort in RBC could only be decreased at the cost of increased energy consumption. It is believed that the slightly lower discomfort in CTRL-DK1 as compared to CTRL-EE is likely due to the stochastic nature of the optimization algorithm. Since the framework had access to 100% accurate occupancy “predictions”, it could theoretically minimize the discomfort to 0 Kh. The fact that the discomfort metric was non-zero indicate that either the solution was still suboptimal, e.g. due to the maximum CPU time reached. The suboptimality of the solution is at least partially true as can be seen in the case of zone 5, CTRL-EE, January 3 in Fig. 29, where the indoor temperature setpoint at night is

slightly above actually needed. The influence of the objectives hierarchy and optimization settings should be investigated further in the future.

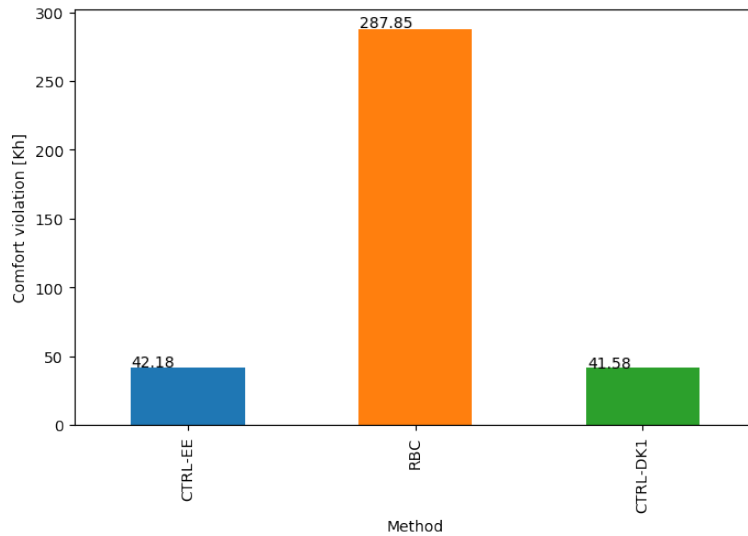


Figure 31 Indoor comfort violations for the three considered scenarios

The indoor heating profiles and the energy price during a subperiod of the analyzed month can be compared in Fig. 32. As in the case of temperature, CTRL-EE and CTRL-DK1 followed a similar trend with one major exception on January 4 when the electric energy price was negative for a short period of time. The controller in CTRL-DK1 decided to consume as much energy as possible in that time, meaning that the second priority objective came into play. However, for most of the time the price signal had no influence on the solution. Possibly higher price variations or different objective hierarchy would be needed to effectively optimize for the total energy cost in a real application.

Contrary to expectations, the CTRL-DK1 yielded slightly higher energy cost than CTRL-EE (Figure 33). However, as argued before, this is likely due to the stochastic nature of the optimization algorithm and the dominant role of the highest priority objective of the thermal comfort maintenance.

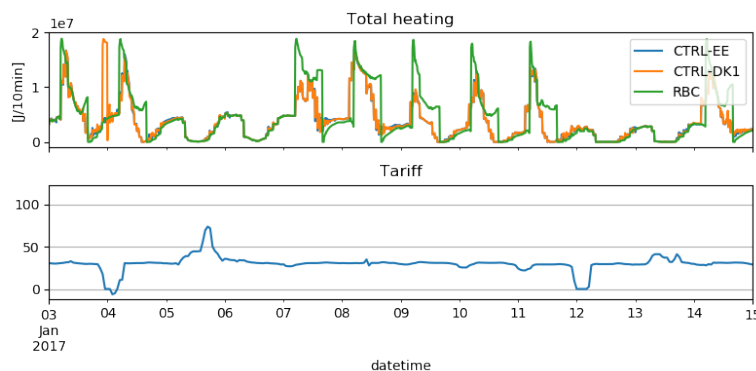


Figure 32 Total heating profiles for the three scenarios (top) vs. energy price (bottom).

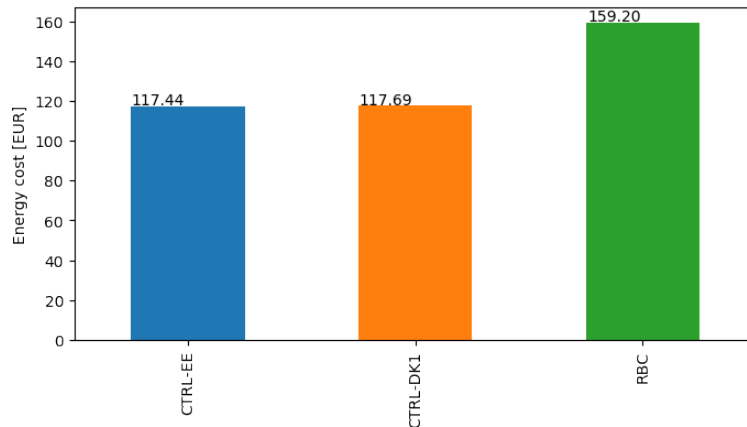


Figure 33 Total energy cost per scenario.

The presented results were computed using code that was only partially parallelized, e.g. Pareto frontier detection was performed on multiple cores. However, the main bottleneck with respect to the CPU time was the simulation of the gray-box zone models, which was performed on a single core. Due to the nature of MOGA, the zone model simulations need to be repeated thousands of times. In this setup a maximum allowed optimization time per each 7h optimization horizon was five minutes. After each optimization, a one-minute time slot was used to synchronize the measurements and control strategy between MOGA and the virtual building. The optimization was repeated every 1h of the virtual building's time. In total, around 3 days of real time were needed to perform a one-month emulation of the virtual building with the MOGA framework (for one scenario). Although the computational requirements of the framework are considerable, they are feasible for implementation in real buildings. However, implementation in large buildings (with hundreds of zones) may require parallelization of the zone model simulations. In general, more investigations regarding the scalability of the framework are required.

Summarily, the MOGA framework reduced the energy consumption by around 25% (compared to RBC), however most of the saving were due to the demand-driven heating and not due to the utilization of the building dynamics. This may be due to either a low thermal inertia of the studied building or due to the deficiency of the dynamic optimization method. The relatively small difference in the results between the case based on the energy efficiency objective and the case based on the energy cost minimization objective shows that dynamic energy pricing might not be a sufficient incentive for increasing energy flexibility in the analyzed building.

5.5 Reference

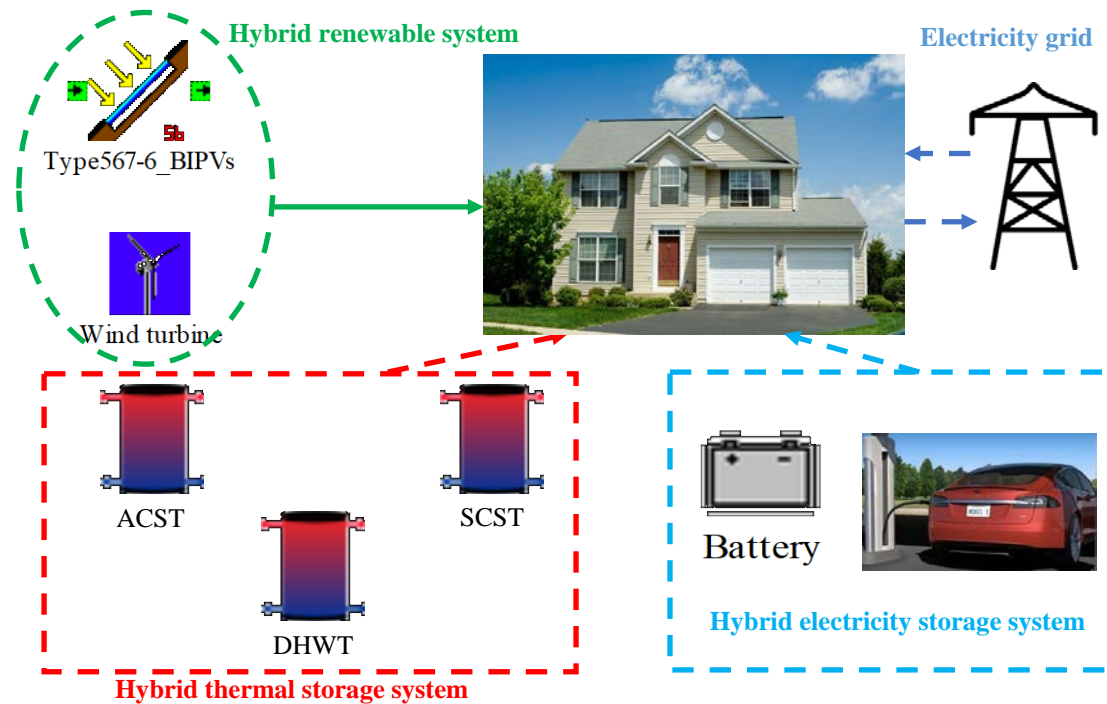
- Arendt, K., Jradi, M., Wetter, M., Veje, C. T., ModestPy: An Open-Source Python Tool for Parameter Estimation in Functional Mock-up Units, in: Proceedings of the American Modelica Conference 2018, Cambridge, MA, USA, 2018, to appear.
- Ascione, F., Bianco, N., De Stasio, C., Mauro, G. M., & Vanoli, G. P. (2016). Simulation-based model predictive control by the multi-objective optimization of building energy performance and thermal comfort. *Energy and Buildings*, 111. <https://doi.org/10.1016/j.enbuild.2015.11.033>
- Bianchini, G., Casini, M., Vicino, A., & Zarrilli, D. (2016). Demand-response in building heating systems: A Model Predictive Control approach. *Applied Energy*, 168, 159–170. <https://doi.org/http://dx.doi.org/10.1016/j.apenergy.2016.01.088>

- Blochwitz, T., Otter M., Åkesson J., et al. (2012). Functional Mockup Interface 2.0: The Standard for Tool Independent Exchange of Simulation Models, Proceedings of the 9th International Modelica Conference, p. 173-184.
- Lazutkin, E., Selassie, A.G.W., Hopfgarten, S., Li, P. (2014). Modified multiple shooting combined with collocation method in JModelica.org with symbolic calculations, Proceedings of the 10th International Modelica Conference, March 10-12.
- Magnusson, F., Åkesson, J. (2015). Dynamic Optimization in JModelica.org, Processes 3:471-496.
- Mattsson, S.E., Elmqvist, H. (1997). Modelica - An international effort to design the next generation modeling language. 7th IFAC Symposium on Computer Aided Control Systems Design, CACSD'97, Gent, Belgium, April 28-30.
- Sørensen, J. C., Jørgensen, B. N. (2017). An Extensible Component-Based Multi-Objective Evolutionary Algorithm Framework. Proceedings of the 6th International Conference on Software and Computer Applications. Association for Computing Machinery, 191-197.

5.6 Relevant publications

- Arendt, K., Clausen, A., Mattera, C.G., Jradi, M., Johansen, A., Veje, C.T., Kjærgaard, M.B., Jørgensen, B.N. (2019). Multi-Objective Model Predictive Control Framework for Buildings. Proceedings of the 16th IBPSA International Conference Building Simulation 2019. *(to appear)*

6. The investigation of the energy flexibility of a residential building via the hybrid energy storages in Hong Kong



Institution

Department of Building Services Engineering,
Faculty of Construction and Environment,
The Hong Kong Polytechnic University

Contact persons

Mr. Yuekuan Zhou
Yuekuan.zhou@connect.polyu.hk
(+852) 3400 3890

Dr. Sunliang Cao
sunliang.cao@polyu.edu.hk; caosunliang@msn.com
(+852) 2766 5837

6.1 Modelling objective

Several objectives are included as shown below:

- 1) Quantitatively investigation of the energy flexibility of a building with specific flexibility indicators and propose technical solutions to enhance the building energy flexibility;
- 2) Investigation of the energy interactions between a flexible building, a smart grid and a electric vehicle in the hybrid net zero energy building and electric vehicle (NZEB-EV) system.

6.2 Building and system description

There are two floors in the studied single-family house with a net floor area of 100 m² and a height of 3 m in each floor. An attic is designed for shedding rain water and shading the solar radiation. The titled angle and the total area of the attic roof are 22° and 108 m², respectively.

Regarding the operational and the control principle, when the renewable generation is higher than the total electric demand, one option is to drive the renewable-air handling unit cooling storage tank (REe-ACST) recharging chiller or the renewable-space cooling storage tank (REe-SCST) recharging chiller to convert the surplus renewable electricity to the cooling storage tank, resulting in the decrease of the total electric demand. Another option is the renewable-domestic hot water storage tank (REe-DHWT) recharging strategy, which will reduce the electric consumption of the auxiliary heater for the DHW heating. This also results in a decrease of the total electric demand. These two recharging strategies will enhance the forced energy in both tanks. If there is still surplus renewable electricity, it will be used to charge the electric vehicle (EV) before charging the static battery. Afterwards, the rest of the surplus renewable electricity will be exported to the electric grid.

During the period when the renewable electricity is insufficient to cover the total electric demand, the delayed thermal energy in both the ACST, the SCST and the DHWT will be used to back up the total electric demand. If the total electric demand is not completely covered when the thermal storages are completely discharged, the static battery will be discharged to cover the total electric demand before discharging the EV battery. In the end, the rest of the total electric demand will be covered by importing electricity from the grid.

6.3 Method and modelling tools

This research is conducted on the Transient System Simulation Program called TRNSYS 18 [2], which is a dynamic simulation environment for building energy technology, HVAC and renewable energy systems. The open source code-based models (Types) make it possible for refining the existing model or developing new models. This enhances the applicability and the practicality of the simulation tool in the building energy simulation.

To quantitatively investigate the building energy flexibility, several flexibility indicators have been proposed from the perspectives of the time-duration, the flexible power and the flexible energy.

Forced period, t_{forced} : the time-duration when the cooling load of the building is lower than the cooling power of the chiller, [h].

$$t_{forced} = \int_0^{t_{end}} GT((C_{chiller,normal} + C_{chiller,recharging} - L_{cooling}), 0) \cdot dt \quad (1)$$

Delayed period, $t_{delayed}$: the time-duration when the cooling load of the building is higher than the power of the chiller, [h].

$$t_{\text{delayed}} = \int_0^{t_{\text{end}}} \text{GT}((L_{\text{cooling}} - C_{\text{chiller,normal}}), 0) \cdot dt \quad (2)$$

REe surplus period, t_{surp} : the time-duration when the REe electricity generation is higher than the total electrical demand, [h].

$$t_{\text{surp}} = \int_0^{t_{\text{end}}} \text{GT}((G_{\text{REe}} - L_{\text{electricity}}), 0) \cdot dt \quad (3)$$

REe shortage period, t_{short} : the time-duration when the REe electricity generation is less than the building total electric demand, [h].

$$t_{\text{short}} = \int_0^{t_{\text{end}}} \text{GT}((L_{\text{electricity}} - G_{\text{REe}}), 0) \cdot dt \quad (4)$$

Forced power, ρ_{forced} : the additional cooling power generation of both the normal chiller and the excess REe-cooling recharging chiller compared to the cooling load, [kW].

$$\rho_{\text{forced}} = \text{Max}(((C_{\text{chiller,normal}} + C_{\text{chiller,recharging}} - L_{\text{cooling}}), 0)) \quad (5)$$

Delayed power, ρ_{delayed} : the decreased cooling power generation of the normal chiller compared to the cooling load, [kW].

$$\rho_{\text{delayed}} = \text{Max}((L_{\text{cooling}} - C_{\text{chiller,normal}}), 0) \quad (6)$$

Flexible energy (E_{forced} , E_{delayed} , E_{DHW} and E_{Aux}): the integration of the flexible power over the corresponding flexible period, [kWh/m².a].

$$E_{\text{forced}} = \int_0^{t_{\text{Forced}}} \rho_{\text{Forced}} dt/A \quad (7)$$

$$E_{\text{delayed}} = \int_0^{t_{\text{Delayed}}} \rho_{\text{Delayed}} dt/A \quad (8)$$

$$E_{\text{DHW}} = \int_0^{t_{\text{surp}}} P_{\text{DHW}} dt/A \quad (9)$$

$$E_{\text{Aux}} = \int_0^{t_{\text{short}}} P_{\text{Aux}} dt/A \quad (10)$$

where P_{DHW} and P_{Aux} are the surplus renewable electricity consumption in recharging the DHW tank, and the electricity consumption of the auxiliary electric heater, respectively. A is the floor area of the single-family house.

The $\text{FF}_{\text{forced}}$ indicates the capability of the flexible energy system for shifting the forced energy to the REe surplus period compared to the REe shortage period. The $\text{FF}_{\text{delayed}}$ indicates the capability of the flexible energy system for shifting the delayed energy to the REe shortage period compared to the REe surplus period. FF_{AC} indicates the capability of the flexible energy system for shifting the forced energy and the delayed energy to the preferable period during both charging and discharging processes. FF_{DHW} indicates the capability of the surplus renewable electricity for heating the DHWT compared to the electricity consumption of the auxiliary heater at the REe shortage period.

$$\text{FF}_{\text{forced}} = \frac{\int_0^{t_{\text{surp}}} \rho_{\text{forced}} dt - \int_0^{t_{\text{short}}} \rho_{\text{forced}} dt}{\int_0^{t_{\text{surp}}} \rho_{\text{forced}} dt + \int_0^{t_{\text{short}}} \rho_{\text{forced}} dt} \quad (11)$$

$$FF_{\text{delayed}} = \frac{\int_0^{t_{\text{short}}} \rho_{\text{delayed}} dt - \int_0^{t_{\text{surp}}} \rho_{\text{delayed}} dt}{\int_0^{t_{\text{short}}} \rho_{\text{delayed}} dt + \int_0^{t_{\text{surp}}} \rho_{\text{delayed}} dt} \quad (12)$$

$$FF_{\text{AC}} = w_1 \cdot FF_{\text{forced}} + w_2 \cdot FF_{\text{delayed}} \quad (13)$$

$$FF_{\text{DHW}} = \frac{\int_0^{t_{\text{surp}}} P_{\text{DHW}} dt - \int_0^{t_{\text{short}}} P_{\text{Aux}} dt}{\int_0^{t_{\text{surp}}} P_{\text{DHW}} dt + \int_0^{t_{\text{short}}} P_{\text{Aux}} dt} \quad (14)$$

where w_1 and w_2 are the weighing factors during both the charging and the discharging processes, respectively. In this study, they are assumed to be 0.5. All flexibility factors range from -1 to 1. The larger the flexibility factors are, the more flexible the system will be.

To vividly demonstrate the flexibility with respect to the above description, Figure 34 demonstrates the flexible time-duration, the flexible power, the flexible energy and the flexibility indicators. As shown in Figure 34(a), when the chiller charges the thermal storage tank, the cooling energy generation of the chiller can be higher than the cooling load, and the forced energy will be stored in the tank. The thermal storage tank will be discharged to meet the cooling load, and thus the operational time-duration of the chiller is postponed. Therefore, the delayed energy is resulting from the stored energy in the tank and the postponement of the operational time-duration of the chiller. Figure 34(b) demonstrates the renewable generation, the total electric demand, the cooling load and the cooling energy generation of the chiller. Both the flexible energy and the flexibility factors are quantitatively calculated by Equations (15)-(23).

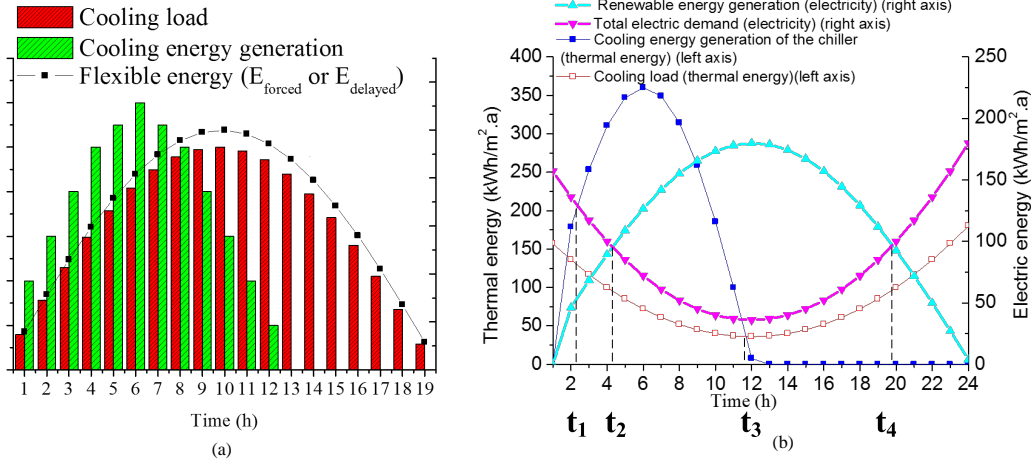


Figure 34 The demonstration of the flexible energy and the flexibility factors for the thermal storage system

$$E_{\text{forced}} = \int_{t_1}^{t_3} [C_{\text{chiller}} - L_{\text{cooling}}] dt / A \quad (15)$$

$$E_{\text{delayed}} = \int_0^{t_1} [L_{\text{cooling}} - C_{\text{chiller}}] dt / A + \int_{t_3}^{24} [L_{\text{cooling}} - C_{\text{chiller}}] dt / A \quad (16)$$

$$E_{\text{forced}}^+ = \int_{t_2}^{t_3} [C_{\text{chiller}} - L_{\text{cooling}}] dt / A \quad (17)$$

$$E_{\text{forced}}^- = \int_{t_1}^{t_2} [C_{\text{chiller}} - L_{\text{cooling}}] dt / A \quad (18)$$

$$E_{\text{delayed}}^+ = \int_0^{t_1} [L_{\text{cooling}} - C_{\text{chiller}}] dt / A + \int_{t_4}^{24} [L_{\text{cooling}} - C_{\text{chiller}}] dt / A \quad (19)$$

$$E_{\text{delayed}}^- = \int_{t_3}^{t_4} [L_{\text{cooling}} - C_{\text{chiller}}] dt / A \quad (20)$$

$$E_{imp} = \int_0^{24} \text{Max}[(L_{\text{electricity}} - G_{\text{REe}}), 0] dt/A \quad (21)$$

$$FF_{\text{forced}} = \frac{E_{\text{forced}}^+ - E_{\text{forced}}^-}{E_{\text{forced}}^+ + E_{\text{forced}}^-} = \frac{\int_{t_2}^{t_3} [C_{\text{chiller}} - L_{\text{cooling}}] dt/A - \int_{t_1}^{t_2} [C_{\text{chiller}} - L_{\text{cooling}}] dt/A}{\int_{t_2}^{t_3} [C_{\text{chiller}} - L_{\text{cooling}}] dt/A + \int_{t_1}^{t_2} [C_{\text{chiller}} - L_{\text{cooling}}] dt/A} \quad (22)$$

$$FF_{\text{delayed}} = \frac{E_{\text{delayed}}^+ - E_{\text{delayed}}^-}{E_{\text{delayed}}^+ + E_{\text{delayed}}^-} = \frac{\int_0^{t_1} [L_{\text{cooling}} - C_{\text{chiller}}] dt/A + \int_{t_4}^{24} [L_{\text{cooling}} - C_{\text{chiller}}] dt/A - \int_{t_3}^{t_4} [L_{\text{cooling}} - C_{\text{chiller}}] dt/A}{\int_0^{t_1} [L_{\text{cooling}} - C_{\text{chiller}}] dt/A + \int_{t_4}^{24} [L_{\text{cooling}} - C_{\text{chiller}}] dt/A + \int_{t_3}^{t_4} [L_{\text{cooling}} - C_{\text{chiller}}] dt/A} \quad (23)$$

where t_1 and t_3 refer to the time when the cooling energy generation of the chiller is equal to the cooling load; t_2 and t_4 refer to the time when the renewable energy generation is equal to the total electric demand.

6.4 Results

- 1) In the cooling dominated region, Hong Kong, the BIPVs can maximumly reduce the cooling load of the residential building by 22.1%. To meet the energy demand of the hybrid NZEB-EV system, the NZEB should be equipped with BIPVs and an 8 kW wind turbine. By implementing the latest grid feed-in tariff, the NZEB will get the net annual operational income of 646.3 HK\$/m².a.
- 2) In this study, the investigated technical solutions for enhancing the building energy flexibility include the excess REe-recharging strategies, the integration of an electric vehicle and the enhancement of both the rated capacity of the on-site renewable system and the storage capacity of hybrid energy storage systems.
- 3) In addition, the integration of the EV with buildings can enhance the building energy flexibility, which is also affected by the interaction time-duration, the storage capacity and the limitation of the discharging condition of the EVs' battery. In the scenario when a 48 kWh EV is integrated with a residential NZEB at daytime, 87.2% of the annual total energy charged to the EV is from renewable energy. Meanwhile, 71.7% of the annual total energy charged to the EV can be used for covering the building demand, and 55% of annual energy demand for the travelling purpose can be covered by the renewable system.

Challenges:

- 1) In this study, despite the electrical-to-thermal energy conversion in the hybrid NZEB-EV system, the energy form for the flexibility indicators is only related to the thermal energy. It is necessary to develop the flexibility factors that contain both the thermal and the electric energy forms.
- 2) In this study, the uncertainty of input parameters is not considered. Moreover, the computational complexity of the energy prediction of the multivariable nonlinear building is not addressed. In the future, an advanced controller considering the uncertainty of the scenario parameters will be developed with the data-driven supervised deep learning technique.

6.5 References

Feed-in Tariff Scheme and Renewable Energy Certificate. https://www.clpgroup.com/en/Media-Resources/site/Current%20Releases%20Documents/20180423/20180423_Factsheet_FiT_RE%20Cert_en.pdf.

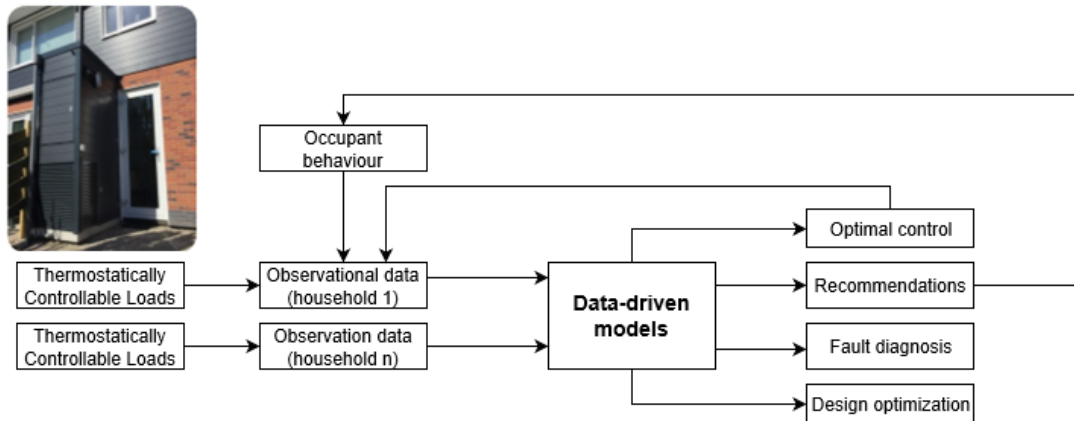
TRNSYS 18. 2017. "A TRANSIENT SYSTEMS Simulation Program." Mechanical Engineering Department, UW Madison. <https://sel.me.wisc.edu/trnsys/>.

6.6 Relevant publications

Further information of this study can be found: Yuekuan Zhou, Sunliang Cao. Flexibility quantification of a residential net-zero-energy building involved with dynamic operations of hybrid energy storages and various energy conversion strategies. Ongoing paper, 2019.

Yuekuan Zhou, Sunliang Cao. Investigation of the flexibility of a residential net zero energy building (NZEB) integrated with an electric vehicle in Hong Kong. 10th International Conference on Applied Energy (ICAE2018), 22-25 August 2018, Hong Kong, China.

7. Few-shot learning: data-driven modelling of hot water systems with extremely limited data



Institution

ELECTA,
Department of Electrical Engineering,
KU Leuven, Belgium



Contact person

Hussain Kazmi
Hussainsyed.kazmi@kuleuven.be
+32 476622614

7.1 Modelling objective

The objective of this study is to model the behaviour of hot water systems in an online, data-driven fashion with minimal sensing requirements. Modelling the hot water system includes characterizing both the storage element (i.e. the hot water storage tank) and the heating element (e.g. an electric or gas boiler, a heat pump etc.).

A number of modelling techniques have been proposed in literature which aim to model the behaviour of hot water systems (Ruelens et al., 2014), (Kazmi, 2016), (Markovic et al., 2017). These include white-box modelling methods which utilize a human modeller’s domain expertise to characterize the system dynamics of the hot water system (Hensen, 2012). At the other end of the spectrum, lie black-box modelling techniques which remove the dependence on the human domain expert by learning the system’s dynamics from sensor data (Kazmi et al., 2018). This can be done both offline (when a model is learnt prior to operation) and online (when a model is learnt during operation). Somewhere between these two extremes lie grey-box modelling methods which calibrate an existing model to observed data (Afram et al., 2014). These methods typically employ explainable models e.g. the popular RC models.

Most of these methods suffer from a number of significant shortcomings. White-box methods are constrained by the expertise and availability of the human modeller. The sheer number of hot water systems to be modelled especially makes it impractical to consider every single one individually. Furthermore, since these methods are typically employed in the design-phase, they seldom reflect operational performance of the modelled systems. The biggest reason for this is occupant behaviour which drives system operation to regions of the state-space which were not adequately modelled. Black-box methods, while avoiding the costly dependence on human domain expertise, rely on complete sensing of the system to model the system accurately. Where the data being gathered does not fully reflect the internal state of the system, these methods break down. This is often the case for hot water systems where only minimal sensing is employed in the form of a solitary temperature sensor. As the temperature distribution inside the storage is nonlinear because of stratification and other nonlinear dynamics, this sensory information is insufficient to learn an accurate dynamics model. Grey-box systems too inherit most of these disadvantages in real world settings (Kazmi et al., 2019).

This example presents a method which resolves most of these issues by leveraging transfer learning, a relatively recent development in machine learning (Pan et al., 2010). At its heart, the methodology provides a structured way of integrating information collected by agents operating in a variety of settings. Being data-driven, it is not limited to homogeneous devices and can also accelerate learning in the context of heterogeneous devices (i.e. devices with different physical and thermal characteristics). This study presents the results of applying transfer learning to two different housing projects comprising of recently refurbished net-zero energy buildings in The Netherlands.

The example also benchmarks the performance of the proposed system with a more conventionally formulated black-box system which relies on raw time series learning to model the hot water system. Furthermore, it highlights the influence increasing agency and data collection periods have on both the benchmark and the proposed system. By successfully learning a reliable system dynamics model in an extremely limited time frame (one week for the storage, one month for the heating element) the example successfully demonstrates few-shot learning (Ravi and Larochelle, 2016). Learning an accurate dynamics model in a timely manner brings about not just the time benefits but also enables smart control to improve energy efficiency and provide ancillary services to the grid.

7.2 Building and system description

We consider two different housing projects in the Netherlands in this case study. All the houses considered (in both projects) are net-zero energy buildings and are insulated to a very high degree. Furthermore, all the houses considered in both projects employ air-source heat pumps which are used to provide both the hot water and the space heating in the building (Kazmi et al., 2019). The storage installed in each house in both projects is 200 litres. However, the hot water system is identical only for houses belonging to the same project. There are considerable differences in the make of the hot water system between the two projects (most important of which is the completely different orientation and dynamics of the storage as well as the way the heat pump interacts with it). In subsequent sections, this distinction is made clear by referring to households (and devices) belonging to the same project as homogeneous, and those belonging to different projects as heterogeneous.

As the example focuses on data-driven modelling of the hot water system, it is important to enumerate the data streams it uses (represented in Fig. 35). These include:

1. Temperature measurement in the storage: for project 1, this was at the halfway point in the storage; for project 2, it was at one third of the storage height
2. Hot water flow from the storage vessel
3. Ambient temperature
4. Electricity consumed by the heat pump for hot water production

Making use of this data, the objective is to learn a system dynamics model for the hot water system. This further comprises of a storage model and a heating model. The purpose of the storage model is to estimate the state of the storage (i.e. its state of charge) at any given instant, while the purpose of the heating model is to estimate the amount of energy required by the heating element (heat pump in this case) to reheat the storage vessel from an initial to a final state of charge. Finally, it is important to note here that while over 50 houses were available for analysis for the first project, there were only eight houses in the second project which constrained data availability considerably.

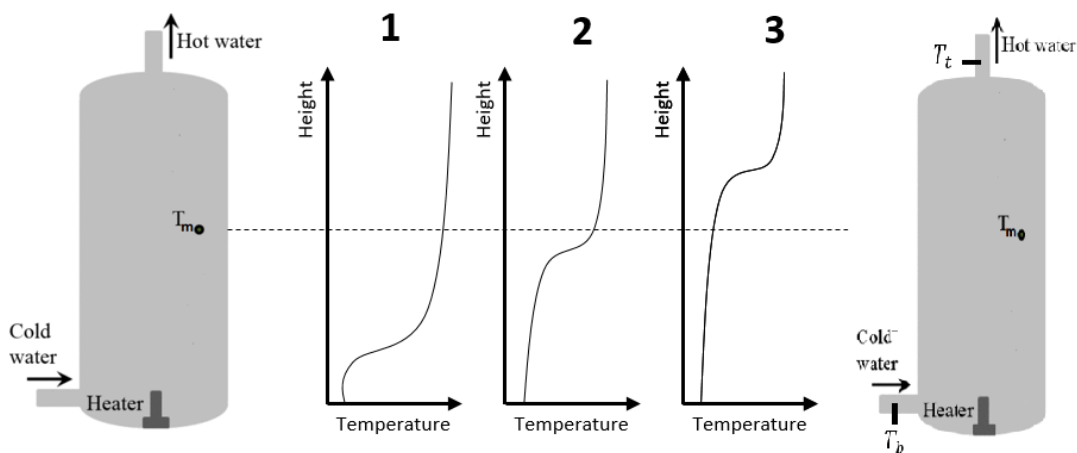


Figure 35 A schematic representation of the sensing employed in the projects and the non-linear temperature distribution inside the storage, which complicates the state of charge estimation.

7.3 Method and modelling tools

This section summarizes both the benchmark black-box method and the developed transfer learning framework to improve the modelling process. The modelling technique used in both cases is a deep neural network (LeCun et al., 2015). The architecture of the neural network is discovered through an extensive grid search over hyperparameters which includes the number of layers, number of neurons in each layer, choice of activation function, regularization and learning rate (Goodfellow, et al., 2016). Keras, an open source library for deep learning, was used with Python to train and evaluate the different neural networks (Chollet, 2015). Numerous metrics can be used to evaluate the performance of a black-box system. In this example, we will focus on two such measures: the R2 metric (or the explained variance in observation data by the fitted model) and the mean absolute error (which is in the units of measurement and is useful to quantify prediction error in absolute terms) (Goodfellow et al., 2016). Additionally, thermodynamic tests designed to test the general validity of model predictions were also developed and included here for completeness. These metrics will be investigated for both the heating and the storage models.

7.3.1 Benchmark black-box method

The black-box model used to benchmark the results learns from time series of raw sensor data. In this case, the only question to consider is which sensor streams to include and their temporal extents (i.e. how much historic data should be fed to the modelling method). On the one hand, increasing the temporal window allows the neural network to detect longer term trends (i.e. low frequency events). On the other hand, increasing the temporal window length can confuse the neural network by providing it unnecessary inputs. Furthermore, this also ties in with the curse of dimensionality where increasing the input feature vector considerably increases the exploration (or amount of data) required by the neural network to learn an accurate representation of the hot water system. In this case, the length of the window was chosen by evaluating model performance for different window lengths. The best performance trade-off was observed at using an entire historic day for all sensors under observation (although the model improvements were marginal).

7.3.2 A taxonomy of transfer learning

Transfer learning offers three key benefits when compared to traditional data-driven (i.e. black box) methods. These include a higher initial performance, a higher asymptotic performance and a faster rate of learning. This is highlighted in Fig. 36.

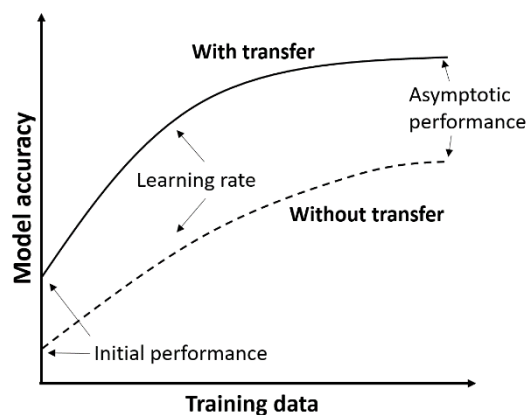


Figure 36 A graphic representation of the potential benefits of transfer learning.

Before discussing key results, a note on terminology is necessary here (Pan et al., 2010). Transfer learning is meant to transfer ‘knowledge’ from a source S to a target T . Often it is the case that a lot of data has been gathered for the source which can potentially be used to help improve the learning performance on the target of interest where training data is sparse (or expensive). However, in reality the separation between source and target is rather arbitrary, and knowledge can flow in both directions. More formally, transfer learning includes a domain and a task. The domain \mathcal{D} consists of (1) the input feature space \mathcal{X} , and (2) the marginal probability $P(X)$. Given a domain $\mathcal{D} = \{\mathcal{X}, P(X)\}$, the task \mathcal{T} consists of (1) the label space \mathcal{Y} , and (2) a predictive function $f(\cdot)$ which is learned in a supervised manner based on training examples $\{x_i, y_i\}$. This can also be seen as the conditional probability distribution $P(Y|X)$.

In all cases considered in this example, the feature space \mathcal{X} and the label space \mathcal{Y} are the same for all agents, i.e. $\mathcal{X}_S = \mathcal{X}_T$ and $\mathcal{Y}_S = \mathcal{Y}_T$ respectively. What this means is that the observed input and predicted output features remain the same for both source and target. However, individual household (occupant) behaviour means that the marginal probability $P(X)$ is different across different agents i.e. $P_S(X) \neq P_T(X)$ where $X = \{x_1, x_2, \dots, x_n\} \in \mathcal{X}$. This is the case because differences in the occupant behaviour drive even identical hot water systems to different operational zones, regardless of the hot water system employed. On the other hand, when the hot water system differs, i.e. for the heterogeneous case, the conditional probability distribution $P(Y|X)$ is also different for the source and target task, i.e. $P(Y_S|X_S) \neq P(Y_T|X_T)$.

7.3.3 Towards few-shot learning

While transfer learning can improve performance of black-box methods, the way the black-box learning problem is posed is incredibly naïve. The most obvious flaw in the formulation is that the task is episodic. An episodic task refers to a problem which has a clearly defined initial and terminal state. An example of an episodic task is chess, where an individual game ends in checkmate. Once the game has ended (i.e. after checkmate), a new game begins and the previous game does not affect future games. However, if an agent were to learn on raw time series, it would have no clue as to when one game ends and when the next one starts. In other words, by defining a static temporal window, the black box method formulated above is forced to also consider data from previous episodes in its learning. This further complicates an already complex learning task.

The realization of the episodic nature of the task allows for meaningful features to be extracted from the time series. More specifically, four features are extracted in this example: (1) initial state of the storage after a reheat cycle (i.e. the mid-point temperature), (2) time elapsed since the last reheat cycle, (3) hot water consumption since the last reheat cycle, and (4) ambient temperature conditions (only for the heat pump model). This leads to a feature set which is roughly two orders of magnitude lower than for raw time series learning, which additionally also help reduce the dimensionality of the input feature vector and circumvents the curse of dimensionality. On the other hand, manual feature extraction detracts from the purely data-driven motivation. However, it compensates for this limitation by further improving the interpretability of the learned model, which is a common problem for black-box methods.

The initial predictions of the neural network before substantial amounts of data have been gathered is usually a contentious issue (as shown in Fig. 36). Two methods can be brought to deal with this. The first is a domain specific algorithm which makes use of constraints imposed on the function learnt by the neural network. These constraints include:

1. Temperature is assumed to monotonically increase with storage height; thus $T_h \leq T_{h+x} \forall x \geq 0$.
2. The water temperature in the storage is always bounded between a lower bound T_b and an upper bound T_u , i.e. $T_b < T_x < T_u$ [$^{\circ}\text{C}$] $\forall x$ where $T_b = 0$ [$^{\circ}\text{C}$] and $T_u = 100$ [$^{\circ}\text{C}$]; even stricter bounds can be introduced by observing that a residential water vessel invariably operates between $10 < T_x < 65$ [$^{\circ}\text{C}$] $\forall x$
3. $T_x \rightarrow T_b \forall x$ as w (the cumulative water consumption) $\rightarrow \infty$ (without reheating the vessel), where T_b is the lower bound as defined above

The second is a principled transfer learning approach which operates either through feature or parameter sharing (Ruder et al., 2017) (Pan et al., 2010). These approaches are explained in greater detail in the results section.

Finally, it is important to keep in mind what the neural networks are actually learning. The storage model learns the temperature distribution in the vessel as a function of thermodynamic and mixing losses, given a certain initial condition. This temperature distribution is then thresholded to obtain a state of charge (i.e. the amount of hot water above a certain temperature threshold). The heating model, on the other hand, learns the amount of energy which would be required to reheat the storage in a given state of charge and ambient conditions.

7.4 Results

This section presents results from applying the formulation presented above on the two different hot water systems. First, the application of the algorithm to the storage model is discussed, which is, in a way, an easier learning problem because of an abundance of data. The heating model is more difficult to learn accurately because the training examples available for this is typically two orders of magnitude fewer than for the storage model. This is because, in a day, there are only a few – usually not more than two or three – reheat cycles but the temperature recordings are made every 5 to 15 minutes.

7.4.1 Storage model

Benchmark black-box

Fig. 37 presents the result of predicting the mid-point temperature in the storage vessel with a neural network trained on increasing amounts of gathered data in a household (1 week, 4 weeks and 32 weeks). While the performance improves over time as more data becomes available to the neural network, the predictive accuracy continues to be low, as evidenced by the poor correlation between predicted and observed temperatures.

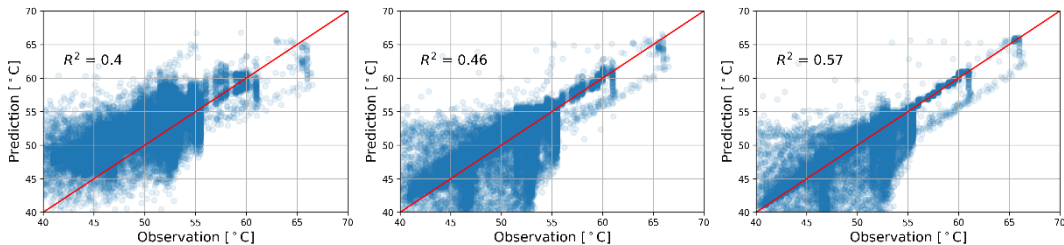


Figure 37 Storage vessel model accuracy with raw time series learning for increasing amounts of data (1 week, 4 weeks, and 32 weeks).

Transfer learning with benchmark

The realization that all individual households are trying to learn the same dynamics model (within the same project) can be leveraged to apply transfer learning. In this case, the gathered features from individual households are combined together to form a single feature vector which is then used to learn the shared dynamics model for all households. As seen in Fig. 38, increasing the data weeks used for learning a model improves its accuracy (or the variance it can explain in the observed data) but only up to a certain extent before asymptoting. In this way, only one of the three benefits (improved initial performance) of transfer learning is achieved (Fig.36).

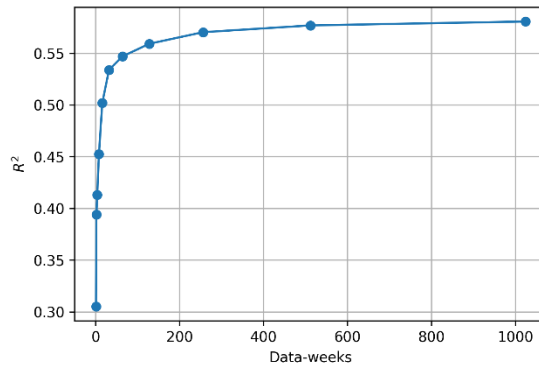


Figure 38 Storage model accuracy with raw time series learning incorporating transfer learning – data-weeks here represents amount of data in weeks used to train the neural network, the source of the data can be from different households achieving transfer.

Extracting features

By reducing the dimensionality of the input feature vector from 288 to 3 (i.e. applying the feature transformations as explained in the previous section), the learning problem is simplified considerably. This is reflected in the improved accuracy of the learned storage model. It also considerably simplifies the calculation of state of charge from the predicted temperature. The extracted state of charge according to the learned model is presented in Fig. 39 as a function of elapsed time and hot water consumption. It is obvious that the neural network has not converged to a reliable model after only a single week of data collection for a single household. However, either increasing the collected data for the single household or increasing the number of households but limiting the data gathering period accelerates the learning process and allows a reliable dynamics model to be learnt.

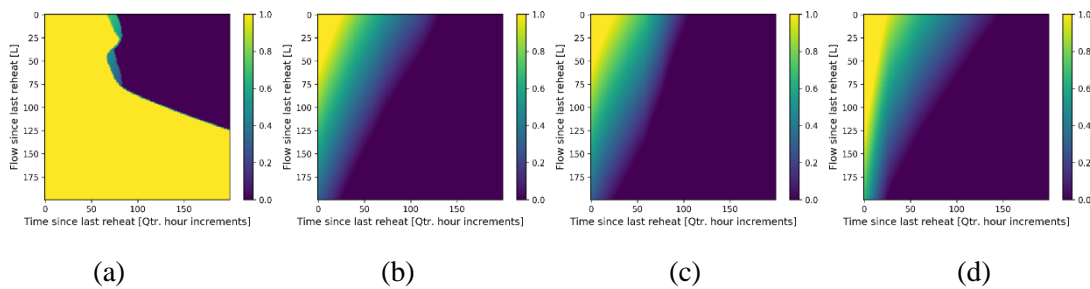


Figure 39 Estimated state of charge as a function of user hot water consumption and thermodynamic losses; the models having been learned with: (a) one week of data for one household; (b) 32 weeks of data for one household; (c) one week of data for 32 households; (d) 32 weeks of data for 32 households.

Adding constraints

While the model converges after only a single week when the neural network has access to data from multiple households, this is not always the case. For instance, as opposed to the 32 houses used for learning the state of charge profile in Fig. 39, only four to eight houses were available in the second project considered in this example. To learn a reliable dynamics model in this case would require a few months at least. However, by leveraging constrained learning, as explained in the previous section, it is possible to learn a reliable model in a very brief amount of time (and data). These results are highlighted in Fig. 40 where it is evident that a smooth state of charge profile is obtained after only a single week of data collection. These state of charges are, on average, accurate to within 10% of the actual state of charge in regions of interest.

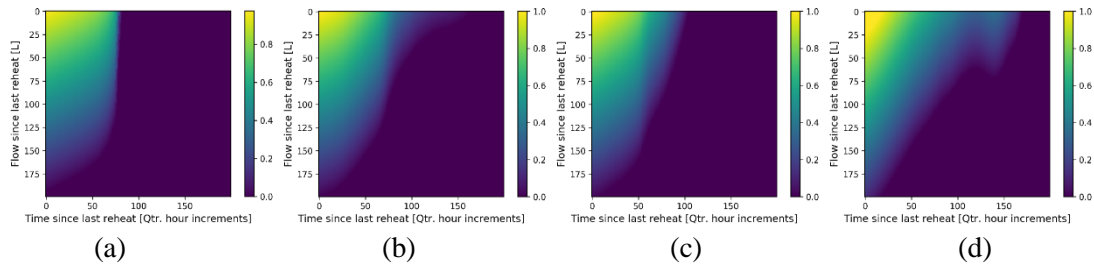


Figure 40 Estimated state of charge as a function of user hot water consumption and thermodynamic losses after constraints have been imposed; the models having been learned with: (a) one week of data for one household; (b) 32 weeks of data for one household; (c) one week of data for 32 households; (d) 32 weeks of data for 32 households.

It is also instructive to summarize the effect of increasing agency and time on the learning model accuracy. This is highlighted in Fig. 41 where it is easy to see that increasing agency and data collection have largely the same effect. This means that gathering data for the learning function for months in a single household can be replaced by collecting data in multiple households for a very brief amount of time. Of course this result holds only for homogeneous devices, but it can also be extended to heterogeneous devices, as we show in the next section. It is also fairly easy to see that while transfer learning allows for a much improved initial performance, the asymptotic performance is not too different.

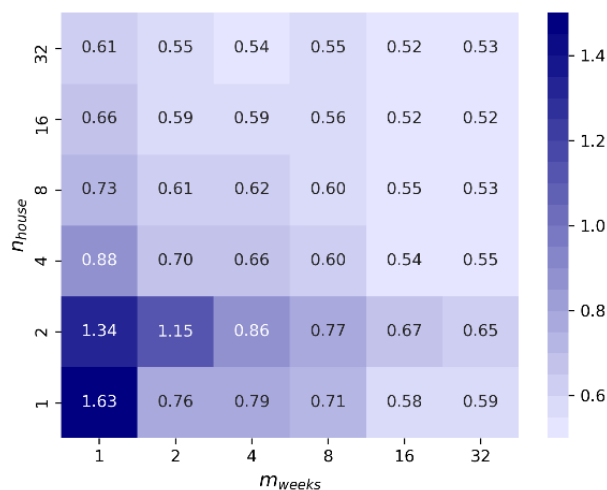


Figure 41 Mean Absolute Error [$^{\circ}\text{C}$] as a function of increasing data collection (weeks) and agency (households).

7.4.2 Heating model

As mentioned previously, the biggest challenge to model the heating element accurately arises from the very limited training dataset the learning algorithm has access to. Practically, this means that the learning algorithm has ten or fewer training examples after a week of interacting with the system. For data-intensive algorithms like deep neural networks, this leads to severe overfitting (Goodfellow et al. 2016), especially when the deep neural network is using the raw time series as its input feature vector. In this case, the dimensionality of the input feature vector is one to two orders of magnitude higher than the number of examples available for learning. This seldom, if ever, works well in practice. Indeed, the neural network failed to converge using raw time series data alone, with or without transfer learning.

Extracting features

As before, to model the heating element, the extracted input feature vector is fed to the neural network which predicts the energy required to reheat the storage given different ambient conditions. On average, this energy is between one and two kWh's (however this can vary considerably as a function of the storage's state of charge and the ambient conditions). Unlike the raw learning case, the model successfully learns to predict the heating element's behavior. This prediction grows progressively better as the agent observes more data. Additionally, the effect holds also as the number of agents (or households involved in the learning process) increases. However, unlike the case of the storage element, the heating model continues to improve until all the gathered data has been used. In this case, transfer learning leads to both improved initial and asymptotic performance (as highlighted earlier in Fig. 36). It is important to note that without transfer, a single household would never have access to almost 20 years of data collected across different devices (which is the amount of data used in this example to make predictions). This information is highlighted in Fig. 42 where it is easy to see that the error rate continues to drop as we increase the amount of data (either through observation period or the number of households).

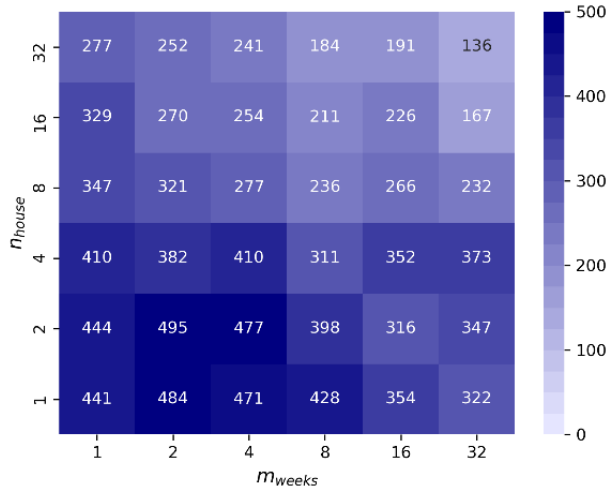


Figure 42 Mean Absolute Error [kWh] as a function of increasing data collection (weeks) and agency (households).

An interesting caveat arises here as, unlike for the storage model, the model improves more significantly for a longer data gathering period with fewer households than it does with additional households with fewer data gathering (i.e. learning a model with data collected for one household over 32 weeks results in a better model than one learnt with data collected over 32

households for one week). This is because of better exploration of ambient conditions over 32 weeks (i.e. the model observes heat pump performance under different conditions) than it does in only one week, even though multiple households are observed.

Induction

The heating model was eventually able to learn an extremely accurate representation of the heat pump (with a relative error less than 10% which is normally distributed). However, it takes almost 20 data-years to do so, implying that a more data-efficient representation can further improve real world learning performance. In the case of the storage model, this was done through constrained learning. However, instead of constraining model output – which requires some domain knowledge – it is also possible to achieve the same effect by induction. This refers to the fourth case of transfer learning highlighted above, where the conditional probability distribution of the source and target are different.

Induction can be achieved by making use of the data gathered in one project in a different project where the hot water system is different by nature. In practice, induction learning can be achieved in one of two ways:

1. Feature sharing: where the input and output feature dimensionality is the same for the source and target, it is possible to simply combine the training features of the source and target to learn a single, unified representation (Pan et al., 2010). It is possible to further select the features based on some metric for similarity or diversity etc. (Ruder et al., 2017).
2. Parameter sharing: it is also possible to use the neural network already trained on the source task as the initialization for the target. In this case, the neural network weights are fine-tuned with target data (i.e. learning is done with a very small learning rate), while possibly freezing one or more layers in the neural network to preserve already learnt knowledge (Pan et al., 2010).

Achieving transfer with either of these two approaches is an active area of research and represents state of the art in many computer vision and natural language processing tasks. In this example, the performance of both types of induction is compared and from Fig. 43, it is obvious that parameter induction (i.e. initializing the neural network with previously trained data) outperforms naïve feature induction. Both are substantially better than the model learnt using just the target data (i.e. project 2). This effect is especially pronounced in the early stages of data collection.

In this case, the workflow for feature sharing is as follows: the training data gathered from project 1 is combined with training data from project 2, which is then used to train a neural network. The workflow for parameter sharing is more involved as first a neural network is trained on the already available data from project 1. Then this neural network is used as the initialization for project 2 where observed data is used to fine-tune the neural network weights through backpropagation (Goodfellow et al. 2016). Results of both these induction learning algorithms are compared with a neural network which is initialized randomly but then sees only the target data (i.e. for project 2). It is obvious that pre-training the neural network drastically speeds up real world performance and reduces data requirements by over an order of magnitude making it realistic to model the heating element through sensor data alone.

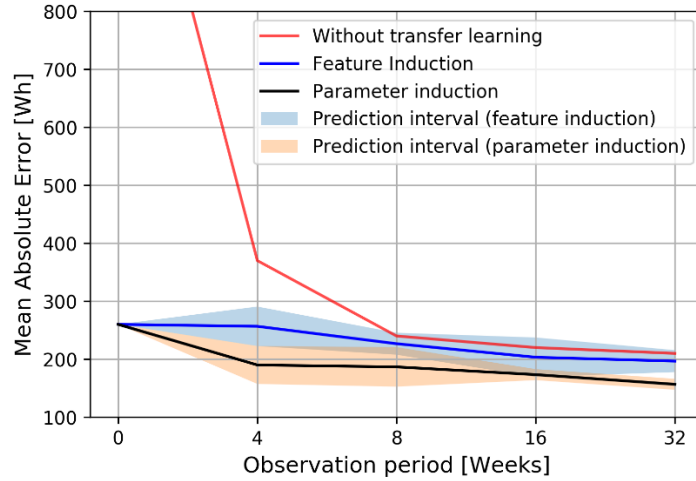


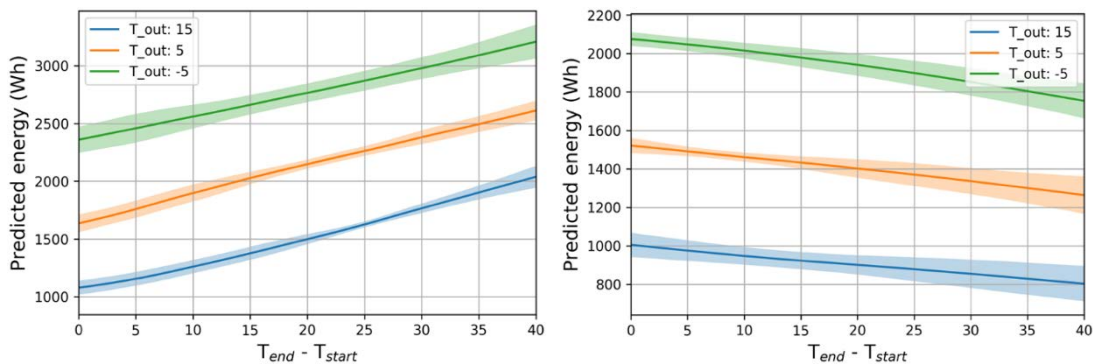
Figure 43 Mean Absolute Error [°C] as a function of increasing data collection (weeks) and different learning frameworks

Thermodynamic validation

While the prediction error in this case is much lower than the benchmark, it is not obvious whether the neural networks learned using data alone can generalize beyond the training and test set. For this, a specifically created test dataset was considered based on evaluating thermodynamic principles. The purpose of this test is to identify whether the model has learnt three properties based on known thermodynamics:

1. As the ambient temperature increases, energy consumption of the heat pump decreases ($T_{out} \uparrow, \hat{E} \downarrow$)
2. As the temperature difference between the start and end of the reheat cycle increases, energy consumption of the heat pump increases ($\Delta T \uparrow, \hat{E} \uparrow$)
3. As the target temperature increases, energy consumption increases ($T_{end} \uparrow, \hat{E} \uparrow$)

As evident from Fig. 44, the model learnt without induction has been able to learn only two of the three fundamental properties correctly after 32 weeks of data collection. This includes arguably the most important property that a higher temperature difference between start and end temperature leads to a higher energy consumption. On the other hand, agents making use of induction were able to learn (retain) all three properties correctly from the source task within four weeks.



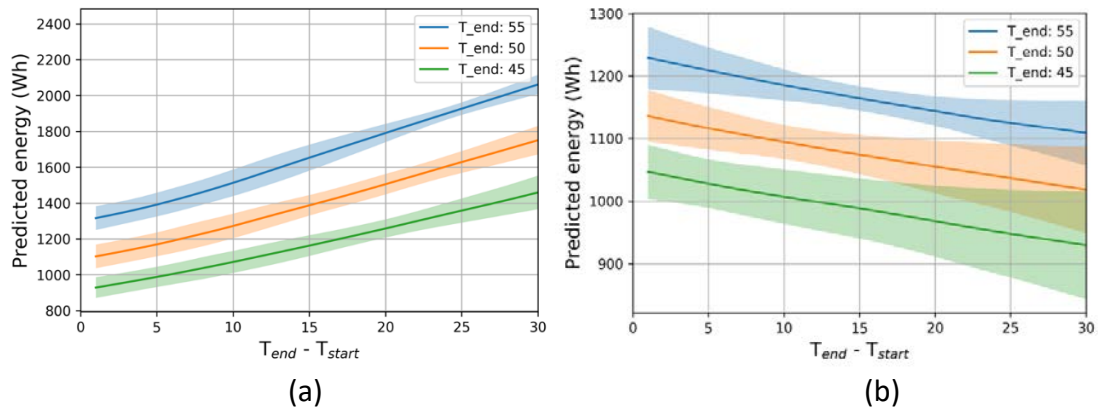


Figure 44 Results of learning with and without induction learning for the heating model; results shown here are to visualize the trends of the learned model for (a) with induction for 2 agents after 4 weeks, and (b) without induction with 2 agents after 32 weeks; the heating temperature (T_{end} is limited to 55°C, above which a booster heater is used to reheat the hot water.

7.4.3 Extension to active control

The models learned in this way were combined with a smart controller to improve the energy efficiency of operation in real world Net-Zero Energy Buildings in The Netherlands (Kazmi et al., 2019). After 11 months of operation, the smart controller resulted in savings of, on average, over 200 kWh / household. In relative terms, this was over 20% of the energy required for the domestic hot water production and reflected the importance of learning accurate dynamics models from data, i.e. without incurring the costs of domain expertise or sensing. The key results of this control are highlighted in Fig. 45, which shows that the energy efficiency group consistently consumed less energy for hot water production than their counterparts employing a naïve rule-based controller. These results were generated after accounting for differences in individual household hot water demand and are aggregated for tens of houses in both category.

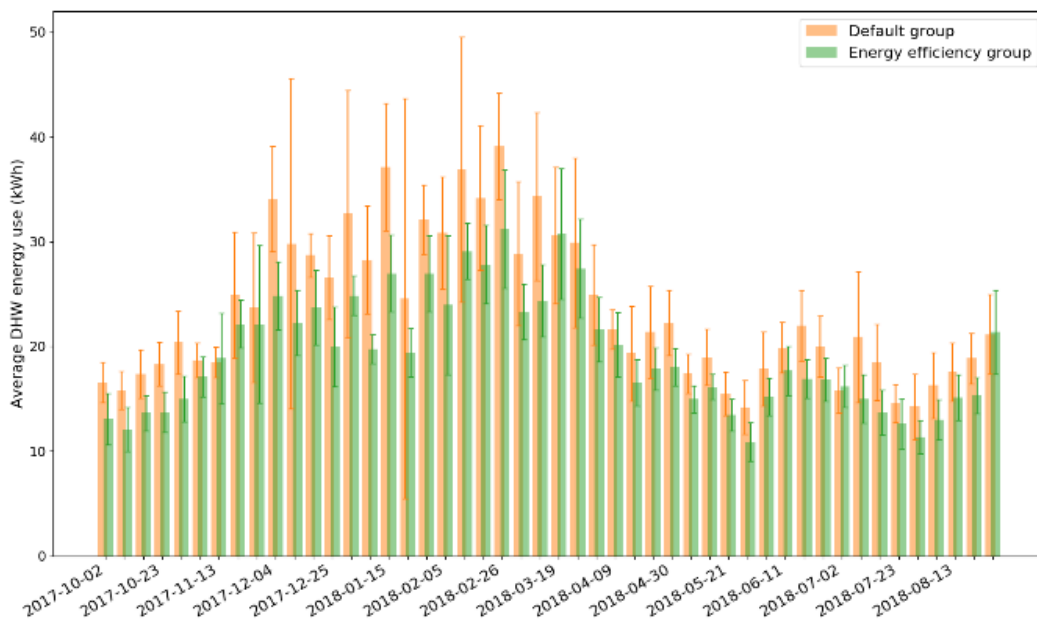


Figure 45 Results of using the developed models to active control of hot water systems.

7.5 Conclusion

This example has presented the methodology and results for modelling a hot water system in detail. The proposed methodology is completely generalizable and avoids most of the limitations of existing white- and black-box methods. The proposed transfer learning technique is, in a way, similar to existing grey box models in the sense that an existing model is calibrated with newly acquired data. However, the innovative part is that the initial model is completely data-driven, thereby removing both human dependence and bias from the modelling process.

The models thus learned can be used seamlessly to both predict and realize energy flexibility in practice. For instance, the developed model has been used extensively in The Netherlands in a large scale H2020 Project REnnovates. The learned models were employed first in a planning step to determine whether or not grid reinforcement would be required with continuing electrification of heat. This will become a more important concern in the future as many neighbourhoods sever the connection to the gas grid and opt for electric heating and hot water production. Concurrently, the models described in this study can also be used to estimate whether the flexibility inherent in the hot water systems can provide adequate demand response to the grid. In doing so, it allows the practitioner a straightforward way to analyse both the causes and potential solutions to the electrification of heat and proliferation of distributed energy resources. As a practical example, employing the flexibility predicted by the models described in this study resulted in savings of many thousands of euros and substantial amounts of greenhouse gas emissions, without compromising user comfort in any way.

7.6 Reference

Afram et al. 2014. Theory and applications of HVAC control systems—A review of model predictive control (MPC). *Building and Environment* 72, 343-355.

Chollet 2015. Keras. <https://keras.io/>

Goodfellow et al. 2016. *Deep learning* (Vol. 1). Cambridge: MIT press.

Hensen, 2012. *Building performance simulation for design and operation*. Routledge.

Kazmi et al. 2016. Generalizable occupant-driven optimization model for domestic hot water production in NZEB. *Applied Energy*, 175, 1-15.

Kazmi et al. 2018. Gigawatt-hour scale savings on a budget of zero: Deep reinforcement learning based optimal control of hot water systems. *Energy*, 144, 159-168.

Kazmi et al. 2019. Multi-agent reinforcement learning for modeling and control of thermostatically controlled loads. *Applied Energy* 238, 1022-1035.

LeCun, Y., Bengio, Y., & Hinton, G. (2015). Deep learning. *nature*, 521(7553), 436.

Pan et al. 2010. A survey on transfer learning. *IEEE Transactions on knowledge and data engineering*, 22(10), 1345-1359.

Markovic et al. 2017. Application of Support Vector Machine for Predicting the Performance of Air-Source Domestic Hot Water Heat Pump Systems. *IBPSA Building Simulation*.

Ravi, S., & Larochelle, H. (2017). Optimization as a model for few-shot learning. In *Proceedings of the 5th International Conference on Learning Representations (ICLR)*.

Ruder et al. 2017. Learning to select data for transfer learning with Bayesian Optimization. *arXiv preprint arXiv:1707.05246*.

Ruelens et al. 2014. Demand response of a heterogeneous cluster of electric water heaters using batch reinforcement learning. Power Systems Computation Conference (PSCC), (pp. 1-7)

7.7 Relevant publications

More information on this study can be found in Kazmi et al. 2019. Multi-agent reinforcement learning for modeling and control of thermostatically controlled loads. Applied Energy 238, 1022-1035.

8. Development of a simulation based design optimization approach for grid independent houses with integrated energy flexibility metrics



Picture is taken from: <https://www.rvo.nl/sites/default/files/bijlagen/4.%20Brochure%20Voorbeeldwoningen%202011%20bestaande%20bouw.pdf>

Institution

Section of Building Performance,
Department of the Built Environment,
Eindhoven University of Technology



Contact persons

Zahra Mohammadi
Z.mohammadi@tue.nl

Dr. Pieter-Jan Hoes
p.hoes@tue.nl

8.1 Modelling objective

This study focuses on the design of a method that can be used to compare the energy flexibility of the performance of overall building designs, including all elements together from thermal mass, electrical storages and the building energy system. Hence, it provides the opportunity to compare different designs in terms of energy flexibility and other desirable performance indicators.

This study proposes a computational performance assessment methodology that integrates relevant energy flexibility indicators regarding energy matching and grid interaction. Furthermore, this study shows how the assessment methodology can be used to design future-proof grid independent buildings by considering various policy scenarios (support schemes). The proposed design optimization approach is demonstrated using a case study of a Dutch (residential) house and the building owner as the main decision maker/stakeholder.

The energy flexibility of single buildings is defined as the ability of a building to manage its load and generation in a way to increase self-consumption and reduce dependency of the energy grid. This methodology integrates uncertainties due to policy scenarios in multi criteria assessment to aid decision makers in selection of robust design options.

8.2 Building and system description

The simulation uses a detailed TRNSYS model of the house, the grid-tied solar system (composed of PV panels, charge controller, inverter and battery bank), as well as an all-electric HVAC system (Air to water heat pump system).

In this study a typical Dutch residential, semi-detached terraced house from 1975, [1] is chosen as the case study building. The building is a heavyweight three-floor construction as shown in Figure 46. Each floor is considered as one thermal zone for calculating the temperature and energy demand of each zone. The living room and kitchen at the ground floor form the first zone, three bedrooms in the first floor constitute the second zone, and the attic in the second floor is the third zone.

Heating is supplied by an air source heat pump and the building is ventilated with balanced mechanical ventilation with a heat recovery unit. Natural ventilation (free cooling) is used in summer instead of mechanical cooling [2].

The domestic hot water (DHW) needs are met either by a standalone solar thermal collector system with an auxiliary heater or a gas boiler. In case of solar thermal collector a storage tank of 200 L with an auxiliary immersion heater of 2 kW capacity is used in this study.

A photovoltaic system with a module efficiency of 18.3% and an inverter with a conversion efficiency of 97.5% were chosen in this study and modelled in TRNSYS. Each panel has a gross surface area of 1.67 m² and a peak capacity of 260 Wp.

8.3 Method and modelling tools

The proposed design optimization approach consists of three main steps. These steps are presented below:

- 1a. Identify the decision makers' preferences and define the relevant performance indicators including energy matching and grid interaction performance indicators.
- 1b. Define the design space, e.g., define the possible renovation measures that should be considered (variations in building envelope properties, HVAC systems, size of onsite-energy generation system and storage systems).

- 1c. Formulate the future scenarios, e.g., in this study based on the various support schemes.
2. Predict the performance of each design solution in the design space using building performance simulation and calculate the performance indicators across all future scenarios.

In this study the performance of each design is predicted using the building performance simulation tool TRNSYS. The performance of each design is assessed based on the defined performance indicators and the energy matching and grid interaction performance indicators. The performance indicators are often conflicting, therefore, a multi-objective optimization approach with the objectives to minimize (or maximize) each indicator is applied. For example, the building owner would like to maximize thermal comfort, but at the same time, he would like to minimize the operational costs.

3. Analyze and present future-proof building designs with low grid dependency using multi-criteria decision making.

Due to the conflicting nature of most indicators, a set of Pareto optimal solutions is obtained for each scenario. This enables the decision maker to perform a trade-off among alternative design solutions based on the preferred performance indicators. Depending on the selected performance indicators, the set of Pareto optimal solutions can vary per scenario.

It is assumed that the probabilities of the occurrence of the scenarios is unknown and hence, it is essential to assess the performance robustness of the design solutions considering all scenarios. The minimax regret method [2] is used to calculate the performance robustness of each Pareto. The Pareto solutions are presented using scatter plots and box plots to show the values for each design parameter.



Figure 46 Layout of a typical Dutch terraced house, showing different floors, front and back view of the building. All dimensions are in mm.

8.3.2 Identify decision makers and performance indicators

The decision maker of this case study is the homeowner. The homeowner wants to renovate his house and requires a comfortable indoor environment at low investment and operating costs. The considered performance indicators are described in Table 8. In order to assess the energy matching and grid interaction of each design the indicators, as described in Table 9, are defined.

Table 8 Overview of thermal comfort and costs performance indicators.

Name	Mathematical description	Characteristic
Weighted overheating hours (WTOH)	$WTOH = \Delta T * h$ <p>h: total number of hours exceeding the allowable maximum indoor temperatures ΔT: degree of temperature excess</p>	Indicating number and magnitude of hours exceeding the allowable indoor temperatures, based on maximum and minimum acceptable indoor temperatures as proposed on [3]
Operational cost (OC)	$OC = (E_{import} * P_E + NG * P_{NG}) - (E_{inc} * P_{inc})$ <p>E_{import} : imported electricity from grid, P_E: price of electricity, NG: natural gas, P_{NG}: price of natural gas, E_{inc}: type of energy receives incentive, P_{inc}: rate of incentive</p>	Annual energy costs for gas and electricity consumption. Exported or self-consumed electricity is also considered in the calculation of operating cost, depending on the policy scenario
Additional investment cost (IC_a)	$IC_a = \sum IC_{design\ options} - \sum IC_{reference\ building}$	Additional amount of required investment by a design compared to the reference building

Table 9 Overview of energy matching and grid interaction performance indicators.

Name	Mathematical description	Characteristic
On-site Energy Matching (OEM)	$\frac{self - consumption [kWh]}{on - site\ generation [kWh]}$ <p>Self-consumption and on-site generation are integrated over summer months</p>	Describe the degree of the utilization of on-site energy generation related to the local energy demand [4].
On-site Energy Fraction (OEF)	$\frac{self - consumption [kWh]}{Energy\ demand [kWh]}$ <p>Self-consumption and energy demands are integrated over winter months</p>	Show the effectiveness of on-site generation, how often demand is lower than supply and how often supply is lower than demand.
Grid dependency [5]	$\frac{\Gamma_{power\ exchange \neq 0}}{\Gamma_{total}}$ <p>Γ : number of time</p>	Represents the frequency of either positive or negative power exchange between a building and the power grid.
Capacity factor [6]	$\frac{energy\ exchange\ with\ the\ grid [kWh]}{nominal\ connection\ capacity [kW] * period [h]}$	Indicates the total energy that has been exchanged with the grid (either supply to or import from the grid) in ratio to nominal connection capacity

8.3.3 Defining design space

Different design options, as shown in Table 10, are varied to form the design space. In order to satisfy different building standards, design options related to building envelopes such as window

type, insulation level of envelopes and infiltration rates are altered at the same time and formed different renovation packages. First renovation package, RP1, meets the energy label B requirements. RP2 is based on the current Dutch building standard [7]. RP4 and RP5 can meet Dutch zero-energy buildings standard [1] and a Passive house standard in respect. Hence, the air to water heat pump system is sized for each building envelope package. Other design options such as size of PV system, size of electrical battery and type of DHW system are varied for all building envelope packages.

PV panels with a module efficiency of 18% and an inverter with a conversion efficiency of 97.5% are chosen for the on-site energy generation system [8]. The size of PV system is varied from 5m² to 25 m² for all building envelope packages where the maximum size of PV system is limited by the available roof area on the south surface. Each panel has a gross surface area of 1.67 m² and a peak capacity of 260 Wp. As it is shown in Table.9, the sizes of the electrical battery capacity [9], with 2.5-3.3 kW charge and discharge power, is changed for each building envelope packages.

Two different systems are assumed to meet the domestic hot water (DHW) needs, one is a standalone solar domestic hot water system with an electrical auxiliary heater and the other one is a gas boiler. Both solar thermal collectors and photovoltaic panels are placed at a tilt angle of 43° facing south, which is also the slope of roof.

Table 10 Design parameter options considered in this study

Renovation package	Reference	RP1	RP2	RP3	RP4	RP5
RC-floor, m ² k/W	1.3	2.5	3.5	5	6	10
RC-wall, m ² k/W	1.3	2.5	4.5	7	8.5	10
RC-roof, m ² k/W	1.3	2.5	6	8	10	10
Window U value, W/m ² K	5.2, 2.9	1.8	1.43	1.01	0.86	0.52
Window g value	0.81, 0.75	0.61	0.60	0.38	0.59	0.58
Infiltration, dm ³ /sm ²	1	0.62	0.5	0.4	0.15	0.1
ASHP nominal capacity, kW _{th}	9.1	7.4	6.0	4.9	4.0	3.5
PV system, m ²	5, 10, 15, 20, 25					
Electric battery, kWh	0, 2.5, 5, 7.5, 10, 12.5, 15					
DHW system	Solar thermal collector (STC), HR 107 gas boiler (GB)					

In this study, the deployed control strategy for load managing between the electric storage, the PV system, the demand and the grid first prioritize to use the produced energy by the PV system to satisfy the demand and then the electric battery will be charged with surplus on-site produced energy. In this mode, if there is no demand and electric storage is fully charged, the surplus electricity will be exported to the grid. In this control strategy, when there is no on-site produced energy, the system supplies the required load by prioritizing to use the energy stored in battery and then import from the grid. This reduces the dependency on the grid, but it will not necessarily minimize the electricity bill since discharging the battery during off or mid peak hours is not always economically beneficial.

8.3.4 Define future scenarios

Various types of support schemes are currently in operation in different countries. Most of the European countries have initially started with production-based support schemes like feed-in tariffs (FiT). In this scheme, the PV system owner receives a fixed rate for each unit of electricity (kWh) fed into the power grid. Other support schemes are based on self-consumption support mechanisms. These schemes are being increasingly promoted in many countries, among others

Germany, Italy, Denmark, Belgium, etc. [10]. In these schemes, energy saving and the use of on-site generated electricity are rewarded instead of rewarding the export of electricity. In these type of schemes, typically the exported electricity is sold at low prices whereas the price of the purchased electricity is high. Therefore, a mismatch between on-site generation and demand can cause a financial loss to the PV owner. Thus when these schemes are in place, it is beneficial for the PV owner to match the building's on-site electricity generation with the electricity demand as much as possible.

The scenarios below are selected to give an overview of possible future policies ranging from production-based support to self-consumption based support schemes. In addition to the considered scenarios, there are investment subsidies, which pay a part of the initial purchase and installation cost of an energy system, without considering the actual operation after the installation [11]. These subsidies are not considered in this case study. The considered scenarios are as follows:

1. Net metering scenario: energy consumption imported from grid and on-site produced energy exported to the grid are measured and their difference determines the electric bill, though negative bills might not be allowed. In this system, exported energy is of equal value to imported energy [11].
2. Guaranteed FiT: a fixed rate is paid for each unit of electricity generated and supplied to the grid.
3. Self-consumption incentives: provide money if locally generated energy being used on-site, instead of being exported to the grid.
4. NO incentive: there will be no incentive for energy fed into grid or used locally.

Table 1 Overview of the policy scenarios and rate of incentives used in this study

Type of support scheme	Policy scenario	Rate of incentive (c€ kWh)	Electricity price (c€ kWh)
Production-based incentive	Net-metering	$\frac{17.06 \text{ c€}}{\text{kWh electricity fed to the grid}}$ As long as : $\sum_{Year} \text{exported}_{energy} \leq \sum_{Year} \text{imported}_{energy}$	17.06
	Guaranteed FiT	$\frac{8.53 \text{ c€}}{\text{kWh electricity fed back to grid}}$	17.06
Self-consumption promoting	Self-consumption based	$\frac{17.06 \text{ c€}}{\text{kWh electricity demand met by own generatio}}$	17.06
	No incentive	$\frac{0 \text{ c€}}{\text{kWh electricity either fed to the grid or consumed locally}}$	17.06

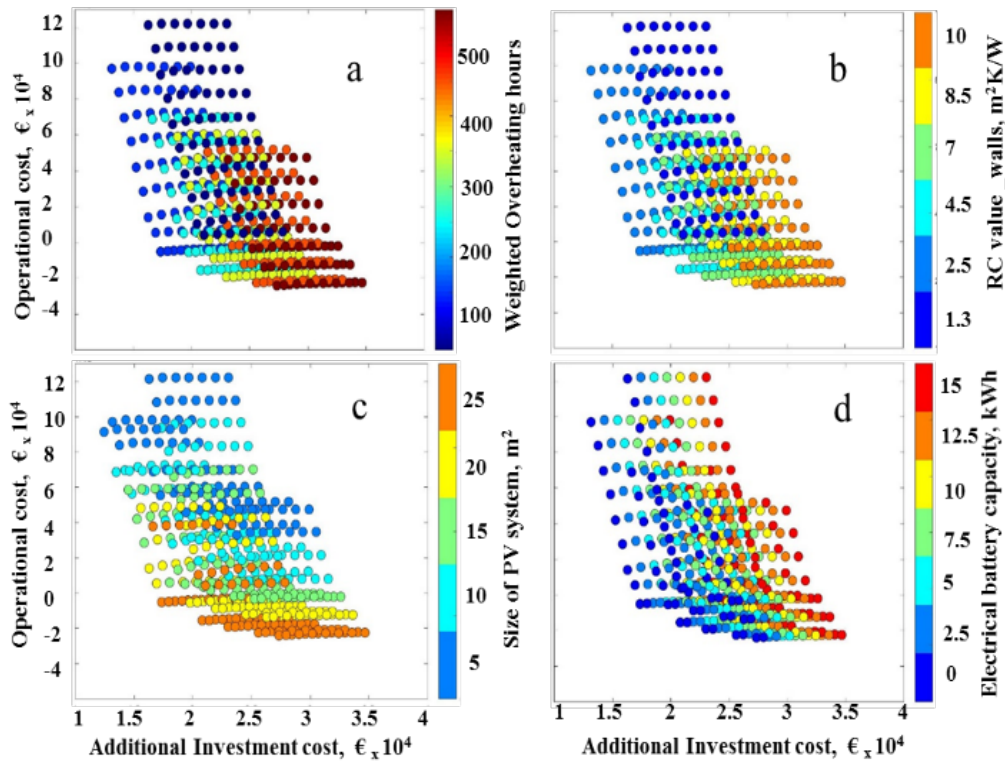


Figure 47 The investment cost and operational cost for total energy consumption of all designs solutions under net-metering scenario.

8.4 Results

8.4.1 Performance prediction and analysis of the design solutions

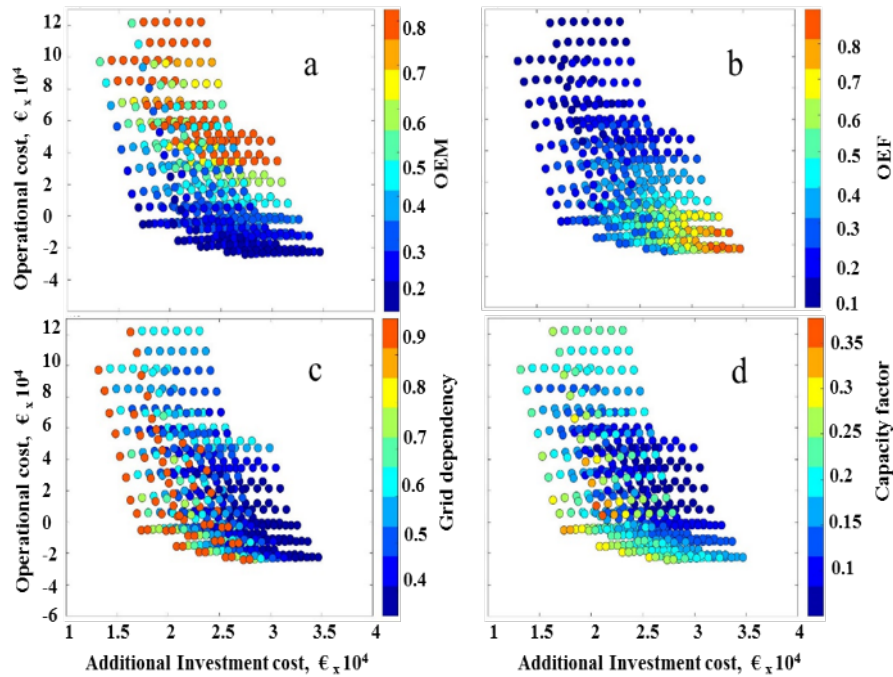
The performance of each design solutions is calculated for all four policy scenarios. However, in this section, first the results are described for the current energy policy scenario in The Netherlands, the net-metering scenario. The results for the other scenarios including the robustness analysis is presented in the next section.

Figure 47a shows the additional investment cost, the operational cost and the weighted overheating hours of all design solutions. Each dot represents the performance of a unique design solution, i.e., a unique combination of the building envelope and infiltration rate, PV system size and electrical storage capacity. To get a better insight of the design variants, RC-values of the walls, the size of PV system and electrical storage capacity are indicated with colors in the scatter plots in Figures 47b, 47c and 47d.

The figures show that the operational cost decreases with higher RC-values and lower infiltration rates, while the number of overheating hours and additional investment cost increases. One can easily distinguish the effect of the size of the PV system on the operational cost; however, the storage capacity does not influence the operational cost for this policy scenario. In this scenario the user will sell the surplus of on-site produced electricity to the grid at the same rate of buying from the grid. Hence, under this policy scenario, the grid is used as a virtual, unlimited electrical storage device. The designs with the variations in electrical storage capacities only differ in investment cost.

Figure 48 shows the energy matching and grid interactions indicators of the design space against the operational cost and the additional investment cost. Comparing Figures 48a and 48b and the

design parameter variations in Figures 47b, c and d, gives some insight about the self-consumption potential of each design solution. The designs with a small PV system reach a higher OEM regardless of the insulation level and infiltration rate of the building (which mainly decide the energy consumption of the designs). However, this happens at the expense of higher operational cost in comparison to the designs with larger PV systems. Designs with high insulation levels [8.5-10 m²K/W] and low infiltration rates show better OEF, since these designs have a very low energy consumption, especially when they are equipped with high number of PV panels and a high electrical storage capacity. These designs operate at very low operational cost; however, they require very high investment cost.



Figures 48c and 48d illustrate the performance of design solutions regarding the frequency and the magnitude of the traded power with the energy grid. Figure 48c shows the effect of the storage capacity on number of times that a design will interact with the grid; designs without electrical energy storage are almost fully dependent on the grid [grid dependency ≥ 0.9].

The figure shows that the dependency on the grid can be reduced to less than 0.5 for the buildings with low energy consumption [8-10 m²K/W] accompanied with large PV systems [20-25 m²] and high storage capacities [10-15 kWh]. The high on-site energy generation can easily meet the demand of these buildings, while the high storage capacity helps to bridge the gap between demand and generation instead of exporting the surplus electricity to the grid.

The effects of building insulation level and the size of the PV system on the capacity factor can be observed in Figure 48d. Designs with high insulation levels typically have low power consumption for space heating demand and consequently the sized air to water heat pumps have low power capacity. These designs along with a small sized PV system use the minimum capacity of the designed power with the grid.

Overall, the designs with low RC-values and high infiltration rates show low overheating hours, but at the expense of high operational cost. Because of their high-energy consumption, they utilize a higher ratio of on-site produced energy (high OEM). However, this is not enough to meet a noticeable amount of energy consumption (low OEF) and consequently they show high and frequent interaction with the grid to satisfy the demand. Similarly, the designs with high RC-values and low infiltration rates (e.g. passive house) are characterized by very low energy

demand, but higher overheating hours. These designs can reach high OEF and very low capacity factors. However, because of the low energy consumption, they do not utilize the on-site production efficiently (low OEM). The designs with intermediate RC-values [2.5-4.5m²K/W] and infiltration rates are having optimal performance in terms of thermal comfort and show moderate operational and investment costs. These designs can utilize on-site production efficiently to meet the demand when they are equipped with appropriately sized of PV systems and storage capacities.

The Pareto solutions (the trade-off solutions; the solutions that perform equally good) can be calculated considering various sets of performance indicators. The dark blue coloured dots in Figure 49.1 show the Pareto solutions in case the homeowner is only interested in operational cost, investment costs and thermal comfort. The cyan coloured dots shows the Pareto solutions in case the homeowner only considers the energy matching and grid interaction indicators. As expected, these two sets of Pareto solutions are quite different under this net-metering scenario, since the scenario does not provide any (financial) incentive to the homeowner to invest in a house with low grid dependency.

8.4.2 Building performance considering all policy scenarios

The previous section showed that there was no incentive for the homeowner to consider low grid-dependency. However in the future the policy scenario is likely to change. This section shows the performance of the design solutions considering all four policy scenarios. Furthermore, it is discussed which design solutions are the most robust performing considering these scenarios.

As discussed above, Figure 49.1 shows the two Pareto solution sets considering policy scenario 1. The Pareto sets for scenarios 2, 3 and 4 are presented in Figures 49.2, 49.3 and 49.4.

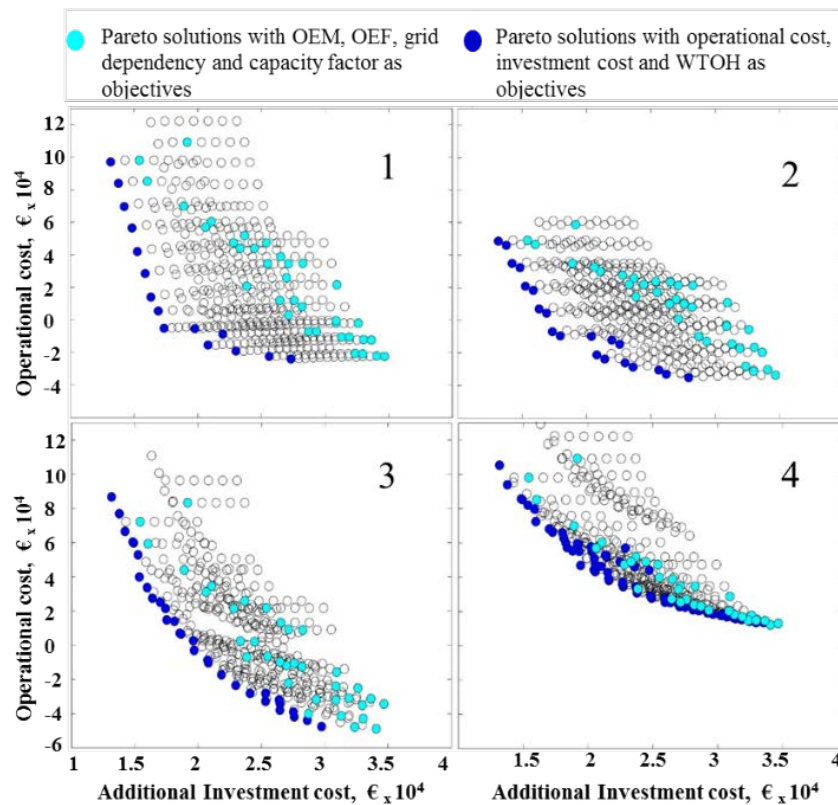


Figure 48 Two sets of Pareto solutions are presented per graph: dark blue dots represent the Pareto solutions based on operational cost, investment cost and overheating hours. Cyan colored dots represent the Pareto solutions based on the energy matching and grid.

The figures show that the gap between the two Pareto sets is more significant in scenarios 1 and 2 (Figures 49.1 and 49.2), which indicates that the solutions with low grid-dependency are

not (financially) attractive to the homeowner under these production-based incentive policies. The reason is that, in these scenarios by selling back the produced energy to the grid, the homeowner can significantly reduce the operational cost. The two sets of Pareto solutions come closer in Figure 49.3, the self-consumption based incentive, and even closer in Figure 49.4, where there is no incentive at all. In these scenarios the more profitable designs for the homeowner are also the ones with higher self-consumption, i.e., lower grid-dependency

Figures 50 and 51 present with colours the values of the design parameters for the solutions of both Pareto sets. The Pareto solutions based on additional investment cost, operational cost and overheating hours are represented with the coloured dots with light-grey edges (from here on referred to as the homeowner set).

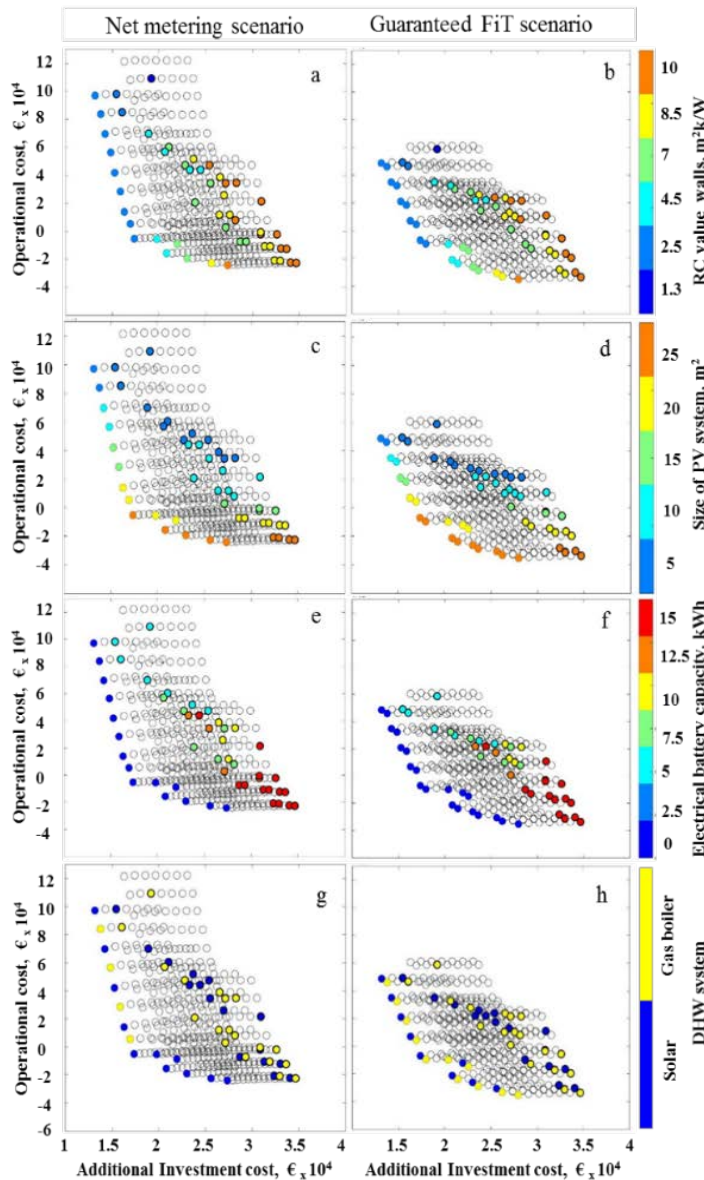


Figure 49 Two sets of Pareto solutions for the production-based incentive policies (scenarios 1 and 2). Dots without edge represent solutions based on additional investment cost, operational

cost and overheating hours. Dots with black edged-lines represent solutions based on energy matching and grid interaction.

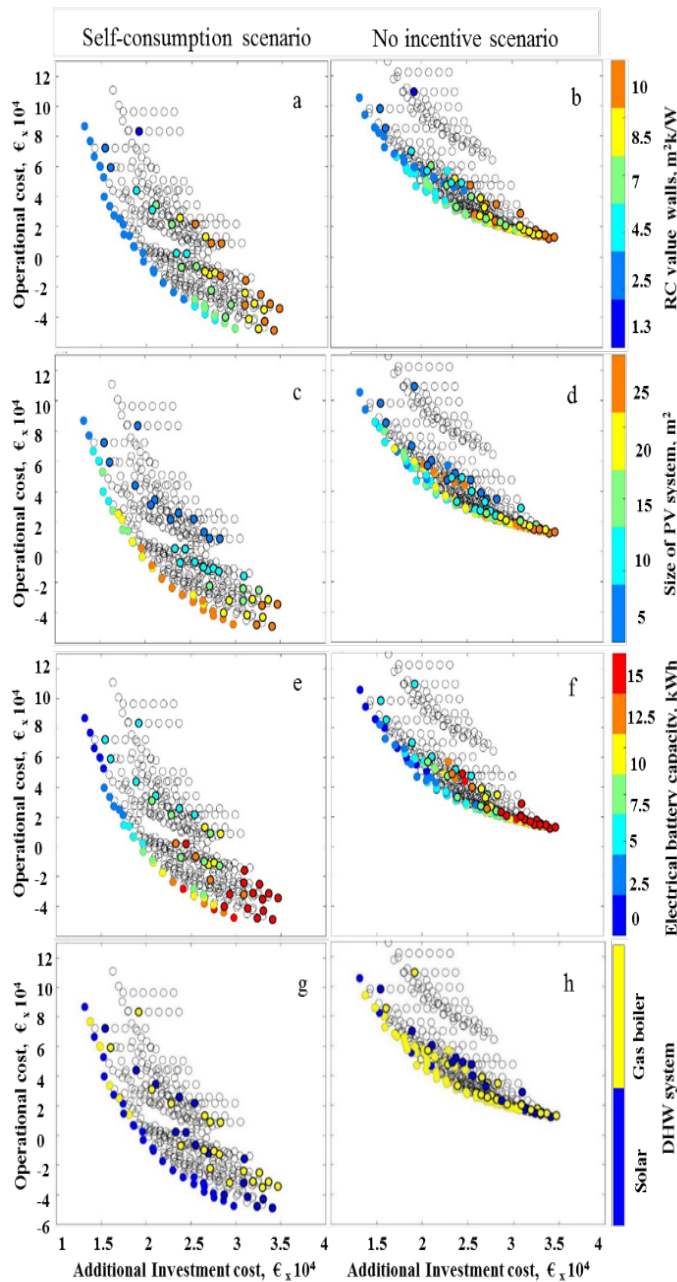


Figure 50 Two sets of Pareto solutions for the self-consumption-based incentive policies (scenarios 3 and 4). Dots without edge represent solutions based on additional investment cost, operational cost and overheating hours. Dots with black edged-lines represent solutions based on energy matching and grid interaction.

The Pareto solutions based on energy matching and grid interaction are represented with coloured dots with the black edges (from here on referred to as the energy flexibility set or EF set). It can be inferred from Figures 50a, 50b, 51a and 51b that the Pareto solutions for the homeowner set are dominated by intermediate insulation levels [2.5-4.0 m²k/W] across all scenarios, i.e., the blue coloured dots dominate the Pareto fronts. These designs show a trade-off between thermal comfort and operational and investment cost. The Pareto solutions of the EF set show a

larger variation of insulation levels; however, the majority of the designs is based on high insulation levels and low infiltration rates. In production-based incentive policies, Figure 50, the operational cost decreases with larger PV systems. Since there is a financial compensation for every kWh of on-site produced electricity fed into the grid, the solutions in the homeowner set show zero storage capacities and large PV systems. Figure 51 shows that in the self-consumption-based policies, the size of storage capacity in homeowner Pareto set increases with the size of PV system in order to increase the self-consumption of on-site produced electricity consequently reducing the operational cost.

8.4.3 Future-proof building designs with low grid dependency considering all policy scenarios

Some design parameters can be replaced relatively easy at any time, such as the size of the electrical storage, while some other design parameters are not easy to change after the renovation, such as the building insulation level. Accordingly, it is useful for the homeowner to understand how robust each design option performs across the policy scenarios. This information is provided by calculating the performance regret for each solution. Figure 52 shows the influence of a chosen design parameter value on the predicted performance of the other homeowner Pareto set solutions.

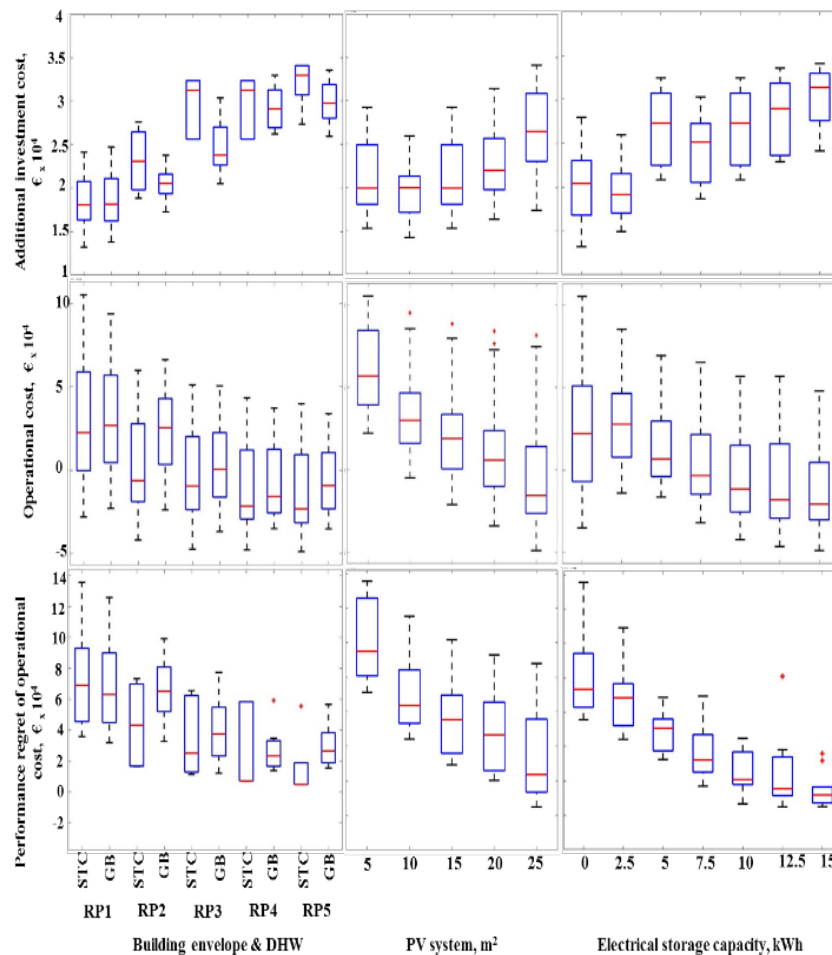


Figure 51 The boxplots show the performance spread for a design parameter value caused by variations in all the other design parameters and by the scenarios. The presented solutions are from the homeowner Pareto set.

Each boxplot show the performance spread for a design parameter value caused by variations in all the other design parameters and by the scenarios. For example, the first boxplot (RP1-STC) is the building design with Renovation Package 1 (RP1) equipped with a Solar Thermal Collector (STC) connected to the DHW system. The performance spread is caused by the variations in the remaining design parameters, in this case by the PV system sizes and the battery sizes. The figure shows that the performance regret of the operational cost decreases with larger sized PV systems and larger electrical storage capacities (bottom graph), which is because by the increase in utilization of on-site produced electricity. It can also be observed that designs with a gas boiler DHW system result in lower performance regrets across the considered scenarios for RP3 and RP4 in comparison to designs with solar DHW system. Designs with higher insulation level and lower infiltration rates have generally lower space heating demands, hence the share of energy consumption due to DHW demands are getting more weight in total energy consumptions. Hence, the designs with higher insulation level can get lower variations of operational cost and consequently lower operational cost regrets with gas boiler DHW system.

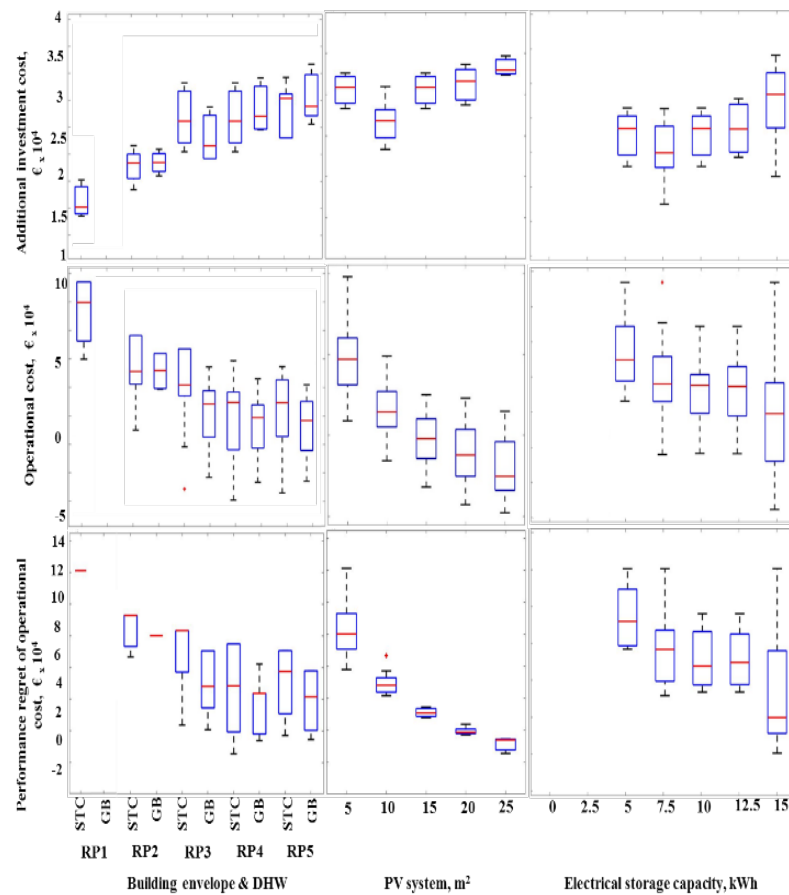


Figure 52 The boxplots show the performance spread for a design parameter value caused by variations in all the other design parameters and by the scenarios. The presented solutions are from the EF Pareto set.

The bottom graph of Figure 52 shows that designs with building envelope RP1 have larger variations of the performance regret for operational cost compared to the designs with building envelope RP5. This indicates that the operational cost of RP5 is more robust across the considered scenarios. However, it requires higher additional investment costs compared to other packages (refer to top graph of Figure 52). The homeowner might prefer the building envelope RP2

equipped with a solar DHW system, which has similar regret variation as RP3 and RP4 without solar DHW, but it requires a lower additional investment cost. Considering variations in operational cost and corresponding performance regrets, the homeowner would prefer larger PV systems and larger electrical storage systems.

Figure 53 shows the influence of a chosen design parameter value on the predicted performance of the other EF Pareto set solutions. Note that some design parameter values are not included in any of the Pareto solutions, e.g., the battery size of 0 kWh. The figure indicates that designs with intermediate insulation levels [2.5-4.5 m²K/W] result in a higher range of operational cost and higher operational cost regrets in comparison to same design options in the homeowner Pareto set. The EF Pareto solutions are equipped with electrical storage capacities of 5 kWh or higher. As mentioned low electrical storage capacities [0-2.5 kWh] are not included in this set of Pareto solutions. High electrical storage capacities are not as robust as in the homeowner Pareto set (compare to Figure 52). However, in the EF Pareto set the variations of operational cost and its corresponding regrets can be reduced with higher size of PV systems. As is shown in Figure 53, the larger PV systems result in very low performance regret for operational cost in expense of high investment costs.

Overall, considering variations in operational cost and corresponding performance regrets, designs with high insulation levels [8.5 m²K/W], large PV systems [25 m²] and high storage capacities [15 kWh] are dominating the EF Pareto set, however because of the high additional investment cost these solutions might not be the homeowner's preferred design solutions.

8.5 Conclusion

This study presents a simulation based design optimization methodology in identifying energy flexible building designs. Energy flexibility is defined as the ability of a building to manage its load and generation in the way to increase self-consumption and reduce dependency to the energy grid. This methodology integrates uncertainties due to policy scenarios in multi criteria assessment to aid decision makers in selection of robust design options.

The performance of the design space for different policy scenarios is assessed by using building performance simulations with multiple energy flexibility, performance indicators and corresponding performance robustness. The methodology is demonstrated using a case study with a homeowner as decision maker.

Results show that the proposed methodology provides a homeowner with information to trade off investment in improving building insulation levels with the other design options like electrical storage and PV system. In addition, the homeowner can choose design options that are more robust to the preferred performance indicators.

The proposed approach also provides the decision makers with information about the possible energy flexibility performance of the design space. As it is observed in this case study, energy flexible designs able to provide higher self-consumption and lower dependency to the grid are more expensive for homeowners specifically in policy scenarios providing incentives to sell on-site produced energy. Considering variations in the operational cost due to different policy scenarios, designs with high insulation levels [8.5 m²K/W], large PV systems [25 m²] and high storage capacities [15 kWh] are dominating solutions obtained with self-consumption and grid dependency objectives. However, because of the high additional investment cost these solutions might not be the homeowner's preferred design solutions.

Further work will aim at extending the proposed methodology to assess the performance of groups of residential buildings considering the energy flexibility potential in increasing local self-consumption and reducing grid dependency.

8.6 References

- [1] “Corner house (M) | RVO.nl.” [Online]. Available: <https://www.rvo.nl/initiatieven/energiezuiniggebouwd/hoekwoning-m>. [Accessed: 29-Jan-2019].
- [2] R. Kotireddy, P. J. Hoes, and J. L. M. Hensen, “A methodology for performance robustness assessment of low-energy buildings using scenario analysis,” *Appl. Energy*, vol. 212, no. August 2017, pp. 428–442, 2018.
- [3] L. Peeters, R. de Dear, J. Hensen, and W. D’haeseleer, “Thermal comfort in residential buildings: Comfort values and scales for building energy simulation,” *Appl. Energy*, vol. 86, no. 5, pp. 772–780, May 2009.
- [4] J. Salom, A. J. Marszal, J. Widén, J. Candanedo, and K. B. Lindberg, “Analysis of load match and grid interaction indicators in net zero energy buildings with simulated and monitored data,” *Appl. Energy*, vol. 136, pp. 119–131, Dec. 2014.
- [5] P. Huang, G. Huang, and Y. Sun, “Uncertainty-based life-cycle analysis of near-zero energy buildings for performance improvements,” *Appl. Energy*, vol. 213, pp. 486–498, Mar. 2018.
- [6] B. Verbruggen and J. Driesen, “Grid Impact Indicators for Active Building Simulations,” *IEEE Trans. Sustain. Energy*, vol. 6, no. 1, pp. 43–50, Jan. 2015.
- [7] “Middle house RVO.nl.” [Online]. Available: <https://www.rvo.nl/onderwerpen/duurzaam-ondernemen/gebouwen/wetten-en-regels-gebouwen/nieuwbouw/energieprestatie-epc/referentiewoningen-epc/tussenwoning>. [Accessed: 29-Jan-2019].
- [8] “Standard Solar Panels CS6P-P | CS6K-P | CS6K-M | Canadian Solar.” [Online]. Available: <https://www.canadiansolar.com/solar-panels/standard.html>. [Accessed: 29-Jan-2019].
- [9] sonnenBatterie.”[Online].Available:<https://sonnen.com.au/sonnenbatterie/>. [Accessed:29-Jan-2019].
- [10] G. Masson -Iea, P. Jose, I. Briano, and M. Jesus Baez -Creara, *REVIEW AND ANALYSIS OF PV SELF-CONSUMPTION POLICIES*.
- [11] J. Hirvonen, G. Kayo, S. Cao, A. Hasan, and K. Sirén, “Renewable energy production support schemes for residential-scale solar photovoltaic systems in Nordic conditions,” *Energy Policy*, vol. 79, pp. 72–86, Apr. 2015.

8.7 Relevant publications

More information on this study can be found in Mohammadi, Zahra; Hoes, Pieter-Jan; Hensen, Jan, Simulation-based design optimization of houses with low grid dependency, The 16th IBPSA International Conference and Exhibition, Building Simulation (BS2019), Rome, Italy, Unpublished.